

TALLINN UNIVERSITY OF TECHNOLOGY
DOCTORAL THESIS
34/2018

Cobalt- and Nickel-Free Titanium and Chromium Carbide-Based Cermets

MÄRT KOLNES



TALLINN UNIVERSITY OF TECHNOLOGY

School of Engineering

Department of Mechanical and Industrial Engineering

This dissertation was accepted for the defence of the degree 02/05/2018

Supervisor:

Prof. Jakob Kübarsepp
School of Engineering
Tallinn University of Technology
Tallinn, Estonia

Co-supervisor:

Assoc. prof. Fjodor Sergejev
School of Engineering
Tallinn University of Technology
Tallinn, Estonia

Opponents:

Igor Konyashin, PhD
Element Six GmbH, Burghaun, Germany
National University of Science and Technology MISIS
Moscow, Russia

Aile Tamm, PhD
Institute of Physics
Faculty of Science and Technology
University of Tartu, Estonia

Defence of the thesis: 20/06/2018, Tallinn

Declaration:

Hereby I declare that this doctoral thesis, my original investigation and achievement, submitted for the doctoral degree at Tallinn University of Technology, has not been previously submitted for doctoral or equivalent academic degree.

Märt Kolnes

signature



European Union
European Regional
Development Fund



Investing
in your future

Copyright: Märt Kolnes, 2018

ISSN 2585-6898 (publication)

ISBN 978-9949-83-273-6 (publication)

ISSN 2585-6901 (PDF)

ISBN 978-9949-83-274-3 (PDF)

TALLINNA TEHNIKAÜLIKOOL
DOKTORITÖÖ
34/2018

Koobalti- ja nikli-vabad titaankarbiid- ja kroomkarbiidkermised

MÄRT KOLNES

Contents

LIST OF PUBLICATIONS.....	6
INTRODUCTION.....	7
ABBREVIATIONS.....	8
SYMBOLS.....	8
1 REVIEW OF LITERATURE.....	9
1.1 Introduction.....	9
1.2 Stainless steels.....	10
1.2.1 Ferritic stainless steels.....	12
1.2.2 Austenitic stainless steels.....	13
1.2.3 Powder metallurgy of stainless steels.....	13
1.2.4 Manganese in powder metallurgy steels.....	15
1.3 Titanium carbide-based cermet with alternative binders.....	16
1.4 Chromium carbide-based cermet with alternative binders.....	19
1.5 Objective and tasks of the study.....	21
1.6 Structure of the work.....	22
2 MATERIALS AND EXPERIMENTAL METHODS.....	23
2.1 Starting materials and materials processing.....	23
2.1.1 Powder preparation and pressing.....	24
2.1.2 Sintering.....	24
2.2 Characterization of materials.....	26
2.2.1 Density, microstructure and phase characterization.....	26
2.2.2 Particle size and thermal analysis.....	26
2.2.3 Mechanical properties measurement.....	26
3 DEVELOPMENT OF TITANIUM CARBIDE-BASED CERMETS.....	27
3.1 Cermets with FeCr binder.....	27
3.2 Cermets with FeCrMn binder.....	35
3.3 Summary.....	40
4 DEVELOPMENT OF CHROMIUM CARBIDE-BASED CERMETS.....	41
4.1 Cermet with FeCr binder.....	41
4.2 Cermets with FeTi binder.....	44
4.3 Summary.....	48
5 CONCLUSIONS.....	50
Titanium carbide-based cermets.....	50
Chromium carbide-based cermets.....	50
Novelty and Further research.....	51
REFERENCES.....	52
ACKNOWLEDGEMENTS.....	56
KOKKUVÕTE.....	57
ABSTRACT.....	59
APPENDIX.....	61
CURRICULUM VITAE.....	112
ELULOOKIRJELDUS.....	113

LIST OF PUBLICATIONS

The list of author's publications, on the basis of which the thesis has been prepared:

- I **Kolnes, M.**, Mere, A., Kübarsepp, J., Viljus, M., Maaten, B., Tarraste, M. Microstructure evolution of TiC cermets with ferritic AISI 430L steel binder. *Powder Metallurgy*, 2018, published online: 15 Mar 2018.
- II **Kolnes, M.**, Kübarsepp, J., Kollo, L., Viljus, M. Characterization of TiC-FeCrMn cermets produced by powder metallurgy method. *Materials Science (Medžiagotyra)*, 2015, 21 (3), 353–357.
- III **Kolnes, M.**, Kübarsepp, J., Viljus, M., Traksmäa, R., Illopmägi, S. Effect of sintering conditions on microstructure and performance of TiC-FeCrMn cermets. *World PM2016 proceedings*, 2016.
- IV **Kolnes, M.**, Pirso, J., Kübarsepp, J., Viljus, M., Traksmäa, R. Structure formation and characteristics of chromium carbide-iron-titanium cermets. *Proceedings of the Estonian Academy of Sciences*, 2016, 65 (2), 138–143.
- V **Kolnes, M.**, Kübarsepp, J., Viljus, M., Traksmäa, R. Technological Peculiarities of Chromium Carbide-Based Iron Alloy Bonded Cermet. *Solid State Phenomena, Trans Tech Publications Ltd.*, 2017, 267, 82–86.

The author`s contribution

The author of this thesis took part in the preparation of experiments, was responsible of carrying out the experiments and interpreting the results. The author also took part of the discussion and was responsible for writing and publishing the papers. All the papers were revised and commented by co-authors.

INTRODUCTION

Due to losses resulting from wear in the life cycle costs of tools and equipment, development of new and cost-effective wear resistant materials has been and is essential. Among other wear resistant materials, ceramic-metal composites (cermets) are featured by favorable combination of hardness, toughness and strength as against ceramics. The most recognised ceramic-metal composites are based on tungsten carbide (WC) and cemented with more tough cobalt. Composites based on titanium carbide (TiC) and titanium carbonitride (TiCN) and chromium carbide (Cr_3C_2) prevalently cemented with Ni and Ni-alloys are also known. However, W and Co as metals of high economic importance are in the list of critical raw materials in Europe while Ni and Co are classified as toxic for human health. Therefore, the motivation of the present research was the need for W-, Ni- and Co-free biocompatible cermets replacing regular WC-Co cemented carbides and TiC-NiMo and Ti(C,N)-NiMo cermets.

The focus was on TiC- and Cr_3C_2 -based cermets bonded with high-chromium FeCr alloys. The goal was to acquire better understanding of microstructure evolution and phase transformation during sintering and find possibilities of improving cermet performance using alloying and/or technological opportunities. The thesis research was organized in two parallel directions: TiC-based and Cr_3C_2 -based cermets. TiC- and Cr_3C_2 -based Fe alloys bonded cermets were produced by the conventional powder metallurgy route using hot consolidation liquid-phase sintering or spark plasma sintering (SPS). Microstructure analysis (optical and scanning electron microscope), X-ray spectroscopy (EDS), X-ray diffraction (XRD), and differential scanning calorimetry (DSC) were used to study microstructure evolution and reveal changes in phase composition during sintering of composites. Ceramic-based composite materials were characterized utilizing regular mechanical properties of cermets - Vickers hardness (HV) and fracture toughness (K_{IC}).

The novelty of this research can be outlined in brief as follows: TiC-based cermets: 1) determination of microstructure evolution and phase transformation features of high-chromium TiC-FeCr and high-chromium and manganese TiC-FeCrMn cermets; 2) revealing technological and chemical (alloying) opportunities for improving structural homogeneity and mechanical performance of TiC-based cermets characterized by high resistance to wear. Cr_3C_2 -based cermets: 1) determination of microstructure evolution and phase transformation features of Cr_3C_2 -based cermets bonded with iron alloys (FeCr, FeTi); 2) revealing technological and chemical (alloying) opportunities that enable improvement of the structure and mechanical performance of Cr_3C_2 -based cermets characterized by excellent resistance to corrosion.

Main results of the research are introduced in the publications – 3 in scientific journals (Powder Metallurgy, Proceedings of the Estonian Academy of Sciences and Medžiagotyra) and 2 in conference proceedings (World Powder Metallurgy 2016 and Materials Engineering 2017). Outcomes of the thesis were presented at following conferences: Materials Engineering 2014, 2015, 2017 and World PM Congress 2016.

ABBREVIATIONS

AISI	American Iron and Steel Institute
a.u.	arbitrary unit
bcc	body-centred cubic
Cr _x C _y	Chromium Carbide
DSC	Differential Scanning Calorimetry
EDS	Energy Dispersive X-ray Spectroscopy
fcc	face-centred cubic
M _x C _y	Metal Carbide
OM	Optical Microscope
PM	Powder Metallurgy
SEM	Scanning Electron Microscopy
SPS	Spark Plasma Sintering
TiC	Titanium Carbide
vol%	volume percent
WC	Tungsten Carbide
wt%	weight percent
XRD	X-Ray Diffraction

SYMBOLS

α -Fe	α -iron allotrope, ferrite, body-centred cubic (bcc) crystal structure
γ -Fe	γ -iron allotrope, austenite, face-centred cubic (fcc) crystal structure
a	the half average length of the diagonal of Vickers indentations
c	The average length of the cracks in the tips of the Vickers indentations
HV30	Vickers hardness, load 298 N (30kgf)
K _{IC}	Indentation fracture toughness
p	Pressure
T	Temperature
ΔG	Change in Gibbs free energy

1 REVIEW OF LITERATURE

1.1 Introduction

Major challenges in engineering (energy production, transportation, mining, clean water etc.) require development of materials superior in performance to those today. New advanced materials enable us to create new, innovative products and applications.

Desirable properties of materials can be met in multiphase material structures produced using the powder metallurgy (PM) technology. PM composites suit well in tribological applications where the wear resistance is an important factor to improve the durability of products. The losses resulting from wear in the life cycle costs of equipment are pronounced. In some industries such as mining, building materials production etc., recycling of wear parts may compose up to 40% of life cycle costs. The challenge is to develop new reliable and cost-effective materials on the basis of advanced technologies and to utilize this technology effectively for new products (EuMaT homepage).

Carbides cemented with metals of the iron group are composite materials where brittle and hard carbide phase is “cemented” in a softer metal matrix. Such composite materials are known due to their high hardness, wear resistance and higher toughness in comparison with ceramics (Schatt, 1997). Therefore, cemented carbides are used extensively as cutting tool material, as well as in other industrial applications (Brookes, 2011). Because of the good combination of hardness and wear resistance, WC-based cemented carbides (hardmetals) are most widely used. Cobalt as a binder of hardmetals is widely used since it wets WC readily and leads to products with excellent strength and ductility. However, hardmetal dust is the reason for hardmetal lung disease, which is a rare disease caused by exposure to particles of hardmetal alloys. WC-Co hardmetal dust has been shown to be more toxic in combination than either pure tungsten carbide or cobalt alone (Fischbein, 1992). In addition, because of the strategic nature of tungsten supply and the shortage of cobalt, great efforts have been made to replace or supplement these metals (Norgren, 2015). Therefore, partly or fully tungsten- and cobalt-free cermets have been developed (Exner, 1979) – most of the efforts have centred on titanium carbide- or titanium carbonitride-based cermets bonded with Ni-Mo alloys (Ettmayer, 1989). Another successful cermet type is chromium carbide bonded with nickel metal. This cermet is called a “stainless steel” of the hardmetal industry. But, the REACH (The Regulation on Registration, Evaluation, Authorization and Restriction of Chemicals) (ECHA homepage) and TSCA (Toxic Substances Control Act) (TSCA homepage) are classifying nickel and cobalt as metals toxic for human health. The allergenic diseases have increased over the past three decades. For example, published reports show an exponential increase in reported nickel allergy cases. The best method to decrease the nickel allergy is to utilize and develop completely Ni- and Co-free materials.

The European Commission has created the list of critical raw materials (European Commission homepage) (see Fig. 1). The purpose of the list is to contribute to the

implementation of the EU industrial policy and to ensure that European industrial competitiveness is strengthened through actions in other policy areas. The list is also being used to help prioritize needs and actions.

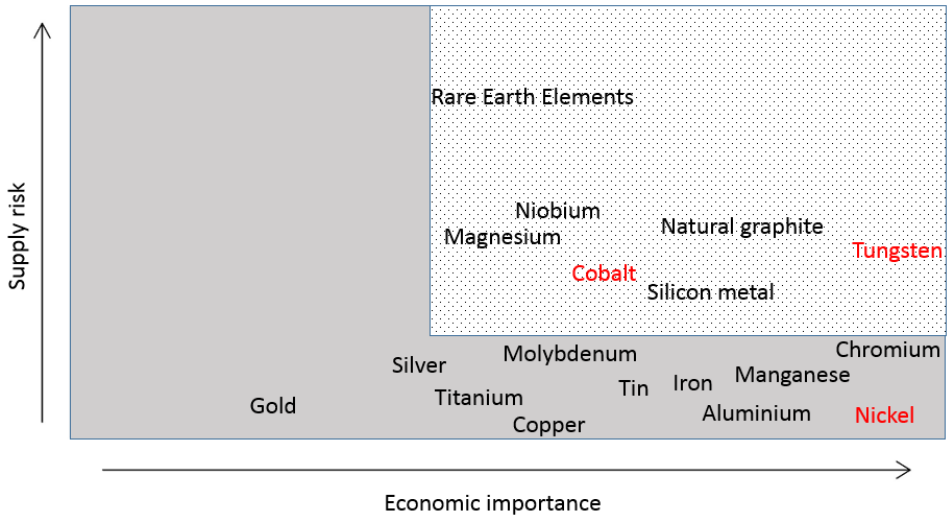


Figure 1. Critical raw materials for EU, upper right corner (European Commission homepage).

Also, according to the European Commission’s list of critical raw materials, utilization of materials with high economic importance and supply risk should be reduced. Tungsten and cobalt are in that list. Titanium, iron and chromium are not included as critical raw materials. Non-toxic titanium carbide and chromium carbide and iron-based binder systems are the top-of-the-line solution for replacing these critical and toxic metals. Since the 1970s, different kinds of alloys (pre-alloyed metal powders and elemental powder mixtures) have been used as an alternative binder phase. Therefore, the law of the thermodynamics and computer simulated programs of different possible phases have been used by many authors.

1.2 Stainless steels

Different stainless steels as a binder phase of cermets and cemented carbides are increasingly used as initial powder in applications where high hardness and corrosion resistance are necessary. Therefore, the structure and phase transformation peculiarities of the binder phase should be observed hand-in-hand with structural evolutions in steels.

Composition of stainless steels is much more complex compared to conventional carbon steels. The more alloying elements, the more opportunities exist to form possible phases and crystal structures. Ferrite, austenite and martensite are the three main phases of stainless steels. Stainless steel contains a minimum of 11 wt% of chromium alone and also other metals like manganese, silicon, nickel, molybdenum,

etc. Chromium forms the passive film that makes stainless steel corrosion resistant (Davis, 1994).

In addition to Cr in stainless steels, other elements include Mo for pitting resistance, Cu, Al and Ti for precipitation hardening, N and Mn for strength and Ta or Nb for sensitization (chromium depletion accompanied by precipitation of chromium carbides at grain boundaries) reduction. Selected compositions and characteristics linkages in the stainless steel family are summarized in Fig. 2.

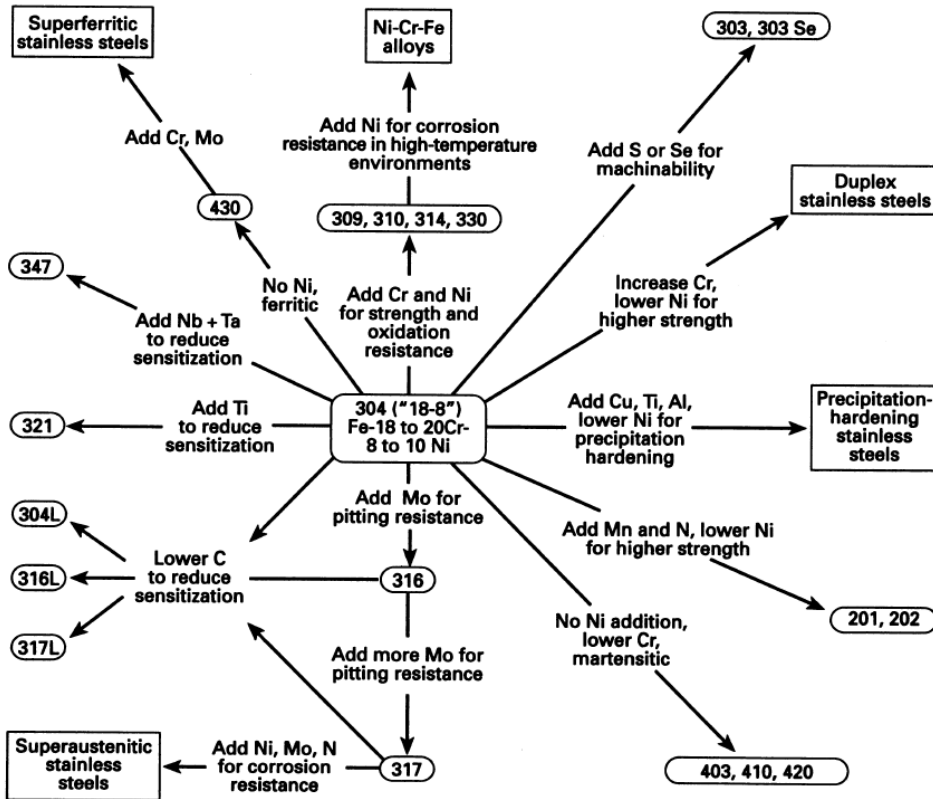


Figure 2. Composition and corresponding properties of different stainless steel families (Al-Mangour, 2015).

The large number of alloying elements in relatively high concentrations causes many stable phases in the steel structure simultaneously. According to the law of thermodynamics, the number of possible solid phases is the same as the number of alloying elements plus one. In addition, most stainless steels have metastable structure. Since the diffusion is too slow for the atomic rearrangements, the structure may not achieve an equilibrium state. To predict the possible phases the calculation of the free energies is required. The phase with the lowest energy is most preferable but other phases may form as well.

There are several families of stainless steel: ferritic, martensitic, austenitic and duplex. These names are derived from the crystal structure of the steels that determines their metallurgical behaviour.

1.2.1 Ferritic stainless steels

Ferrite has a bcc structure and the main alloying element in stainless steels, chromium, is the principal ferrite stabilizing element. Silicon, molybdenum, niobium, tungsten, aluminium and titanium all have a similar effect, but none produces the ability of stainlessness. The bcc structure of ferrite allows very fast diffusion rates of all elements – interstitial (carbon, nitrogen, oxygen, boron and helium) and substitutional diffusion of all other elements. The diffusion rates are two or three orders of magnitude higher than in austenite. Martensite is principally ferrite that has been formed with supersaturation of carbon (Nayar, 2000).

Nitrogen and carbon solubility in ferrite is essentially zero at room temperature; therefore, to retain the ferrite structure, free carbon must be eliminated. Also, during cooling, the solubility of carbon and nitrogen decreases and they must precipitate. Thermodynamically, the most likely compound with chromium (chromium carbide) can form. Therefore, to avoid the depletion of chromium by the formation of chromium carbide, other strong carbide formers such as titanium and niobium are used (Davis, 2001).

$M_{23}C_6$ is the primary carbide found in stainless steel structure particularly at grain boundaries (see Fig. 3) and it contains also iron that can substitute the chromium up to 50 wt%. Tungsten, molybdenum and vanadium can also dissolve in this carbide. At higher carbon contents, M_7C_3 and M_3C carbides may form and additional stabilizing elements form MC type carbides (Roberts, 1998).

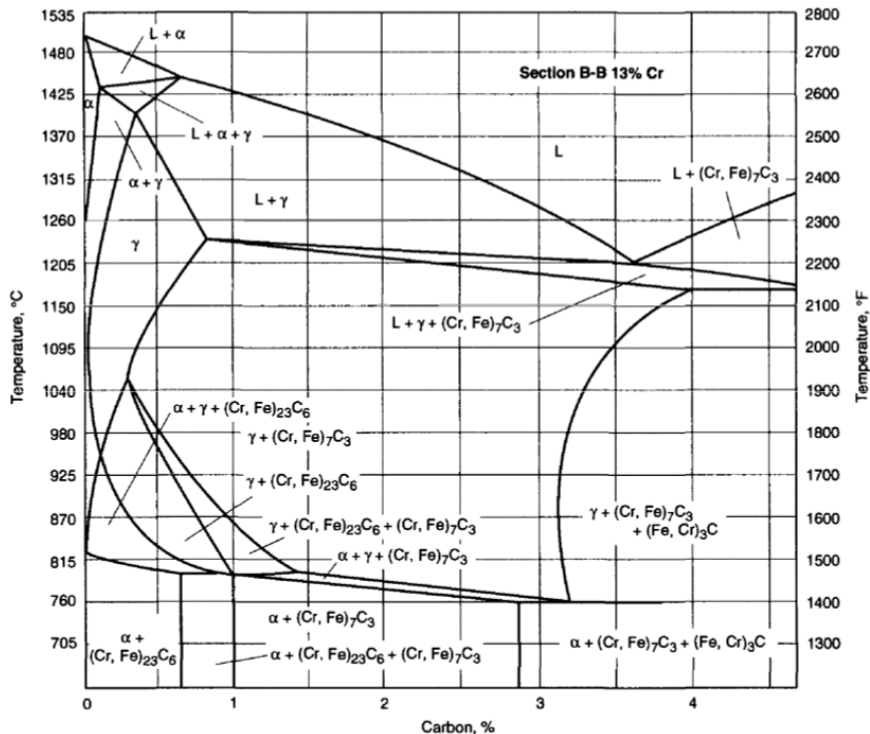


Figure 3. Vertical section of the Fe-Cr-C system at 13% Cr (Roberts, 1998).

The similar metal carbides with relatively complex structure can be presented are presented in the structure of cermets that contain iron and other even stronger carbide forming elements (Cr, Mo, Mn). Formation of metal carbides is due to the high carbon content of ceramic-based composites.

1.2.2 Austenitic stainless steels

Austenite has a fcc crystal structure. Interstitials, carbon and nitrogen, are the most effective austenite stabilizing elements but nickel and manganese are also stabilizers (Nayar, 2000). To ensure the austenitic structure of stainless steel, it must contain about 11 wt% of nickel. The austenite stabilizing effect of manganese is half of that of nickel. Chemical composition of the selected Ni-free or low-nickel austenitic stainless steels is presented in Table 1 (Yang, 2010; Kuroda, 2002).

Table 1. Chemical composition wt% of Ni-free or low-nickel austenitic stainless steels.

Steel	C	Cr	Mn	Mo	Cu	Ni	Si	S	P	N
BIOSS4	0.029	17.05	12.58	2.38	1.44	0.03	0.42	0.007	0.014	0.43
ASTM	0.080	21.00	22.00	1.00	0.25	0.05	0.75	0.010	0.030	0.95
AISI 205	0.200	17.25	14.75	-	-	1.35	1.00	0.030	0.060	0.35
AISI XM-31	0.120	17.50	15.00	-	-	1.00	0.70	0.030	0.045	-
AISI 18-2Mn	0.150	17.25	12.50	-	-	1.50	1.00	0.030	0.045	0.30
AISI 18-18+	0.150	18.00	18.00	1.00	1.00	-	1.00	0.030	0.045	0.50
HNS	0.034	23.50	0.13	2.04	-	0.04	0.07	0.001	0.009	1.34

Manganese acts largely through its ability to promote nitrogen solubility. Despite the fact that manganese is two times weaker austenite stabilizer, fully nickel-free stainless steels have been developed and produced recently. These steels with sufficient corrosion resistance and biocompatibility have proved to be good surgical implantable materials. In addition, many austenitic stainless steels are used as a binder phase of ceramic-based composites.

1.2.3 Powder metallurgy of stainless steels

Powder metallurgy of stainless steels and cermets with stainless steel binder are principally similar in many aspects: reduction of residual oxides, sintering atmosphere due to the high vapor pressure of alloying elements, low level of undesirable interstitials and effect of additional elements with improved sinterability and performance.

To a large extent, compositions of PM stainless steels have been taken over from some of the popular grades of wrought stainless steels. As a result, the characteristics of those steels are similar. Nevertheless, the chemical composition of PM stainless steels often differs by minor but important amounts from those of their wrought counter-parts. This is mainly true in the case of carbon, silicon, and manganese contents (Klar, 2007). The compositions of the standard grades and some of the more

common custom grades of PM ferritic and austenitic stainless steels are listed in Tables 2 and 3, respectively.

In the case of powder metallurgy (PM) stainless steels, the primary goal is to guarantee excellent corrosion resistance along with good mechanical properties (German, 1998). But the amount of oxygen in PM steels is often an order of magnitude higher than in wrought stainless steels. The higher content of oxygen increases the corrosion of the sintered parts – unreduced oxide particles initiate the pitting corrosion and lower the mechanical properties. Therefore, vacuum sintering is very effective for powder metallurgy stainless steels because it combines the high-temperature sintering with superior oxide reduction. The main surface oxide of gas-atomized stainless steels is Cr₂O₃, which starts to decompose at temperatures above 900 °C because of the low stability of this oxide. The common content of carbon in stainless steel powder is regularly in deficiency to reduce all of its oxides. Therefore, some free extra carbon has been added but it should be kept at optimal level to avoid the precipitation of chromium carbides. Additionally, some stabilizing elements are used to avoid the formation of chromium carbides. Among sintered stainless steels, so far niobium has been used successfully.

The second process precaution during vacuum sintering of stainless steels is the high vapor pressure of chromium at elevated temperatures. The surfaces of sintered parts demonstrate the depletion of chromium and it leads to the deterioration of overall corrosion resistance. Therefore, partial pressure of argon or nitrogen (up to 2 mbar) was applied during sintering of PM stainless steels.

Table 2. Typical chemical composition wt% of powder metallurgy Ni-free ferritic stainless steels (Klar, 2007).

Grade	S*	**	Fe	Cr	Ni	Mn	Si	C	S, P, N	Other
409L	X		bal	10.5-11.7		>0.1	>0.1	>0.03	0.03-0.3	Nb
409LE	X		bal	11.5-13.7	0.5	>0.1	>0.1	>0.03	0.03-0.3	Nb
410L	X		bal	11.5-13.5		>0.1	>0.1	>0.03	0.03-0.3	
430L	X		bal	16-18		>0.1	>0.1	>0.03	0.03-0.3	
430LN2	X		bal	16-18		>0.1	>0.1	>0.08	0.04-0.3	
434L	X		bal	16-18		>0.1	>0.1	>0.03	0.03-0.3	Mo
434LN2	X		bal	16-18		>0.1	>0.1	>0.08	0.04-0.3	Mo
434LNb		X	bal	16-18		>0.1	>0.1	>0.03	0.03-0.3	Mo, Nb
434L-M		X	bal	17.19		>0.1	>0.1	>0.03	0.03-0.3	Mo
444L		X	bal	17.5-19.5	0.8	>0.1	>0.1	>0.03	0.03-0.3	Mo, Nb

* Standard grades

** Non-standard grades

Table 3. Typical chemical composition wt% of powder metallurgy austenitic stainless steels (Klar, 2007).

Grade	S*	**	Fe	Cr	Ni	Mn	Si	Mo	C	S, P, N	Other
303L	X		bal	17-19	8-13	0.2	0.8		0.03	0.03-0.2	
303N1	X		bal	17-19	8-13	0.2	0.8		0.03	0.1-0.6	
304L	X		bal	18-20	8-12	0.12	0.8		0.03	0.01-0.04	
304N1	X		bal	18-20	8-12	0.12	0.8		0.03	0.01-0.6	
316L	X		bal	16-18	10-14	0.12	0.8	2.5	0.03	0.01-0.04	
316N1	X		bal	16-18	10-14	0.12	0.8	2.5	0.03	0.01-0.6	
303LSC		X	bal	17-19	8-13	0.2	0.8		0.03	0.01-0.2	Sn, Cu
303L-U		X	bal	17-19	8-13	0.2	0.8		0.03	0.01-0.2	Sn, Cu
304LSC		X	bal	18-20	8-12	0.12	0.8		0.03	0.01-0.04	Sn, Cu
304L-U		X	bal	18-20	8-12	0.12	0.8		0.03	0.01-0.04	Sn, Cu
316LSC		X	bal	16-18	10-14	0.12	0.8	2.5	0.03	0.01-0.6	Sn, Cu
316L-U		X	bal	16-18	10-14	0.12	0.8	2.5	0.03	0.01-0.6	Sn, Cu
317L		X	bal	19.5	14.8	1.0	0.8	3.5	0.03	0.01-0.04	
SS-100		X	bal	20.0	18.0	1.0	0.8	6.0	0.03	0.01-0.04	
316-B			bal	23	18	1.0	1.0	3.5	0.05	0.05-0.2	B

* Standard grades

** Non-standard grades

1.2.4 Manganese in powder metallurgy steels

Among classic low-alloyed structural steels, one of the most common alloying elements is manganese. The reason lies in the following: manganese is a low-priced element, it increases the mechanical properties, it is an active deoxidizer and it improves the machinability. In comparison with classical steelmaking techniques, alloying powder metallurgy steels and compounds with manganese is much more complicated. Therefore, manganese has not been widely used among powder metallurgy steels and a number of additional aspects influencing the sintering parameters have to be considered (Hryha, 2011).

The first effect is the sublimation of manganese – it has high vapor pressure. The substantial sublimation starts at around 700–750 °C when the partial pressure of manganese is about 10^{-5} mbar. Subsequent increase of temperature causes the exponential increase of manganese partial pressure (see Fig. 4) – 10 mbar corresponds to the temperature of 1450 °C (Desai, 1987). The huge amount of manganese vapor specifies a number of interconnected processes: manganese distribution through the pore system, manganese oxidation and its loss. Although high vacuum sintering demonstrates superior oxide reduction, it is not acceptable for chromium and manganese containing steels because of the depletion of these elements during the sintering cycle. Therefore, the conventional vacuum sintering technology is improved with several process precautions: vacuum sintering is conducted with low partial pressures of argon or nitrogen, introduction of high affinity elements in the pre-alloyed state.

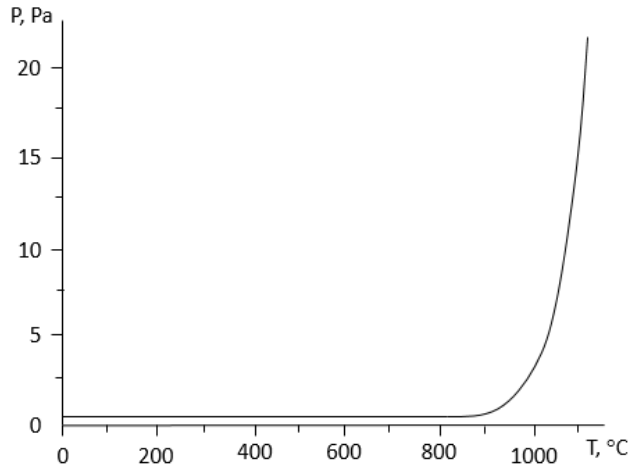
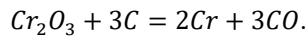
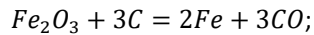


Figure 4. Equilibrium partial pressure of Mn with temperature (Hryha, 2011).

According to different researchers, in different alloys, above 600 °C and above 900 °C carbothermal reduction of iron and chromium surface oxides starts, respectively. This leads to the production of carbon monoxide according to reactions (Aigner, 1997; Klar, 2007):



Carbon monoxide is also considered as an oxidizing agent for manganese vapor and manganese vapor reacts with carbon monoxide according to the following reactions (Hryha, 2011):



Schubert et al. have also reported that high vacuum liquid-phase sintering is inappropriate for manganese containing WC-FeMn cemented carbides. Therefore, manganese vapor “microatmosphere” within the graphite crucible was applied. Consequently, the sintering was performed at 1250 °C under an argon partial pressure of 8 mbar and in a Mn vapor-saturated environment. Using these sintering conditions, up to 16 wt% of Mn could be maintained in the iron matrix. At such high Mn values, the binder remained partly austenitic during cooling (Schubert, 2015).

1.3 Titanium carbide-based cermet with alternative binders

Beginning from the 1930s, mostly because of the shortage of tungsten, efforts were made to replace or supplement tungsten carbide used as a hard phase in cemented carbides. Therefore, titanium and chromium carbide-based cermets have been investigated (Brookes, 1997).

Titanium has very high affinity to nitrogen and carbon and forms titanium carbonitride, Ti(C,N), in a full range from TiC to TiN. Furthermore, because of the high chemical and thermal stability of TiC, its solubility in iron is marginal and particles of titanium carbide are precipitated in steels at low content of titanium at elevated temperatures (Jonsson, 1998).

TiC-based cermets have been investigated for use in the cutting tool material since the 1930s, because of the high melting point and low density of TiC. Therefore, these cermets are used in applications where low density, high wear or high temperature oxidation resistance is needed. Iron-group metals (Ni, Co, Fe) have been used as a binder phase. Usually TiC- and TiCN-based cermets demonstrate core-rim structure, consisting of TiC or Ti(C,N) core with a complex carbide rim grown through the reprecipitation process (see Fig. 5).

Liquid-phase and melt infiltration sintering are the two most used production techniques for processing TiC- and Ti(C,N)-based cermets. Nickel is most popular as a metallic binder of these cermets, due to its low wetting angle with solid TiC (Humenik, 1956) and its low solubility in TiC and TiCN is low (Kocich, 2013). Extra molybdenum is used because it decreases the wetting angle of Ni-Mo alloy with TiC to zero (Lenel, 1980). This minimizes the porosity of cermets and therefore good mechanical properties are achieved. A full densification of cermet with Mo₂C addition can be achieved due to improvement of the wettability between Ti(C,N) and iron (Guo, 2009). The increasing content of Mo in cermet decreases the final grain size of the carbide phase and the microstructure becomes more homogeneous and compact (Dai, 2012).

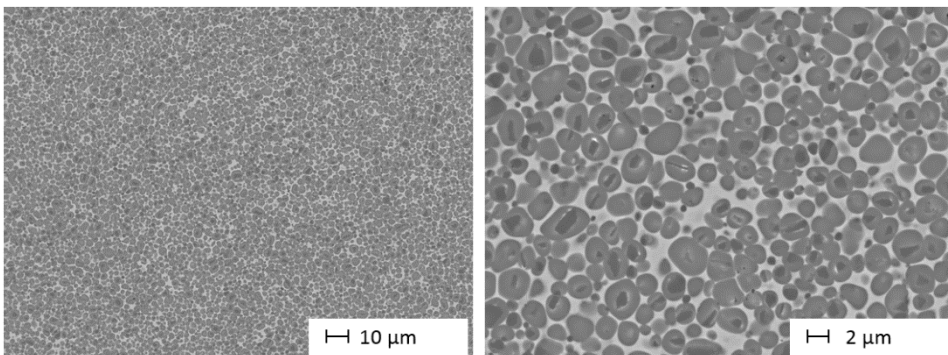


Figure 5. Microstructure of TiC-20NiMo cermet.

Throughout the whole last century there has been a flurry of activity to find alternative binder systems for TiC-based cermets. In the 1950s, the focus was on the development of different nickel containing binder systems (Ni-Mo-Al, Ni-Co, Ni-Co-Cr) for temperature critical applications (Eisen, 1998), but these were utilized as metal working tools. Additionally, since the 1970s, major scientific efforts have been made to develop iron-based binders.

Findings show that TiC-Fe cermets have insufficient wettability between iron and titanium carbide (Humenik, 1956). Also, Jing et al. concluded that in the case of TiC-Fe cermets, the formation of carbide Fe₃C due to the eutectic reaction between remanent C and Fe takes place during sintering (Wang Jing, 2007). Kübarsepp et al. have studied corrosion and mechanical performance of TiC-based cermets with different iron-based binder systems (low-alloyed Si-steel, corrosion resistant Cr-Ni steels, Ni-steels) (Kübarsepp, 1980; Kübarsepp, 1993). They reported that sinterability and therefore also

mechanical characteristics of TiC-based cermets with high chromium steel as a binder can be improved by alloying them with silicon (Kübarsepp, 1986; Reshetnyak, 1994). Silicon facilitates reduction of chromium oxides at sintering temperatures (Kübarsepp, 1986; Kübarsepp, 1994). Recent studies have addressed the influence of the different sintering modes on the performance and reliability of TiC-based Fe-alloy bonded cermets (Kübarsepp, 2014).

In the 1980s, many scientists focused on the aluminide compounds with nickel, titanium and iron as a binder for TiC. Iron aluminide is an intermetallic alloy known as extremely resistant to corrosion under oxidizing and sulfurizing atmospheres (Deevi, 1996). Fe₃Al intermetallic matrix composites reinforced with 0–50 vol% of TiC have been reported. The consolidation was performed using hot pressing, pressureless infiltration or pulse discharge sintering (spark plasma sintering, SPS) and nearly full density, improved mechanical properties, nanoscale grain size is retained (Krasnowski, 2007; Li, 2008). Also, Subramanian et al. stated that conventional liquid phase sintering is successful for TiC-FeAl cermets production (Subramanian, 1996). Durlu investigated a reaction sintering technique for processing of TiC-Fe₃Si and TiC-FeAl composites. He demonstrated high density and hardness with moderate bending strength (Durlu, 1999).

In previous decades, different steel grades (austenitic and ferritic) have been used as binders of Ti(C,N)-based cermets. Among researchers today, austenitic stainless steel as a binder phase of Ti(C,N)-based cermets is relatively popular. The most commonly used steel is AISI316L (EN 1.4016) because of its good mechanical characteristics and excellent corrosion resistance. Chenxin Jin et al. fabricated TiC-316L (TiC-FeCrNi) stainless steel cermets using a simple melt-infiltration process. They showed that a complex core-rim structure was developed and no intermediate or reaction phases were observed (Jin, 2016). Furthermore, Akhtar et al. fabricated TiC-based cermets alloyed with elemental powders of Fe and Cr (Akhtar, 2007) and AISI 465 (Cr – 12 wt%) maraging stainless steel (Akhtar, 2008). They stated that in the case of both binder systems, TiC-based composites showed no reaction between TiC particles and the binder phase. Also, good wettability of TiC particles with AISI 465 stainless steel was demonstrated and these composites showed the homogeneous distribution of TiC grains in the binder phase (Akhtar, 2008).

Chromium containing ferrite has high requirements for thermal processing to maintain the homogeneity of chromium for proper corrosion-resistance performance (McGuire, 2008). The limit of solubility of carbon is much lower in ferritic stainless steels, and the diffusion rates of interstitials are much higher due to their body-centered cubic structure. In contrast to the face-centered cubic austenitic stainless steels, the diffusion rate of chromium atoms in the ferritic matrix is approximately hundred times faster (Klar, 2007). In addition, chromium is known as a very active carbide forming element and carbon solubility in ferrite is fractional. Chromium carbide formation in cermets decreases the chromium content in stainless steel binder (McGuire, 2008). Therefore, it affects the corrosion resistance and mechanical properties of TiC-based chromium containing cermets.

Alvaredo et al. investigated the influence of carbon content on the sinterability of a FeCr matrix cermet with Ti(C,N). The calculated equilibrium phase diagram (Fig. 6) shows the presence of the following phases at temperatures below 500 °C: ferrite, austenite, sigma phase, Ti(C,N) and carbides $M_{23}C_6$ and M_7C_3 (Alvaredo, 2013). Regardless of that, the XRD analysis revealed no peaks of sigma phase or carbides – XRD diffractograms exhibited peaks that correspond to ferrite and TiC(C,N). This is most likely because they constitute a relatively low percentage of carbon in the cermet.

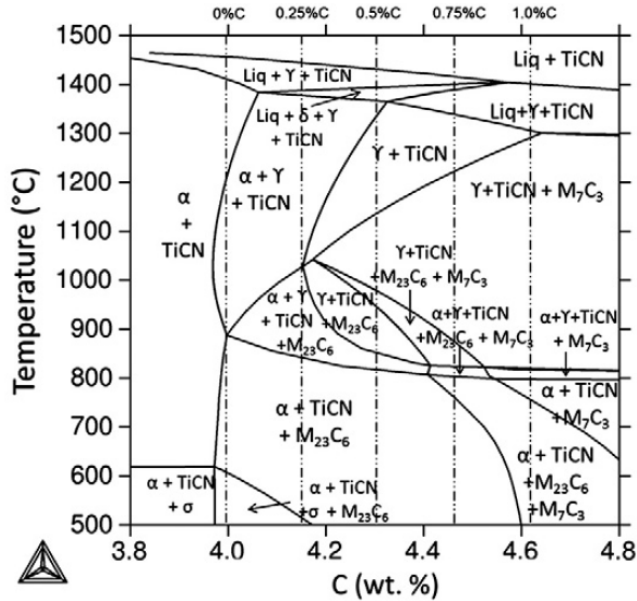


Figure 6. Calculated equilibrium phase diagram for a material with a composition of AISI 430L (EN 1.4016) steel and Ti(C,N) 50 vol%, as a function of C content (Alvaredo, 2013).

1.4 Chromium carbide-based cermet with alternative binders

Chromium carbide cermets are suitable for general and special application areas where both wear and corrosion resistance are needed. Chromium carbide-based cermets bonded with nickel demonstrate high hardness and excellent oxidation, corrosion, erosion and abrasive resistance. Microstructure of the chromium carbide-based nickel bonded cermet is presented in Fig. 7. These cermets are even called “stainless steel” of cemented carbides (Brookes, 1997). However, the major disadvantages of this material are its low mechanical properties: fracture toughness and transverse rupture strength. The second drawback is the cost and toxicity of nickel. Therefore, efforts have been made to replace nickel with low-priced and harmless iron or its alloys.

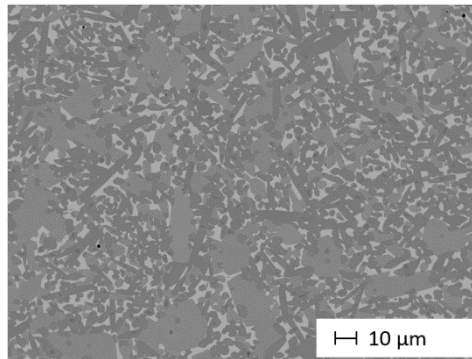


Figure 7. Microstructure of Cr_3C_2 -20Ni cermet.

Previous results from different studies demonstrate that iron and iron-based alloys could replace nickel as a metal matrix of chromium carbide-based cermets. Radomyselskii et al. focused on the development of tungsten- and nickel-free chromium carbide and white cast iron composites (Maslyuk, 2014). Unfortunately, because of high brittleness and low toughness, these cermets have not been utilized yet. Coarse carbide grains in the microstructure are one of the main reasons behind that. Despite this, Radomyselskii's followers – Maslyuk and Vlasyuk – continued research in this area. They examined the interaction between chromium carbide Cr_3C_2 and iron alloys and according to their findings, vertical section of the Cr-Fe-C phase diagram was developed (Maslyuk, 2013), (see Fig. 8).

The Fe- Cr_3C_2 section demonstrates that iron-based phases are not in equilibrium with starting Cr_3C_2 : carbide $(Cr,Fe)_7C_3$ forms during sintering and two phased regions are wide enough to produce composites with acceptable characteristics. They also stated that it would be most promising if the cermet is produced by liquid phase sintering containing 50–60 wt% of Cr_3C_2 carbide. When the content of iron is lower than 40 wt%, almost all of iron is dissolved in complex carbide $(Cr,Fe)_7C_3$. During heating, in the carbide Cr_7C_3 , up to 60 wt% of chromium atoms can be replaced by iron atoms (Vlasyuk, 1984). Also, Yakovenko et al. reported that despite the differences in the chemical composition of the initial metal matrix (iron or iron-chromium steel), the phase transformation mechanisms are similar (Yakovenko, 2011).

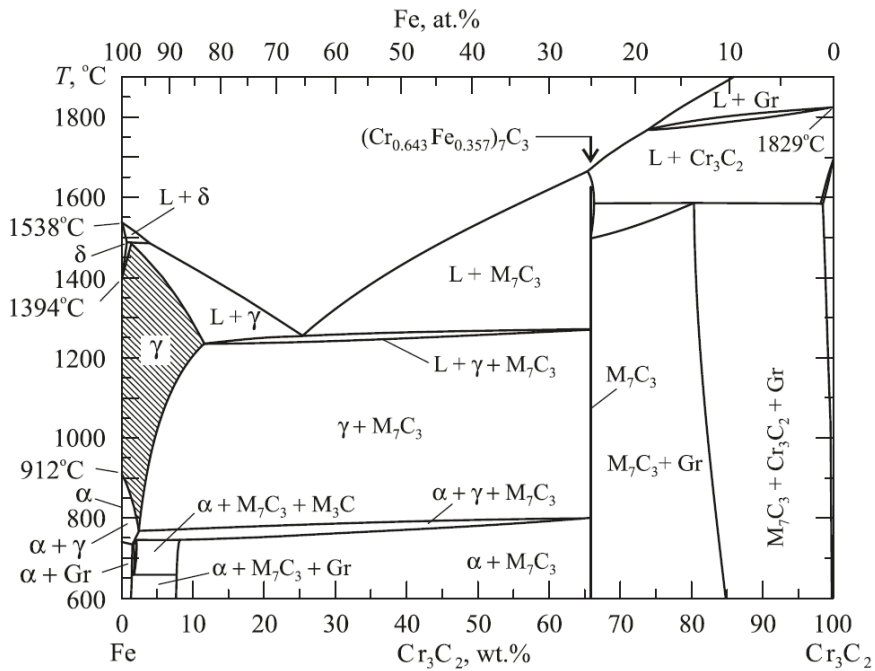


Figure 8. Vertical section of the Fe-Cr₃C₂ phase diagram (Maslyuk, 2013).

Sintering temperature and time are very important technological parameters designating the structure and properties of the chromium carbide-based cermets. Marked grain growth during sintering is the second main disadvantage of these cermets. Tolochin et al. proved that in the case of chromium carbide cermets with powder metallurgy steel addition, shock-wave sintering in vacuum improves the mechanical properties of cermets (Tolochin, 2017). Also, because of the fast nature of the spark plasma sintering, it would be an optional technology in chromium carbide-based cermets production.

1.5 Objective and tasks of the study

The motivation of the study is the need for tungsten, cobalt and nickel free ceramic-metal tribomaterials having capacity to replace regular WC-Co hardmetals and TiC-NiMo or Ti(C,N)-NiMo cermets.

The main objectives of the thesis research are: (1) to acquire deeper understanding of microstructure evolution and phase transformations during sintering of TiC- and Cr₃C₂-based cermets bonded with Ni-free FeCr alloys and as a result, (2) to develop composition and sintering parameters for optimized microstructure, hardness and toughness of composites.

The main goals of the research of titanium and chromium carbide-based cermets are as follows:

1. Determine hot consolidation features of high chromium FeCr alloys bonded cermets;
2. Reveal microstructure evolution and phase formation of cermets during sintering;
3. Demonstrate possibilities of improvement of high-chromium FeCr alloys bonded cermets performance using alloying and/or technological opportunities;
4. Characterize mechanical properties of composites.

1.6 Structure of the work

This thesis covers two main parts (research directions) – titanium carbide- and chromium carbide-based cermets with iron-based binder systems. The first part contains three subthemes: study of structure evolution of titanium carbide-based ferritic steel bonded cermets (Paper I); problems with the manganese loss of titanium carbide ferro-chromium-manganese cermets during sintering (Paper II); challenges in the development of the sintering conditions for titanium carbide – FeCrMn cermets (Paper III). The second main part addresses two subthemes: the influence of technological factors on the structure evolution and mechanical properties of chromium carbide ferritic FeCr cermets (Paper V); study of technological peculiarities of chromium carbide FeTi steel cermets (Paper IV).

Structure of the thesis research:

- Titanium carbide-based cermets:
 - TiC-FeCr,
 - TiC-FeCrMn.
- Chromium carbide-based cermets:
 - Cr₃C₂-FeCr,
 - Cr₃C₂-FeTi.

2 MATERIALS AND EXPERIMENTAL METHODS

This chapter describes the characteristics of starting powders, powder materials processing peculiarities and methods of materials characterization. It is divided into three parts: starting materials, materials processing and methods of characterization.

2.1 Starting materials and materials processing

Chemical composition and characteristics of starting carbide and steel powders are presented in Table 4. Additionally, elemental powders of iron, manganese, chromium, molybdenum and silicon were used. Materials processing contains three stages: powder preparation, pressing of green compacts and sintering.

Table 4. Chemical composition, average particle size and producer of starting powders.

Powder	Chemical composition, wt%		Average particle size, μm	Producer or supplier
	Basic components	Impurities		
TiC	$C_{\text{comb}} - 19.12$; $C_{\text{free}} - 0.15$; Ti - bal.	O - 0.30; N - 0.02	2.10	PPM Ltd.
Cr_3C_2	Cr - 86.7; C - 13.2	Fe - 0.1	1.88	PPM Ltd.
AISI430L X2Cr17 (EN 1.4016)	Cr - 16.8; Mn - 0.69; Si - 0.64; Fe - bal.	C - 0.02; P - 0.01; S - 0.01	10 - 45	Sandvik Osprey Ltd.
AISI446 X18CrN28 (EN 1.4762)	Cr - 24.2; Mn - 1.2; Si - 0.85; Fe - bal.	N - 0.25; C - 0.03; P - 0.011; S - 0.008	10 - 45	Sandvik Osprey Ltd.
AISI316L X2CrNiMo17-12-2 (EN 1.4435)	Cr - 17.1; Mn - 1.2; Ni - 10.9; Mo - 2.3; Si - 0.67; Fe - bal.	N - 0.1; C - 0.02; P - 0.022; S - 0.006;	10 - 45	Realizer GmbH.
Fe	Fe - 99.72	Si - 0.01; P - 0.07; Mn - 0.02	< 100	Rio Tinto
Mn	Mn - 99.84	O - rest	7.95	PPM Ltd.
Cr	Cr - 99.5	O - 0.38; Fe - 0.01	6.65	PPM Ltd.
Mo	Mo > 99.80	Fe - 0.0025; O - 0.110	2.48	PPM Ltd.
Si	Si - 99.50	Al - 0.15; Ti - 0.002; Fe - 0.2; P - 0.004; Ca - 0.05; B - 0.0005	44	Whole Win, Materials Sci. & Tech.
Fe-Si	Fe - 50.1; Si - 48.2	Al - 1.1; Cr - 0.2; Mn - 0.4	< 100	Comminute foundry ferrosilicon

2.1.1 Powder preparation and pressing

Cermets were produced using the conventional powder metallurgy method: mechanical milling in the ball mill followed by uniaxial pressing and sintering. Powders were mechanically ball milled (grinding and mixing) in liquid media (isopropyl alcohol) using a laboratory ball mill with a rotating speed of 60 rpm during 72 h. Powder mixture milling in the ball mill using WC-Co lining and balls results in alloy moderate contamination with tungsten. The ball to the powder mass ratio was 10:1. Additionally, the influence of technological factors on the carbide grain growth of chromium carbide-based cermets was studied by attritor milling. The charge ratio in the attritor was 5:1 and the rotation speed of the impellers 560 rpm. Milled powder mixture was dried and plasticized with paraffin wax (approx. 1–2 wt%) and granulized. Granulized powder was compacted into green bodies with 80–100 MPa of uniaxial pressure.

2.1.2 Sintering

Two sintering techniques – vacuum sintering and spark plasma sintering (SPS) were used (Fig. 9).

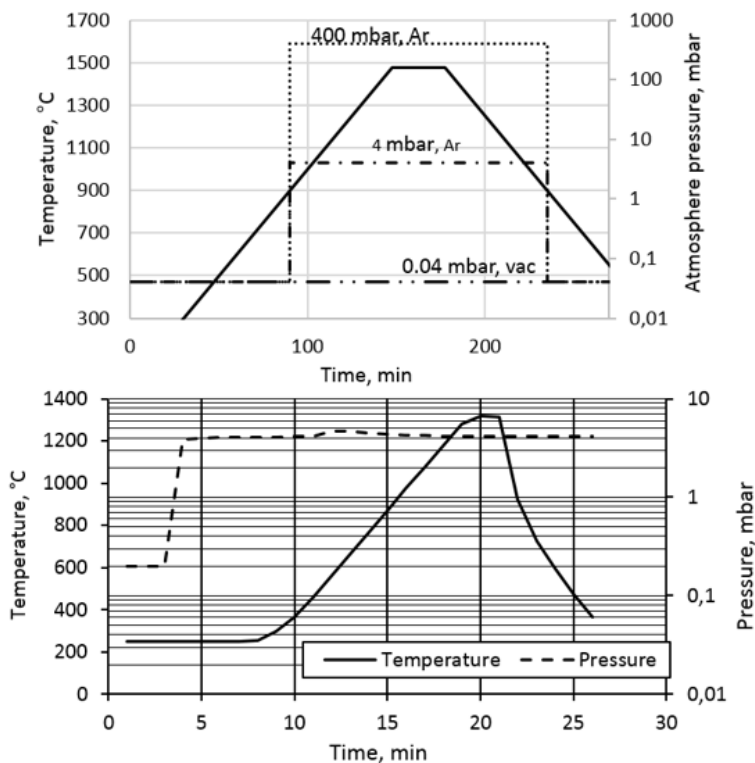


Figure 9. Sintering regimes: vacuum low-partial pressure (top) and spark plasma sintering (bottom).

Liquid phase vacuum sintering at different temperatures (600–1500 °C) in a furnace with graphite heaters was used (semi-industrial FPW-300/400-2-1600-100KS/SP). Pressed specimens were sintered on a ZrO_2 powder in graphite crucible support. The

compacted samples were sintered at the sintering temperature for 30 min using an approximate heating rate of $10\text{ }^{\circ}\text{C}\cdot\text{min}^{-1}$.

Manganese loss during sintering of manganese containing cermets was studied by a special built-up system (see Fig. 10) that includes manganese vapor "microatmosphere" in the presence of 4 mbar of argon gas pressure (Paper III).

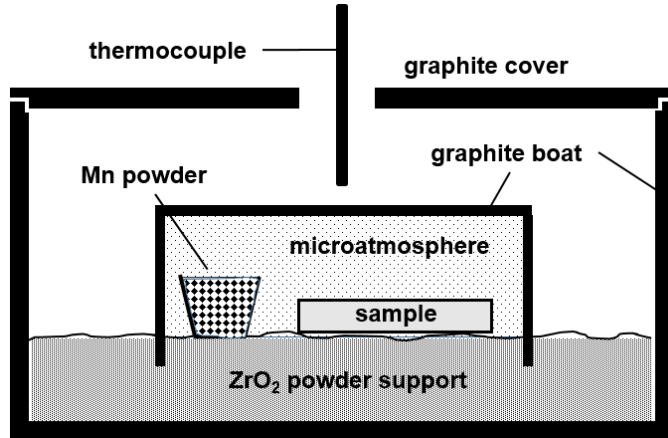


Figure 10. Schematic built up of the graphite crucible which includes the manganese vapor "microatmosphere" (Paper III).

To consolidate the powders via the SPS method, the furnace HPD 10-GB from FCT Systeme GmbH with graphite dies was used (see Fig. 11). Pulsating current and uniaxial pressure were applied simultaneously. The temperature was measured using a pyrometer from inside the top graphite punch. Spark plasma sintering was performed in vacuum under partial pressure of 4 mbar of argon gas using a load of 60 MPa, heated up to the sintering temperature with the heating rate of $100\text{ }^{\circ}\text{C}/\text{min}$ and dwelled at the final temperature for 2 min (Paper III). Natural cooling with furnace was followed. Detailed sintering parameters are described in the published papers (Papers I – V).

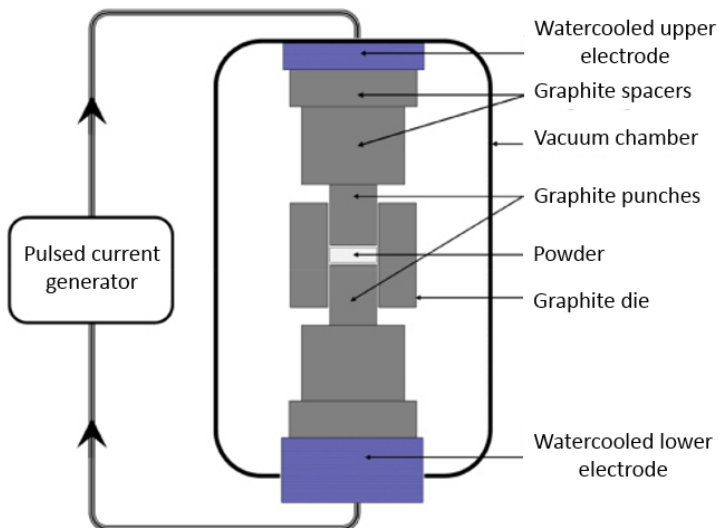


Figure 11. Schematic of the spark plasma sintering (Guyot, 2012).

2.2 Characterization of materials

2.2.1 Density, microstructure and phase characterization

The density was measured according to the Archimedes' method using analytical balance Mettler Toledo ME204. In the calculated density of the cermet composition, the formation of new phases and evaporation or dissolution of chemical elements were not taken into account. The porosity was evaluated by measuring the surface area of pores on the optical image of the microstructure at the magnification of 200 times. Optical microscope Axiovert25 and software Buehler Omnimet were used.

Phase identification of cermets was conducted using X-ray diffraction (XRD) with a Rigaku (D.Max.C) X-ray diffractometer (having $\text{CuK}\alpha$ ($\lambda = 1.5405 \text{ \AA}$) radiation and Ni filter operated at 30 kV and 20 mA). In the microstructural analysis, scanning electron microscope (SEM) JOEL JSM 840A was used. Distribution of chemical elements and chemical composition of sintered cermets were analysed using X-ray spectroscopy (EDS).

2.2.2 Particle size and thermal analysis

Particle size distribution of milled powders was determined with laser diffraction. The wet as-milled powder was used to determine the concentration of particles and cumulative frequency. In the particle size analysis Laser Particle Sizer Analysette 22 COMPACT was used.

For the differential scanning calorimetry analysis (DSC), the specimens were analysed using a NETZSCH STA 449 F3 Jupiter® TG-DSC apparatus. The samples were heated in a pure argon (5.0) atmosphere from 40 °C to 1240 °C using constant heating rates set to 5 and 20 °C/min. A protective gas flow of 50 mL/min was used. The samples were analysed in Pt/Rh alloy crucibles with removable thin walled liners of Al_2O_3 .

2.2.3 Mechanical properties measurement

Fracture toughness and hardness were measured using grinded and polished test samples of 5x5x17 mm. Vickers hardness was measured in accordance with the standard EN-ISO-6507. The fracture toughness (K_{IC} , $\text{MPa}\cdot\text{m}^{1/2}$) was determined by the method of fracture by indentation with the most commonly used empirical equation for fragile materials proposed by Evans (Evans, 1976):

$$K_{IC} = 0.16 \cdot \left(\frac{c}{a}\right)^{-1.5} \cdot \left(H \cdot a^{\frac{1}{2}}\right),$$

where c is the average length of the cracks obtained in the tips of the Vickers indentations, (μm); a is the half average length of the diagonal of Vickers indentations, (μm); H is Vickers hardness, (MPa).

Detailed characteristics and parameters of the mechanical characterization methods can be found in the published papers.

3 DEVELOPMENT OF TITANIUM CARBIDE-BASED CERMETS

TiC-based cermets with two different high-chromium binder systems – FeCr (Paper I) and FeCrMn (Paper II and III) – were studied. The focus was on technological peculiarities, microstructural evolution and phase transformation of these cermets. From the applicability point of view, the goal was to propose ways of performance improvement on the basis of better understanding of consolidation processes.

3.1 Cermets with FeCr binder

Calculated chemical composition of 70 wt% TiC-based ferritic FeCr steel AISI 430L (EN 1.4016) bonded cermet for phase and microstructural evolution is presented in Table 5. Pre-alloyed ferritic stainless steel powder was used to achieve homogeneous chromium distribution in the binder phase. Additionally, TiC-based ferritic steel bonded cermet alloyed with strong carbide forming element (TiC-FeCrMe) was used to improve microstructural and chemical homogeneity of cermets. Austenitic stainless steel AISI 316L (EN 1.4435) was used to produce reference TiC-FeCrNi cermet (Paper I).

Table 5. Calculated chemical composition wt% of TiC-based (70 wt% TiC) cermets after milling.

Designation	C	Ti	Cr	Ni	Mo	WC*	Mn	Si	Me**	Fe
TiC-FeCr	12.7	54.6	4.8	-	-	4.5	0.2	0.2	-	23.0
TiC-FeCrMe	12.7	54.6	4.6	-	-	4.5	0.2	0.2	1.2	22.0
TiC-FeCrNi	12.7	54.6	4.8	3.6	0.8	4.5	0.4	0.3	-	18.3

* Contamination with tungsten carbide as a result of ball milling with WC-Co balls

** Strong carbide forming element

Densification

Particle size distribution and SEM image of the ball milled TiC-FeCr powder are presented in Fig. 12. Although the mean particle size of initial un-milled ferritic stainless steel powder is 10–45 μm and of TiC powder 2.1 μm (see Table 3), the average particle size of ball milled TiC-FeCr powder is below 2 μm .

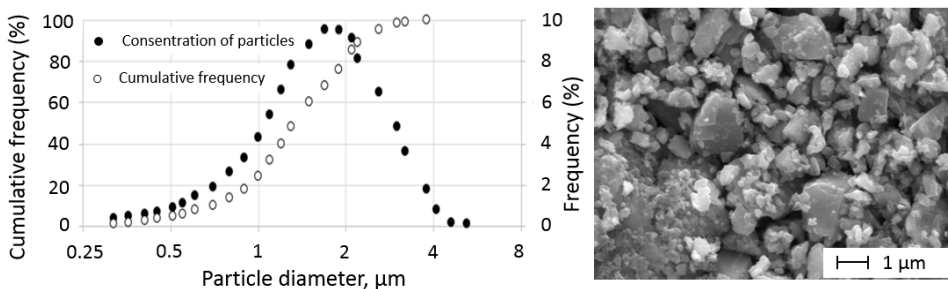


Figure 12. Particle size distribution (left) and SEM image of milled TiC-FeCr powder (right).

Fig. 13 presents the mass loss and density (measured and relative densities as against calculated density) of TiC-FeCr cermets depending on the sintering temperature. It shows the start of densification and formation of liquid phase at low sintering temperatures around 1300 °C, but the liquid binder is not fully soaked up by the porous core (see Fig. 13, right). This is a sign of insufficient sinterability. Also, findings of Humenik et al. show that it could be insufficient wettability between iron alloy and titanium carbide (Humenik, 1956). The fully dense cermets were obtained at the sintering temperature of 1500 °C as the wetting ability of the liquid phase improves significantly with the increase of the sintering temperature (Paper I).

During vacuum sintering, marked mass loss took place (Fig. 13, left). Mass loss can be divided into two parts: first minor decrease in mass (from 800 up to 1300 °C) is due to the reduction of residual surface oxides which corresponds to the results from Kübarsepp's work: the oxygen removal process of TiC-Fe-Cr-Si system is completed before reaching the liquid-phase sintering temperature (Kübarsepp, 1988). The second more intensive part of mass loss (between 1300 and 1500 °C) is caused by the evaporation of metals with the high vapour pressure during vacuum sintering. The reason partly is in the decrease of chromium content – the vacuum level during sintering was approximately 0.04 mbar while the vapour pressure of chromium at 1400 °C is approximately 0.01 mbar (Paper I). Vacuum sintering with the presence of liquid phase also provokes the loss of iron. The higher the sintering temperature, the higher the marked loss of Fe and Cr (see Fig. 13) is.

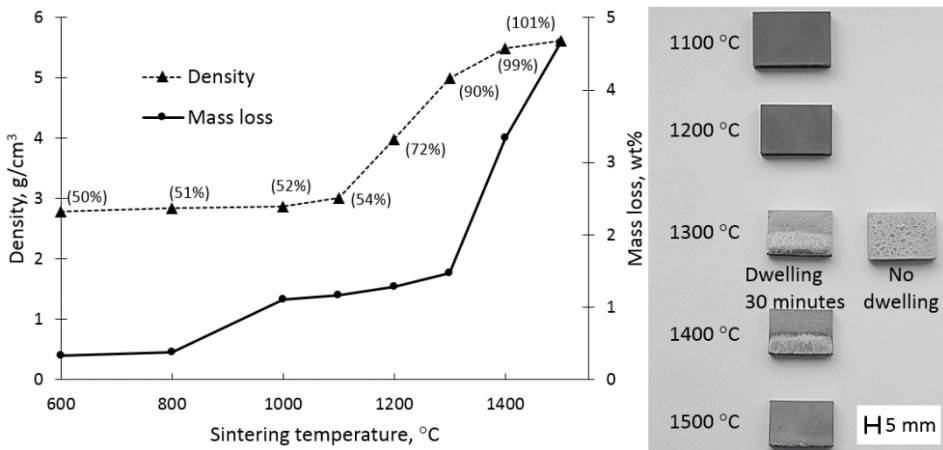


Figure 13. Density and mass loss of TiC-FeCr cermets (left), appearance of specimens after different sintering temperatures (right).

Phase transformation

The phase evolution was studied after sintering at (800–1500 °C). It follows from the XRD patterns of sintered specimens presented in Fig. 14 that as-milled powder mixture consists of three phases: titanium carbide, ferrite and also tungsten carbide as a result of contamination from the milling equipment. During the solid state sintering at 800 °C for 30 min, an additional M_7C_3 phase appeared. After sintering at 1200 °C for 30 min,

WC lines disappeared as WC dissolves mainly in the inner rim of titanium carbide (Mari, 2014). During the sintering in the temperature range 1200–1500 °C, no remarkable changes in the phase composition occurred (see Fig. 14). The final phase composition forms approximately at around 1300 °C, when the eutectic liquid phase formed – eutectic transformation of α -Fe and TiC takes place (Jonsson, 1998). The fully dense composite consists of three main phases: chromium ferrous complex carbide $(Cr,Fe)_7C_3$, α -Fe (solid solution Fe(Cr)) and nonstoichiometric titanium carbide TiC (Paper I). According to the equilibrium phase diagram composed using Thermocalc software obtained by Alvaredo et al., TiCN-FeCr cermets have also three-phased structure: TiCN, α -Fe and M_7C_3 carbide (Alvaredo, 2013).

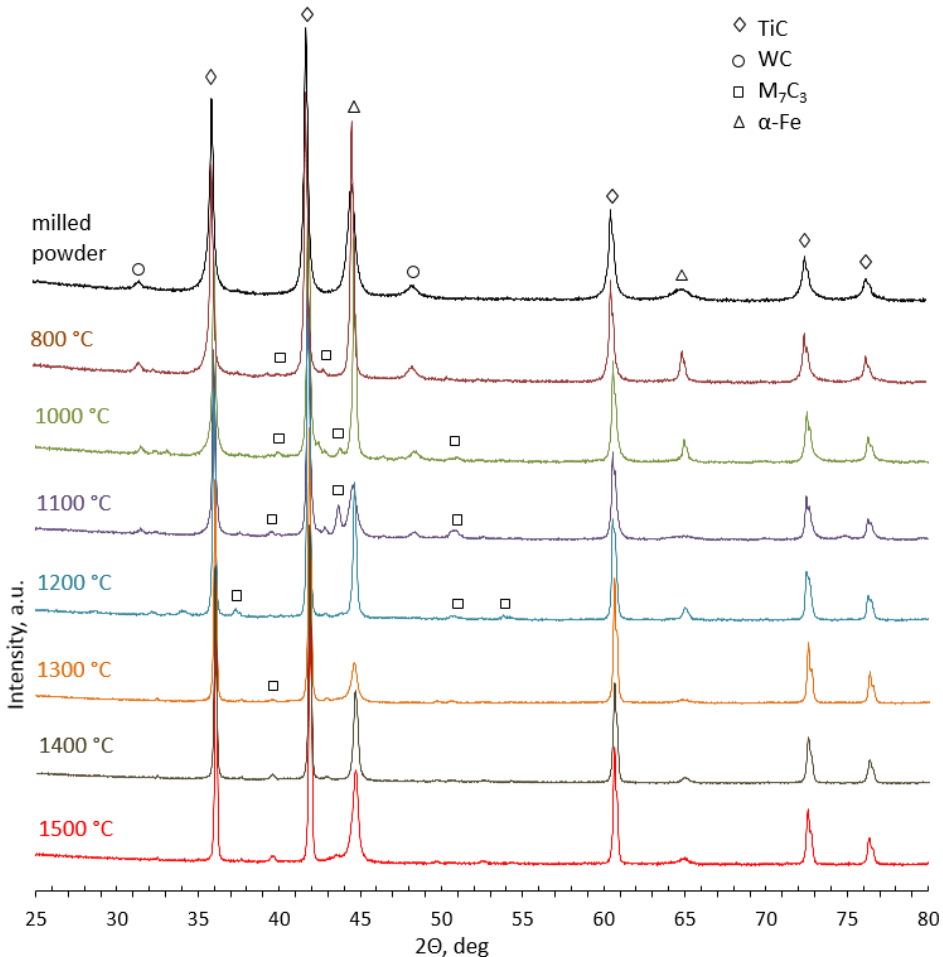


Figure 14. X-ray diffraction pattern of TiC-FeCr cermet at different temperatures.

Because of the allotropic changes during heating/cooling and the different carbon solubility levels in α -Fe and γ -Fe, the formation of free carbon may take place. Therefore, different types of metal carbides can be formed during cooling from the sintering temperature. In addition, the formed carbides will be present as a

combination of several carbide-forming metals if they have a similar lattice parameter – chromium containing iron-based alloy consists of $(Cr, Fe)_x C_y$ carbides (Paper I).

Although the phase transformation calculations show that the two most probable carbide phases after sintering of TiC-FeCr cermets are TiC and M_7C_3 carbides, other types of metal carbides can be formed (see Fig. 15). Traces of the following phases have been detected: $M_{23}C_6$, M_3C , M_6C and γ -Fe. Formation of complex metal carbides M_xC_y are the result of the free carbon connected with decomposing of γ -Fe during cooling. The residual γ -Fe is the result of the unfinished allotropic change $Fe_\gamma \rightarrow Fe_\alpha$. The similar phase transformations show also reference TiC-FeCrNi cermet with primarily austenitic steel binder (see Fig. 15).

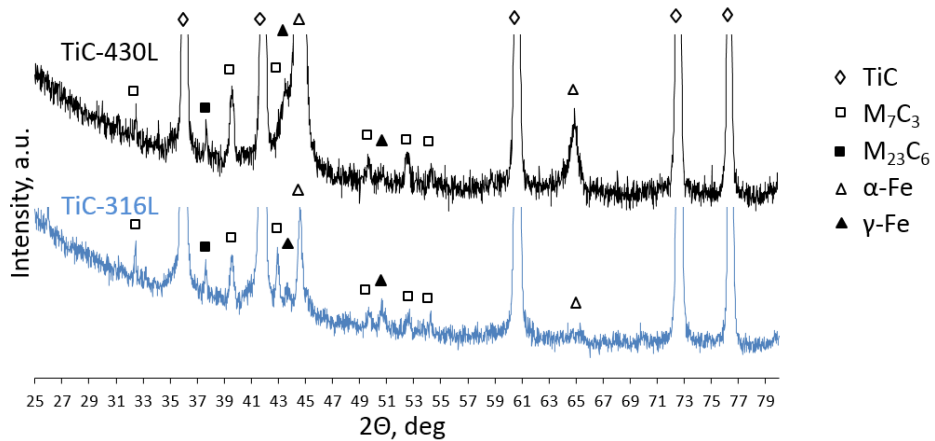
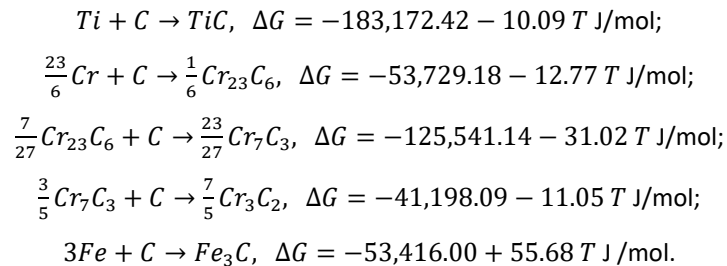


Figure 15. Close-up view of XRD patterns of TiC-FeCr (top) and reference TiC-FeCrNi (bottom) cermets sintered at 1500 °C (Paper I).

Although the Gibbs free energy values are useful in equilibrium conditions, these can be used to predict phase evolutions. Free energy from binary systems can be extrapolated to obtain free energies of ternary and quaternary systems. The information about the reactions in the system Ti-Fe-Cr-C provides the following thermodynamic equations (Fahlman, 2011; Frage, 2002):



The thermodynamic equations prove that the Gibbs free energy of formation of titanium carbide and chromium carbide Cr_7C_3 are thermodynamically more probable than the formation of other carbides. Although the equations are useful in equilibrium conditions, they enable also prediction of phase transformations in sintered alloys.

The differential scanning calorimetry analysis (DSC) thermogram of TiC-FeCr cermet is demonstrated in Fig. 16. Heat-up followed by cooling was used to simulate real sintering cycle up to 1240 °C when most of the carbides formed and no remarkable changes in phase composition took place. The two pronounced changes of the DSC curve at the temperature of 600 °C are due to the change in the heating and cooling rates. Also, at 1240 °C, when heating gives place to cooling, the DSC curve showed a marked change. Three endothermic peaks were observed on the DSC graph. The first peak at temperatures around 700 °C arises from the reduction of oxides. The second peak with a maximum at approximately 1200 °C is due to the formation and the decomposition of different metal carbides. The result is in agreement with the XRD analysis (see Fig. 14), when marked changes take place at sintering temperature up to 1200 °C. The third endothermic reaction with a maximum at 1150 °C during cooling is attributed to the formation of metal carbides from the decomposed γ -Fe (Paper I).

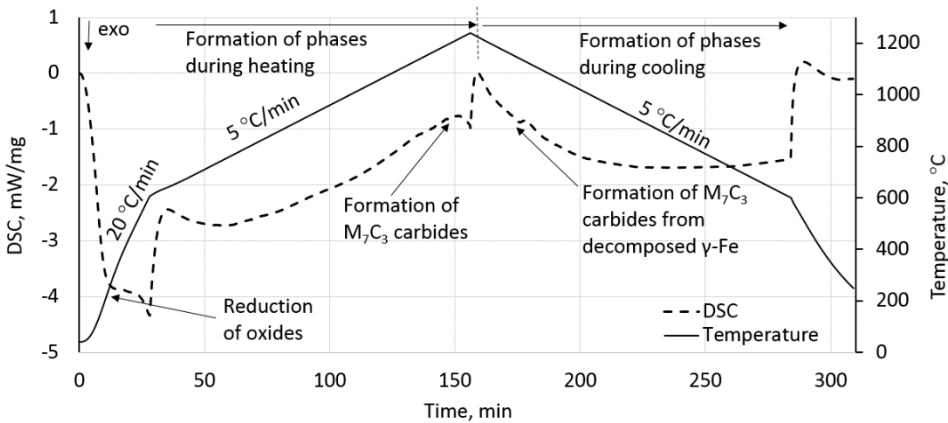


Figure 16. Differential scanning calorimetry thermogram of TiC-FeCr cermet system (heating followed by cooling) (Paper I).

Microstructural evolution

The final three main phases in the microstructure of the sintered TiC-FeCr cermet are: carbides with TiC core, exhibiting a traditional “core-rim” structure, M_7C_3 complex carbides and iron-based metallic phase. The light grey binder region is the solid solution of chromium in the iron matrix and dark grey region is a complex metal carbide based on chromium carbide (see Fig. 17, left). Additionally, the inner and outer rim of TiC could be identified – the inner rim is very thin and unevenly distributed around the cores and contains a large amount of tungsten.

The chemical compositions of different phases are presented in Table 6 (Paper I). WC-FeCr systems also demonstrated the formation of metal carbides with similar chemical composition (Tarraste, 2018). The EDS analysis shows that the content of iron and chromium in the cermet has been decreased during vacuum sintering (compare Tables 5 and 6). It is the result of the evaporation of these elements. Also, some amount of chromium dissolves in titanium carbide and a pronounced part forms the

complex metal carbide M_7C_3 . As a result, chromium content in the metal binder is much below that in the starting AISI 430L steel (see Table 4).

Table 6. Chemical composition wt% of TiC-FeCr cermet phases after sintering at 1500 °C.

Phase	C	Ti	Cr	W	Mn	Si	Fe
Total	14.2	58.4	4.5	4.8	0.5	-	17.6
Binder	-	6.6	4.6	-	1.8	1.0	86.0
Metal carbide, M_7C_3	10.2	10.1	37.3	0.8	2.1	-	39.5
TiC outer rim	15.1	77.4	0.9	6.0	-	-	0.6
TiC inner rim	16.5	68.2	1.2	12.0	-	-	2.1
TiC-core	15.9	81.4	0.3	2.0	-	-	0.4

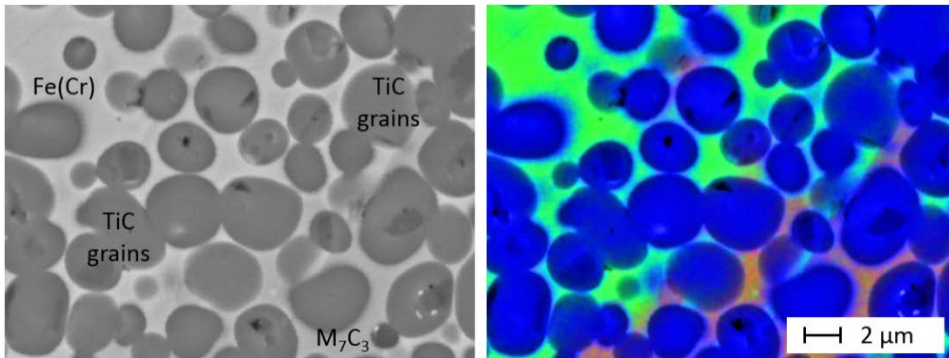


Figure 17. Microstructure (left) and elemental signals mapping (right) of TiC-FeCr cermet sintered at 1500 °C: blue – titanium, red – chromium and green – iron.

Fig. 18 shows the microstructure and binder phase distribution of cermet TiC-FeCr sintered at temperatures 1300 (left), 1400 (middle) and 1500 °C (right).

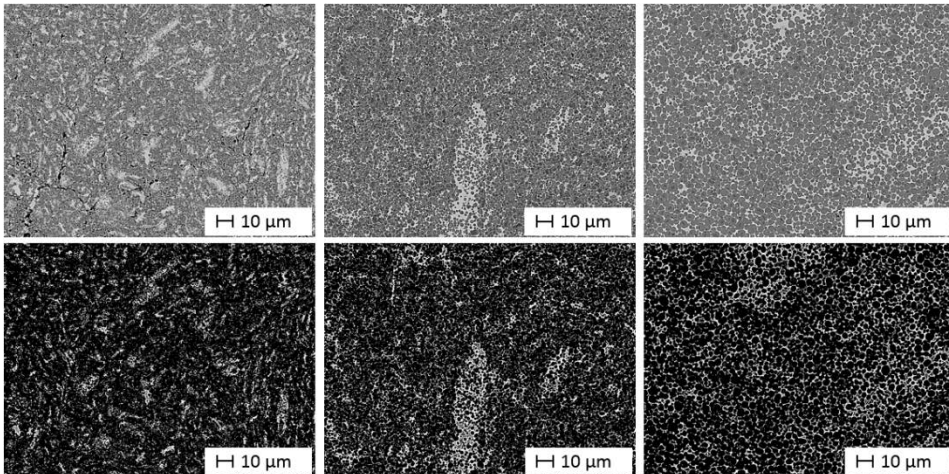


Figure 18. Microstructure (top) and binder distribution (bottom) of TiC-FeCr cermets sintered at different temperatures: 1300 (left), 1400 (middle) and 1500 °C (right).

Distribution of the binder phase and homogeneity of cermets demonstrate some improvement with the increase of sintering temperature which is due to the decrease of the wetting angle between the solid carbide grains and liquid metal. Despite that, cermets sintered at 1500 °C do not exhibit complete homogeneity of the binder phase distribution (Paper I).

Improving the structure and performance

Elements with high affinity to carbon (Ti, Nb, Ta, etc) are used for alloying the corrosion resistant steels. These elements improve the grain refining, retard recrystallization and precipitation hardening of stainless steels. These effects, in turn, increase the toughness, strength, formability, and weldability (Mohrbacher, 2008). These elements have low solubility in ferrite and are strong carbide formers. In cermet TiC-FeCrMe, the majority of strong carbide former dissolves in the rim of TiC (more in the inner rim, like tungsten) but it also dissolves in the M_7C_3 carbide (see Table 7). The most significant differences between EDS patterns of TiC-FeCr (Table 6) and TiC-FeCrMe (Table 7) are the marked increase of Ti content in M_7C_3 carbide and the increase of chromium fraction in the metallic binder. Nevertheless, according to the XRD analysis, no remarkable differences were found in the phase composition of TiC-FeCr and TiC-FeCrMe cermets because the majority of strong carbide former (Me) dissolves in TiC (see Table 7). Both cermets exhibit mainly three-phased structure: TiC, α -Fe and M_7C_3 carbide (Paper I).

Homogeneity of microstructures and binder phase distribution of TiC-FeCr, TiC-FeCrMe and TiC-FeCrNi cermets are presented in Fig. 19. Our result demonstrates that both TiC-FeCrNi and TiC-FeCrMe cermets exhibit microstructural homogeneity and also homogeneity of Cr and Fe distribution (see Fig. 20).

Table 7. Chemical composition wt% of TiC-FeCrMe cermet phases after sintering at 1400 °C (Paper I).

Phase	C	Ti	Cr	W	Mn	Si	Me	Fe
Total	14.8	53.4	4.2	4.5	-	-	1.1	22.0
Binder	-	4.7	6.7	0.3	0.5	0.9	-	86.9
Metal carbide, M_7C_3	12.8	21.6	35.8	2.0	-	-	0.5	27.3
TiC outer rim	16.4	72.3	1.0	5.6	-	-	1.5	3.2
TiC inner rim	16.5	63.0	1.3	12.1	-	-	3.2	3.9
TiC core	17.5	76.6	1.2	2.3	-	-	0.7	1.7

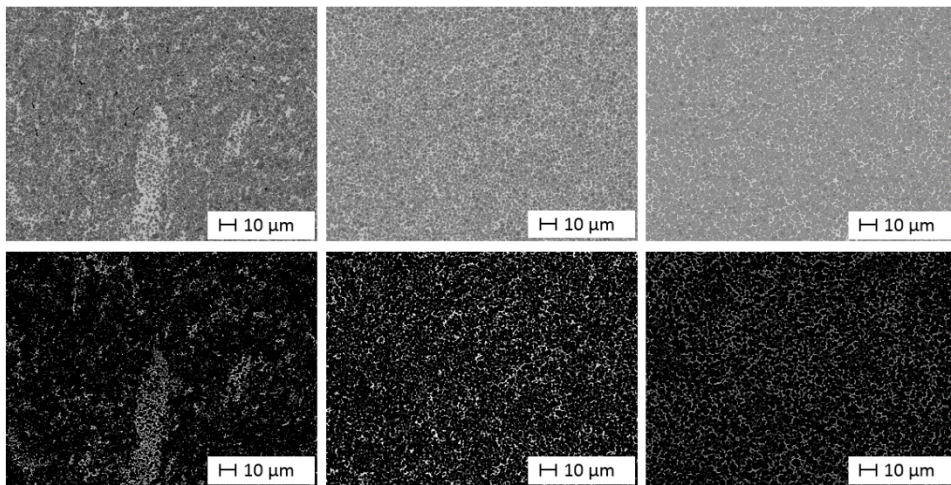


Figure 19. Microstructures (top) and binder distribution (bottom) of TiC-FeCr (left), TiC-FeCrMe (middle) and TiC-FeCrNi (right) cermets (Paper I).

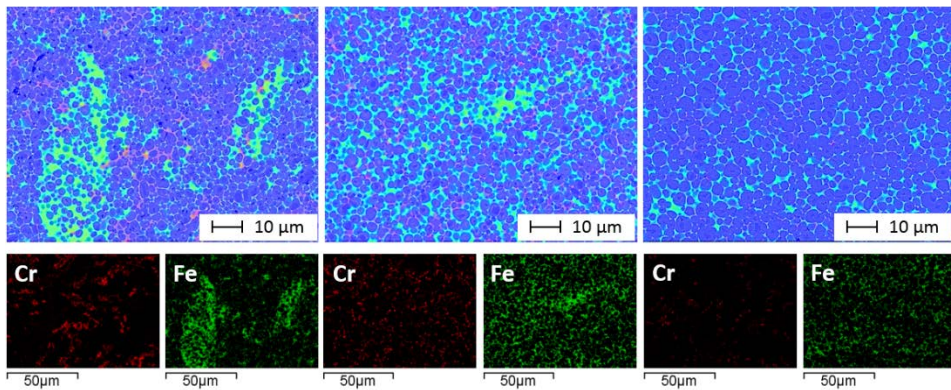


Figure 20. EDS mapping results (top) and elemental distribution of chromium and iron (bottom) of TiC-FeCr (left), TiC-FeCrMe (middle) and TiC-FeCrNi (left).

Mechanical properties and porosity of TiC-FeCr and TiC-FeCrMe cermets are presented in Table 8.

Table 8. Porosity and mechanical characteristics of TiC-FeCr and TiC-FeCrMe

	Hardness, HV30	Fracture toughness, MPa·m ^{1/2}	Porosity, %	Density, g/cm ³
TiC-FeCr	1459±36	10.0±0.3	0.34	5.62
TiC-FeCrMe	1104±10	10.4±0.2	0.31	5.66
TiC-FeCrNi	1158±20	11.0±0.3	0.56	5.55

3.2 Cermets with FeCrMn binder

Results of screening experiments demonstrated that during vacuum sintering of the Ni-free manganese containing TiC-FeCr26Mn20 cermet, drastic reduction of manganese content took place (Paper II). Chemical composition of TiC-FeCrMn cermet after milling and after different sintering regimes is presented in Table 9. It can be concluded that marked depression of manganese loss can be achieved by using gas compression during sintering.

Table 9. Chemical composition, porosity and mechanical characteristics of 70TiC-FeCr26Mn20 cermet after different sinterings.

Sintering conditions	Chemical composition, wt%						Porosity %	Hardness, HV30	Fracture toughness MPa·m ^{1/2}
	C	Ti	Cr	W	Mn	Fe			
After milling	12.7	54.6	7.3	4.5	5.6	15.3	-	-	-
1450°C, 5·10 ⁻⁵ bar	14.5	60.3	5.3	7.2	0.5	12.2	0.56	1520±43	6.9±0.2
1450°C, 1bar (Ar)	14.2	54.1	7.2	6.0	4.1	14.4	2.33	1220±35	-

However, sintering in gas atmosphere (Ar) at 1 bar leads to the decrease of the sinterability and increases the porosity of consolidated samples. It is stated that sinterability and therefore also mechanical characteristics of TiC-based cermets with high chromium steel can be improved by alloying them with silicon (Kübarsepp, 1993; Kübarsepp, 1994). In addition, the TiC-FeSi alloy containing approximately 5 wt% of silicon, demonstrates the contact angle of zero between hard phase and metallic binder (Panasyuk, 1985). Therefore, TiC-FeCrMn cermet with silicon addition was investigated. Cermet alloyed by silicon (nominally 0.6 wt% in alloy 2 wt% in binder) demonstrates more homogeneous microstructure and reduced porosity (see Fig. 21) (Paper II).

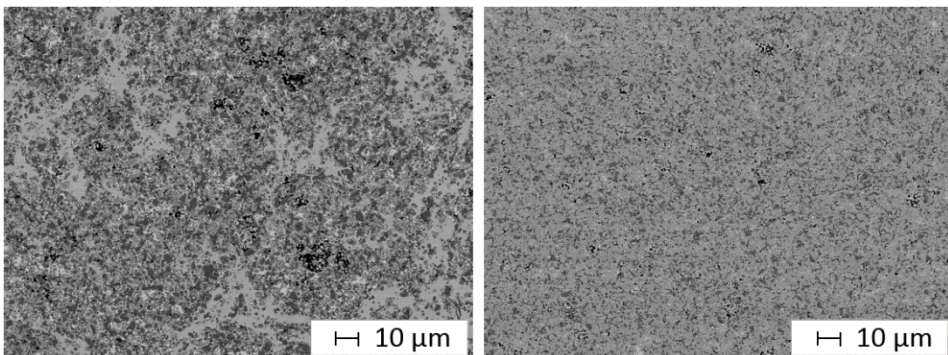


Figure 21. Microstructure of cermets TiC-FeCr26Mn20 (left) and TiC-FeCr26Mn20Si2 (right) after sintering in argon (1 bar).

An additional approach to increase structural homogeneity is using chromium steel powder instead of elemental powders. Therefore, well-known high-chromium pre-alloyed super ferritic stainless steel powder AISI 446 (EN 1.4762) was used to achieve

more homogeneous distribution of chromium in the cermet. In addition, silicon was used to improve the sinterability and reduce porosity of cermets. Chemical composition of TiC-FeCrMnSi cermet is presented in Table 10 (Paper III).

Table 10. Calculated chemical composition wt% of TiC-FeCrMnSi (70 wt% TiC) cermet after milling.

Designation	C	Ti	Cr	WC*	Mn	Si	Fe
TiC-FeCrMnSi	12.7	54.6	5.2	4.5	5.9	1.3	15.8

* Contamination with tungsten carbide as a result of ball milling with WC-Co balls

Phase transformation

The phase composition of TiC-FeCrMnSi cermet was determined after sintering at 1475 °C using 400 mbar of argon partial pressure. XRD pattern is presented in Fig. 22. Sintering using partial argon pressure enables retaining the majority of manganese and also chromium in the alloy. Sintered TiC-FeCrMnSi cermet consists of two carbide and two metallic phases – titanium carbide (TiC) and secondary metal carbide M_7C_3 ($M=Cr,Fe,Mn$) and iron-based solid solutions Fe(Cr), prevalently austenitic γ -Fe with traces of α -Fe (Paper III).

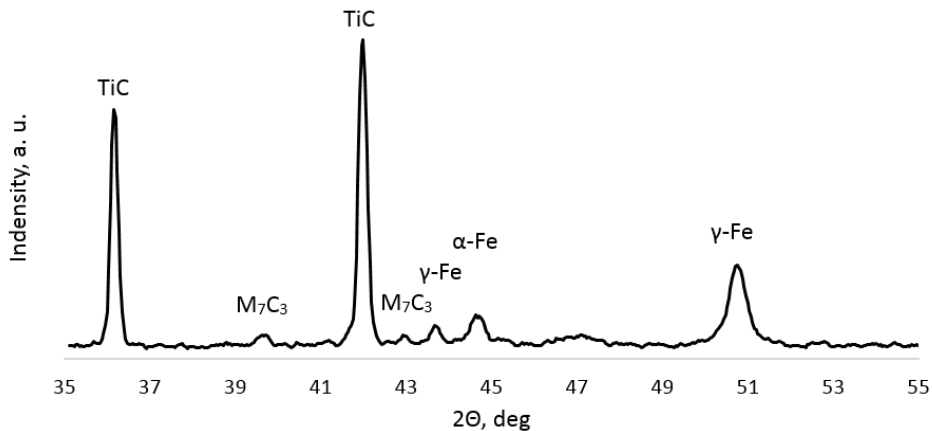


Figure 22. X-ray diffraction pattern of TiC-FeCrMnSi cermet (Sintering under 400 mbar of argon) (Paper III).

Microstructural evolution

All sintered TiC-FeCrMnSi cermets, except for spark plasma sintered, demonstrate typical core-rim structure formed during liquid-phase sintering (see Fig. 23). Most of the carbide grains consist of dark TiC cores and grey (Ti, W)C rims that have noticeable inner and outer part. The lighter binder phase is the solid solution of chromium in iron matrix with prevalently austenitic structure and the darker binder area is the complex metal carbide M_7C_3 .

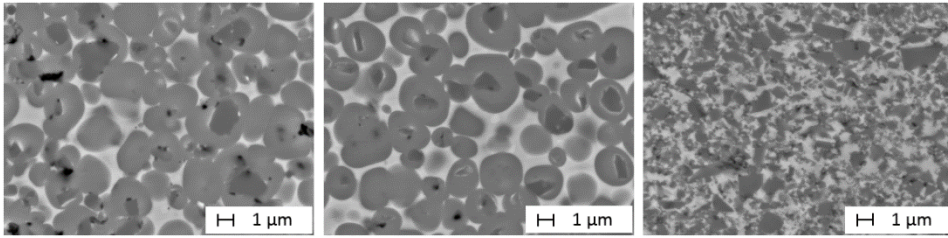


Figure 23. Microstructure of TiC-FeCrMnSi cermets using different sintering regimes: vacuum (left), argon partial pressure (middle) and SPS technology (right) (Paper III).

Elemental signal analysis (EDS mapping) demonstrates that manganese is partly dissolved in the iron-based binder and also in the complex metal carbide M_7C_3 (see Table 11 and Fig. 24). Despite utilizing sintering under partial argon gas pressure enabling majority of manganese retaining in the alloy, the final content of manganese in the metallic binder phase is too low to ensure the fully austenitic structure of that phase (Table 11).

Table 11. Chemical composition wt% of TiC-FeCrMnSi cermet phases after sintering at 1475 °C using 400 mbar of argon partial pressure.

Phase	C	Ti	Cr	W	Mn	Si	Fe
Total	14.4	54.2	5.8	4.4	4.6	0.8	15.8
Binder	-	3.2	3.9	1.3	9.5	4.1	78.0
Metal carbide, M_7C_3	9.8	4.8	39.3	-	11.4	-	34.7
TiC rim	15.2	76.0	2.3	5.4	-	-	1.1
TiC-core	15.9	81.1	0.6	1.7	-	-	0.7

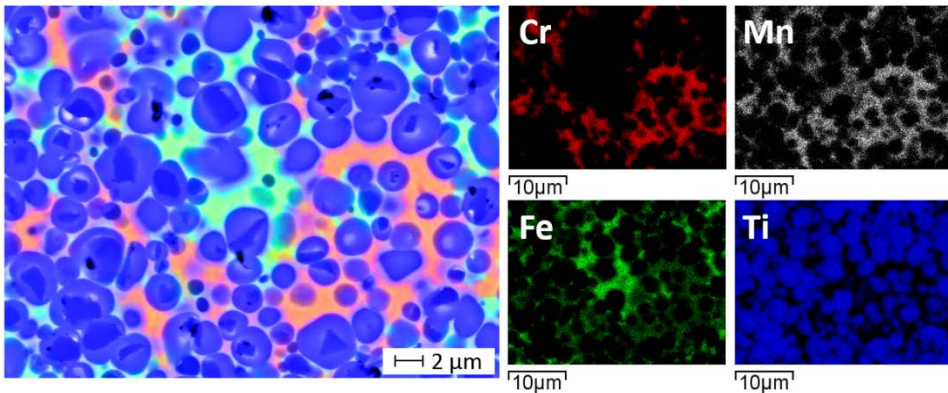


Figure 24. EDS mapping analysis of TiC-FeCrMnSi cermet: blue – titanium, red – chromium, green – iron.

Improving the structure and performance

Schubert et al. stated that high vacuum liquid-phase sintering is inappropriate for manganese containing WC-FeMn cemented carbides (Schubert, 2015). Therefore, in this research, we used manganese vapor “microatmosphere” within the graphite crucible and partial pressure of argon (4 mbar and 400 mbar) to produce TiC-FeCrMnSi cermets. Furthermore, the sintering temperature should be as low as possible. To prevent manganese loss during sintering, two main sintering parameters were changed: temperature and gas partial pressure during sintering. Three different final sintering temperatures (1375, 1425 and 1475 °C) and three pressure levels (0.04, 4 and 400 mbar) during sintering were applied (see Fig. 25). Additionally, spark plasma sintering was used to produce TiC-FeCrMnSi cermets because of the very fast nature of this technology (Paper III). Heating rate of 100 C·min⁻¹ and short dwelling time (2 min) in the presence of argon partial pressure of 4 mbar were applied to minimize manganese loss.

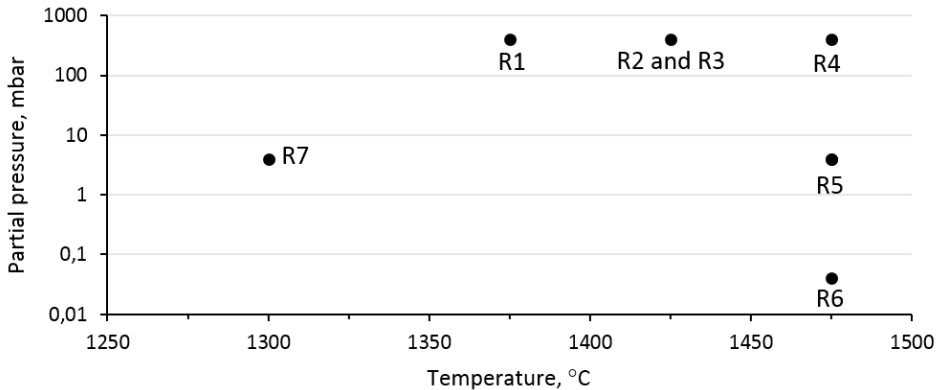


Figure 25. Sintering parameters (Table 12) – temperature and partial gas (Ar) pressure.

Manganese and chromium loss using different sintering modes (conventional vacuum sintering, sintering in two different partial pressures of argon and sintering in manganese vapor) were determined using X-ray spectroscopy. Chemical compositions after milling and using different sintering modes are presented in Table 12 and Fig. 26. As a result of ball milling using WC-Co balls, tungsten (up to 4...6 wt%) was revealed in all cermets.

Results in Table 12 and Fig. 26 demonstrate a substantial depletion of manganese and a fractional loss of chromium and silicon during vacuum liquid-phase sintering. When sintering under 4 mbar of argon, manganese content decreases drastically. Alternatively, cermet sintered under 400 mbar of argon has minor manganese loss.

High vacuum sintered ($p=0.04$ mbar) cermets demonstrate unacceptable porosity. Reduced sintering temperatures (1425 °C and 1375 °C) minimize evaporation and as a result retain manganese in the cermets. On the other hand, cermets sintered using decreased temperatures have quite high residual porosity (see Table 12) and also demonstrate considerably lower Vickers hardness and fracture toughness (Paper III).

Table 12. Chemical composition (content of Cr, Mn and Si), porosity and mechanical characteristics of TiC-FeCrMnSi cermet sintered in different conditions (Paper III).

Sintering Technology	Cr, Mn, Si content, wt%			Mass loss	Hardness, HV30	Fracture toughness	Porosity
	Cr	Mn	Si	%		MPa·m ^{1/2}	%
After milling	5.3	6.0	1.3	-	-	-	-
R1 1475 °C, 0.04 mbar (vac)	4.0	0.3	0.6	7.81	1321	n/a	2.0
R2 1475 °C, 4 mbar (Ar)	5.3	0.8	0.7	6.81	1315	7.1	0.6
R3 1475°C,4mbar(Ar)*	5.2	3.6	0.7	3.80	1232	11.4	0.4
R4 1475 °C, 400 mbar (Ar)	5.8	4.6	0.8	2.27	1244	9.6	0.6
R5 1425 °C, 400 mbar (Ar)	5.7	6.0	0.9	1.04	1156	n/a	2.3
R6 1375 °C, 400 mbar (Ar)	6.5	6.3	1.0	1.11	1081	n/a	3.0
R7 SPS,1300°C,4 mbar(Ar)	5.9	5.5	1.2	n/a	1341	4.1	0.2

* Sintering in manganese “microatmosphere” in graphite container

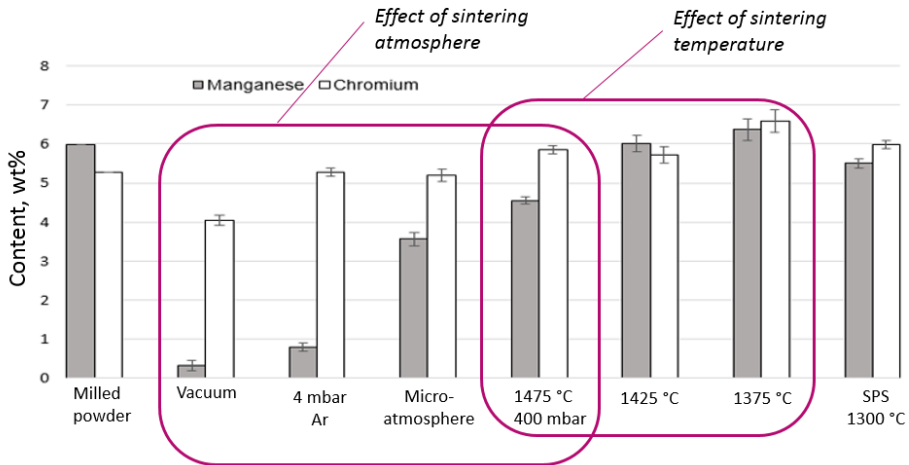


Figure 26. Manganese and chromium content in TiC-FeCrMnSi cermets after different sintering regimes.

SPS employs very high heating rates for powder consolidation at decreased the sintering time and temperature. Therefore, it is not surprising that SPS enables retaining Mn and Cr in the alloy. Also, the fast nature of SPS technology helps reduce drastically average grain size (see Fig. 23) and decrease residual porosity. However, such structural peculiarity – fine microstructure - results in low fracture toughness of spark plasma sintered cermets (see Table 12).

Marked difference in the manganese content was revealed using partial pressure sintering (4 mbar) and partial pressure sintering in manganese vapor “microatmosphere” within the graphite crucible (Fig. 26). The mass loss and manganese depletion were noticeably smaller using sintering in the manganese vapor atmosphere (see Table 12). Cermets using sintering, which includes a manganese vapor

“microatmosphere” within the graphite crucible in the presence of 4 mbar of argon partial pressure at 1475 °C, demonstrate the best combination of hardness, fracture toughness and porosity (Paper III).

3.3 Summary

Our research results of the influence of the composition and technological conditions on the structure formation and performance of titanium carbide-based (Fe-Cr and Fe-Cr-Mn alloys) bonded cermets can be summarized as follows:

FeCr binder

- Vacuum sintered TiC-FeCr composites consist of three main phases – titanium carbide TiC, metal carbide M_7C_3 and iron-based solid solution Fe(Cr). Formation of the M_7C_3 carbides takes place during solid state sintering at temperatures below 1200 °C.
- The decrease of Cr content in the alloy and in the metallic binder is caused by the evaporation during vacuum sintering, formation of complex Cr and Fe carbides M_7C_3 and solution in TiC.
- The heterogenous distribution of Cr both in a composite and metallic binder is caused by the formation of complex metal carbides M_7C_3 .
- Alloying the TiC-FeCr cermets by strong carbide formers enables improvement of structural homogeneity – both of the metallic phase and Fe and Cr distribution.

FeCrMn binder

- Production of corrosion resistant Ni-free TiC-FeCrMnSi cermets with high fraction of both Cr (for attaining resistance to corrosion) and Mn (as austenitizing element) is challenging because of depletion of these elements during vacuum sintering ($p=0.04 - 4$ mbar), formation of secondary carbides M_7C_3 ($M=Cr, Fe, Mn$) and as a result, decrease of chromium content in the metallic binder.
- Retaining both Mn and Cr in cermets is achievable using sintering under partial gas (Ar) pressure of about 400 mbar and higher. Pressure increase during sintering, however, may lead to impairment of sinterability resulting in increased porosity and decreased structural homogeneity. Sinterability in such condition can be improved using alloying by silicon.
- An alternative approach for retaining Mn and Cr is utilizing vacuum sintering under low partial pressure of about 4 mbar using manganese “microatmosphere”. In terms of structure (porosity, structural homogeneity), sintering under such conditions is most effective.
- Retaining of Mn and Cr in cermets is possible utilizing sintering at decreased temperatures under very short sintering regimes – spark plasma sintering. Structural peculiarities decreased carbide grain size in particular; however, as a result, fracture toughness decreased.
- Sintered TiC-FeCrMnSi cermets consist of four main phases – titanium carbide TiC with coaxial structure, secondary metal carbide M_7C_3 ($M=Cr, Fe, Mn$) and iron- based solid solutions Fe(Cr), prevalently austenite (γ -Fe) with traces of ferrite (α -Fe).

4 DEVELOPMENT OF CHROMIUM CARBIDE-BASED CERMETS

Chromium carbide-based cermets with iron-based binders Fe-Cr (Paper V) and Fe-Ti (Paper IV) were studied. The focus was on phase transformations, microstructural evolution and technological peculiarities of these cermets. From applicability point of view, the goal was to achieve improvement in mechanical performance through better understanding of consolidation, structure formation, in particular, grain growth.

4.1 Cermet with FeCr binder

The chromium carbide (Cr_3C_2) and ferritic stainless steel AISI 430L (EN 1.4016) powders were used to fabricate chromium carbide-based FeCr alloy bonded cermets. During heating, up to 40 wt% of iron dissolves in the carbide Cr_7C_3 (see Table 14) and there is also additional chromium from the starting steel. Therefore, the starting (calculated) chromium carbide Cr_3C_2 content of 50 wt% was used. Calculated chemical composition of studied cermets is presented in Table 13.

Table 13. Calculated chemical composition wt% of Cr_3C_2 -FeCr (50 wt% Cr_3C_2) cermets after milling.

Designation	Cr_3C_2	Cr	WC*	Mn	Si	Fe
Cr_3C_2 -FeCr	50	8.1	1.5	0.4	0.3	39.7

* Contamination with tungsten carbide as a result of ball milling with WC-Co balls

Phase transformations

The phase composition of Cr_3C_2 -FeCr cermet was determined after vacuum sintering at 1300 °C. X-ray diffraction pattern of this cermet is shown in Fig. 27. According to the XRD results, the vacuum sintered Cr_3C_2 -FeCr cermet demonstrates two main phases: iron-based ferritic solid solution Fe(Cr) and complex chromium-ferrous carbide $(\text{Cr,Fe})_7\text{C}_3$ (Paper V).

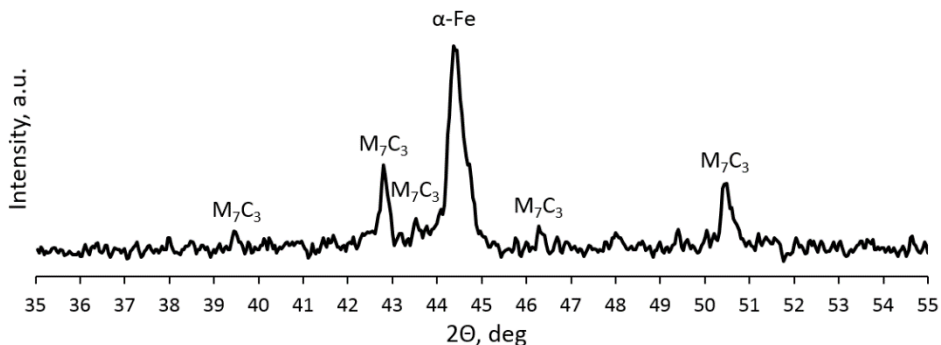
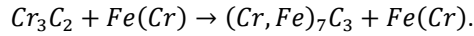


Figure 27. X-ray diffraction pattern of Cr_3C_2 -FeCr (Paper V).

The change in the structure of chromium carbide ($\text{Cr}_3\text{C}_2 \rightarrow (\text{Cr,Fe})_7\text{C}_3$) observed during heating is also connected with its composition, since in the carbide Cr_7C_3 , up to 60% of chromium atoms can be replaced by iron atoms (Yakovenko, 2011).

The following reaction mechanism can be presented during heating: Cr_3C_2 recrystallization into lower carbon containing carbide Cr_7C_3 , iron from metal matrix dissolves into chromium carbide, forming the complex $(\text{Cr,Fe})_7\text{C}_3$ carbide and chromium diffuse into the metallic iron-based matrix. The reaction during sintering of the alloy can be described as follows (Paper V):



The resulting thermodynamic equation remained unbalanced because the equation does not address a single chemical reaction, but rather the sum of several simultaneous reactions.

Microstructural evolution

Microstructure and elemental mapping of cermet is presented in Fig. 28. EDS mapping demonstrates the two-phase structure of sintered cermets – the dark grey region is the complex $(\text{Cr,Fe})_7\text{C}_3$ carbide and light grey is a solid solution of chromium and iron.

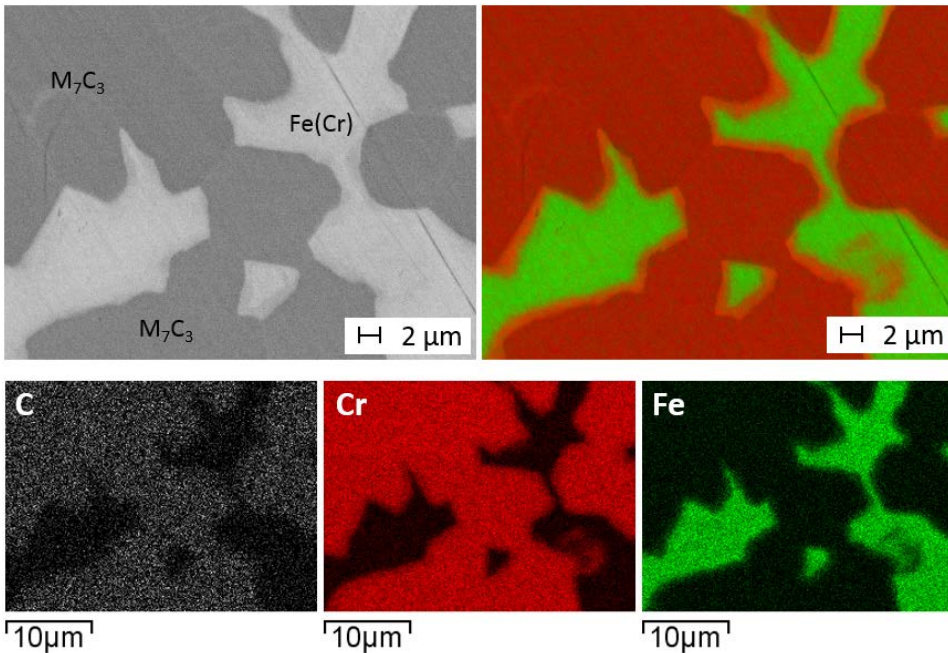


Figure 28. Microstructure (left) of vacuum sintered Cr_3C_2 -FeCr cermet and its elemental signals mapping analysis (right): red – chromium, green – iron (Paper V).

The chemical composition of Cr_3C_2 -FeCr cermet and its phases after sintering are presented in Table 14 (Paper V). The table shows that carbon content in the complex metal carbide $(\text{Cr,Fe})_7\text{C}_3$ is approximately 9 wt.% (~ 30 at.%). Iron content in the complex carbides is approximately 20 wt% (Paper V). It is the result of iron diffusion and dissolution in the carbide matrix. As a result, the chromium content of the binder phase is higher than that in the starting AISI 430L steel (see Table 4).

Table 14. Chemical composition wt% of Cr_3C_2 -FeCr cermet phases sintered in vacuum.

Phase	C	Cr	W	Mn	Si	Fe
Total	6.9	49.8	1.5	0.5	0.3	41.0
Binder	-	19.5	1.9	0.5	1.0	77.1
Carbide	9.1	69.3	1.0	0.4	-	20.2

Improving the structure and performance

The main disadvantage of chromium carbide-based cermets is the rapid carbide grain growth during liquid-phase sintering. Although the milled powder particles average size is around 2 μm , the average grain size of vacuum sintered cermet is by an order of magnitude greater – approximately 20 μm . To suppress carbide grain growth, more rapid sintering technology – spark plasma sintering (SPS) – at decreased temperature was used. Lower temperature and shorter sintering cycle have positive effect on the grain size of Cr_3C_2 -FeCr cermet (Fig. 29).

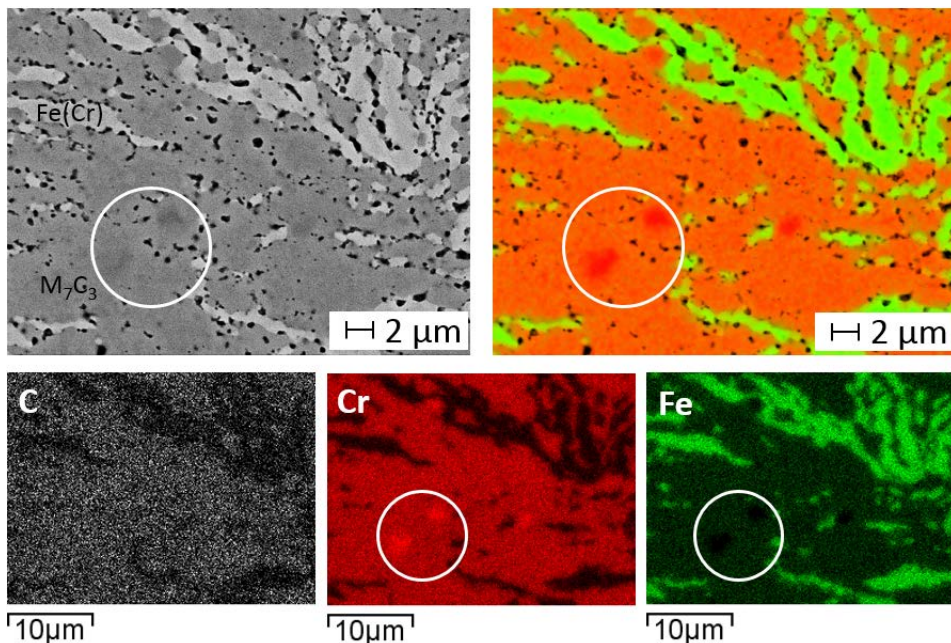


Figure 29. Microstructure (left) of spark plasma sintered Cr_3C_2 -FeCr cermet and its elemental signals mapping analysis (right): red – chromium, green – iron.

The chemical composition of Cr_3C_2 -FeCr cermet and its phases after spark plasma sintering are presented in Table 15. According to the EDS analysis, there can be distinguished two different carbide phases. As can be seen from Fig. 29, (circled) darker carbide regions are presented with average size of approximately 2 μm . Both carbides have M_7C_3 structure (carbon content is the same), but the iron content of darker carbide grains is smaller. The reason for the fast nature of SPS technology lies in the heterogeneity of the carbide phase composition.

Table 15. Chemical composition wt% of Cr₃C₂-FeCr cermet phases sintered using SPS technology.

Phase	C	Cr	W	Mn	Si	Fe
Total	7.6	50.4	1.6	0.6	0.4	40.4
Binder	-	16.3	1.5	-	0.4	81.8
Metal carbide, light	9.5	61.5	1.4	-	-	26.6
Metal carbide, dark	9.5	82.2	0.3	-	-	8.0

Mechanical and structural characteristics of sintered chromium carbide ferritic steel bonded cermets using two different sintering regimes are presented in Table 16. Although spark plasma sintered cermets have small evenly distributed porosity, they outperform vacuum sintered Cr₃C₂-FeCr cermets by smaller grain size and higher fracture toughness.

Table 16. Structural and mechanical characteristics of Cr₃C₂-FeCr cermets consolidated using different sintering technology (Paper V).

Sintering technology	Hardness, HV30	Fracture toughness K _{IC} , MPa·m ^{1/2}	Porosity, %	Density, g/cm ³
Vacuum sintering	1132±33	n/a	0.2	7.2
SPS	1167±16	6.4±0.3	0.6	7.1

4.2 Cermets with FeTi binder

One of the alternative approaches to reduce the grain size of chromium carbide-based cermets is utilization of grain size inhibitors. Strong carbide former – titanium – was used for that purpose (Paper IV). Table 17 shows the calculated chemical composition of the studied cermets with the iron-titanium binder.

Table 17. Calculated chemical composition wt% of Cr₃C₂-FeTi cermets after milling.

Cermet	Cr ₃ C ₂	Fe	Ti	WC*
50Cr ₃ C ₂ - FeTi	50	38.5	10	1.5
60Cr ₃ C ₂ - FeTi	60	30.5	8	1.5
70Cr ₃ C ₂ - FeTi	70	22.5	6	1.5

* Contamination with tungsten carbide as a result of ball milling with WC-Co balls

Phase transformations

The phase evolution study was performed after sintering at 800–1420 °C. XRD patterns of sintered specimens are presented in Paper IV. As it follows from the Paper IV, as-milled powder mixture consists of four phases: Cr₃C₂, Fe, Ti and WC as a contamination from milling equipment. During sintering at 800 °C for 30 min, Cr₃C₂ recrystallizes into lower carbon content Cr₇C₃ carbide and iron dissolves in the matrix of this carbide forming complex carbide (Cr,Fe)₇C₃. After sintering at 1000 °C, additional TiC lines appeared. Ti reacts with carbon and forms TiC already at the temperatures below 1000 °C (Paper IV). Therefore, the carbon content of complex chromium-ferrous carbide decreases even more, resulting in significant changes in the XRD pattern. After sintering

at 1200 °C, the recrystallization of $(Cr,Fe)_7C_3$ into even lower carbon content carbide $(Cr,Fe)_{23}C_6$ takes place. During the sintering at 1420 °C for 30 min, no remarkable evolution in the phase composition was noticed (Paper IV).

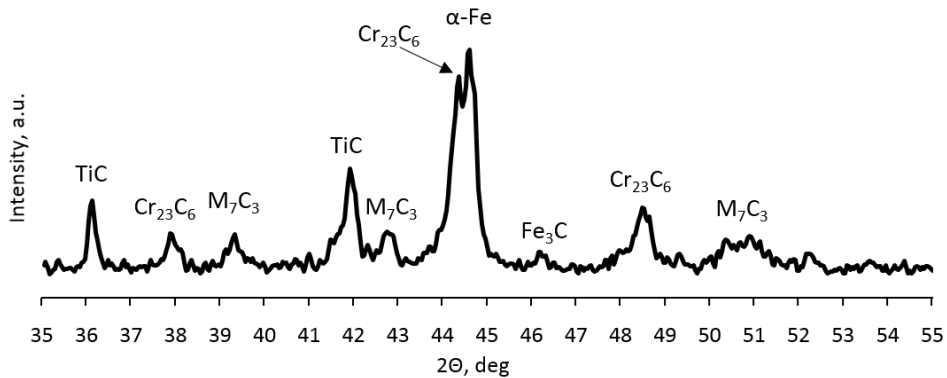
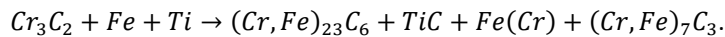


Figure 30. X-ray diffraction pattern of the Cr_3C_2 -FeTi composite at different sintering temperatures (Paper IV).

According to Fig. 30, the Cr_3C_2 -FeTi composite consists of four phases: iron-based ferritic solid solution $Fe(Cr)$, complex metal carbide $(Cr,Fe)_{23}C_6$, traces of carbide $(Cr,Fe)_7C_3$ and *in situ* synthesized titanium carbide TiC. The reaction during sintering of the alloy can be described as follows (Paper IV):



The resulting thermodynamic equation remained unbalanced because the equation does not address a single chemical reaction, but rather the sum of several simultaneous reactions. Two step recrystallization of chromium carbides $(Cr_3C_2 \rightarrow (Cr, Fe)_7C_3 \rightarrow (Cr,Fe)_{23}C_6)$ is the fundamental difference in the phase formation of Cr_3C_2 -FeCr and Cr_3C_2 -FeTi cermets.

Microstructural evolution

As seen from Fig. 31 (lower right), the dark grey region is prevalently dicarbide $(Cr,Fe)_{23}C_6$. The light grey region is the solid solution of chromium in the iron matrix. Ultrafine (below 1 μm) black near-spherical grains are TiC dispersed in the metallic $Fe(Cr)$ binder phase between dicarbide $(Cr,Fe)_x C_y$ particles (Paper IV).

Rapid grain growth during solid and liquid phase sintering is one of the main disadvantages of chromium carbide-based cermets. As can be seen in Fig. 31 (upper right), the cermets solid-state sintered at 1000 °C have fine particles – the average carbide grain size is below 1 μm . Remarkable carbide grain growth takes place in alloys sintered at 1200 °C – the average carbide grain size is 2–3 μm (Paper IV). However, the structure contains marked share of pores. High porosity of cermets is caused by the low liquid phase fraction at this temperature. The microstructure of the cermets sintered at 1420 °C shows coarse $(Cr,Fe)_{23}C_6$ carbide grains regardless of submicron TiC grains between them (Fig. 31 lower right). The chemical composition of Cr_3C_2 -FeTi cermet and

its phases after vacuum sintering are presented in Table 18. The EDS analysis shows that chromium content in the metallic binder (~ 16 wt%) is sufficient to assure resistance to corrosion of Cr_3C_2 -FeTi cermets. Iron content in the complex metal carbide (~ 20 wt%) is similar to that in Cr_3C_2 -FeCr cermets (see Table 14).

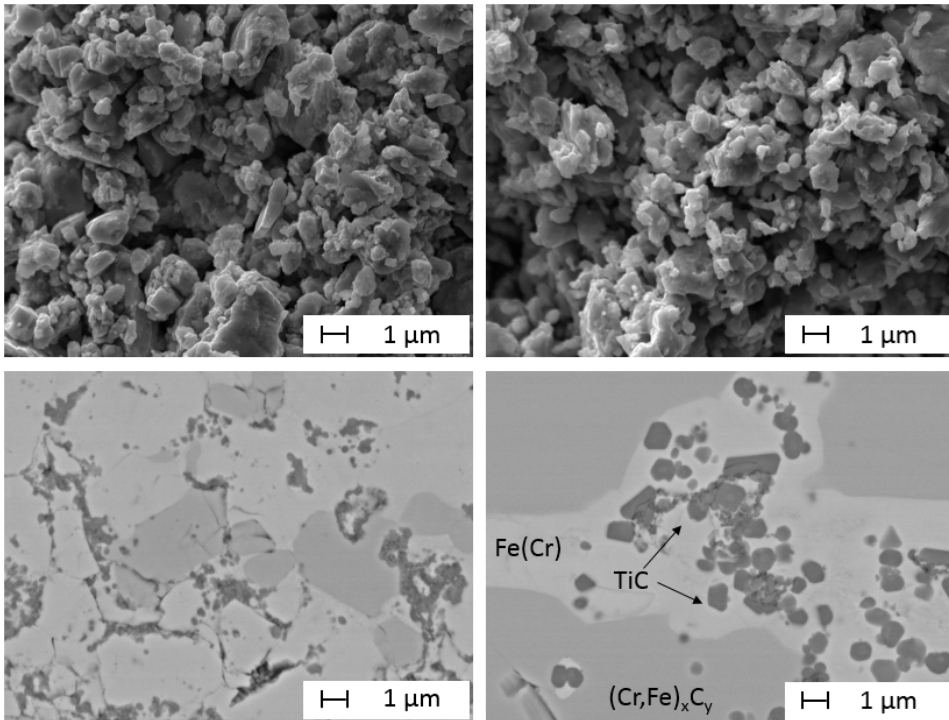


Figure 31. Microstructure of $50\text{Cr}_3\text{C}_2$ -FeTi cermet after milling (upper left) and sintering at different temperatures: 1000 (upper right), 1200 (lower left) and 1420 °C (lower right) (Paper IV).

Table 18. Chemical composition wt% of vacuum sintered Cr_3C_2 -FeTi cermet phases.

Phase	C	Cr	W	Ti	Fe
Total	9.9	38.9	4.1	10.6	36.5
Binder	-	16.1	3.9	1.2	78.8
Metal carbide	10.0	65.6	2.2	1.2	21.0
Titanium carbide	16.1	11.7	6.7	43.1	22.4

Improving the structure and performance

Technological parameters (milling device, sintering time and temperature) and mechanical properties of Cr_3C_2 -FeTi cermets are shown in Table 19. The properties of cermets are dependent on their chemical composition and technological peculiarities. The hardness of the cermets depends mainly on the Cr_3C_2 content in the initial powder mixture – hardness increases with the increase of the carbide content. A coarse microstructure of Cr_3C_2 -FeTi cermets is the main reason behind moderate fracture toughness (Paper IV). However, cermets Cr_3C_2 -FeTi outperform those of Cr_3C_2 -FeCr in

toughness. Cermets sintered at lower temperature during a longer time demonstrate the best complex of hardness and toughness.

Table 19. Technological parameters, porosity and mechanical characteristics of vacuum sintered Cr₃C₂-FeTi cermets.

Composition, wt%	Milling device	Sintering parameter		Porosity, %	Hardness, HV30	Fracture toughness, MPa·m ^{1/2}
		Temp, °C	Time, min			
50Cr ₃ C ₂ - FeTi	Attritor	1390	30	0.29	979±95	7.8±0.8
60Cr ₃ C ₂ - FeTi	Attritor	1450	30	0.55	995±11	4.8±0.5
60Cr ₃ C ₂ - FeTi	Ball mill	1450	30	2.01	1008±21	n/a
70Cr ₃ C ₂ - FeTi	Attritor	1420	30	0.37	1180±19	5.6±0.9
70Cr ₃ C ₂ - FeTi	Attritor	1470	30	0.84	1349±17	3.9±0.2
70Cr ₃ C ₂ - FeTi	Attritor	1420	60	0.47	1067±20	7.7±0.7
70Cr ₃ C ₂ - FeTi	Ball mill	1420	30	1.38	1274±33	n/a
70Cr ₃ C ₂ - FeTi	Ball mill	1470	30	0.15	1133±31	5.4±0.1
70Cr ₃ C ₂ - FeTi	Ball mill	1420	60	0.92	1163± 6	6.0±0.4

Both pure Ti metal and pre-synthesized TiC powders were used for refining the grain size (see Fig. 32). However, this structural peculiarity (TiC particles in the microstructure does not offer reduction of the size of chromium carbides – grain size of Cr₃C₂-Fe, Cr₃C₂-FeTi and Cr₃C₂-TiC-Fe cermets turned out to be similar (Paper IV).

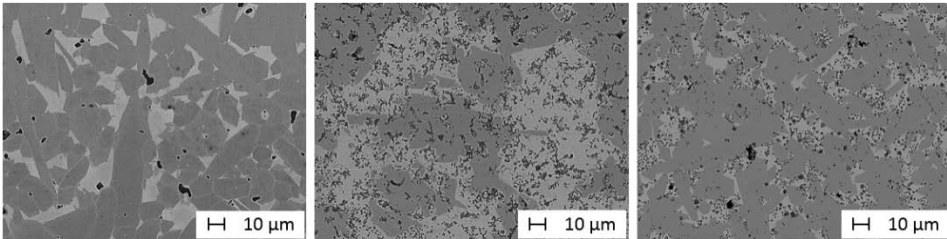


Figure 32. Microstructures of Cr₃C₂-Fe (left), Cr₃C₂-FeTi (middle) and Cr₃C₂-Fe-TiC (right) (Paper IV).

In the case of chromium carbide-based cermets, the FeCrMn binder system was also investigated but these cermets demonstrated relatively high porosity. The reason behind it is unclear and needs further research.

Corrosion and oxidation resistance

Oxidation tests were performed to evaluate the oxidation rates of different carbide-based composites at the air brazing temperature of 900 °C. Oxidation rates of composites are presented in Table 20. Chromium carbide cermets with ferritic steel binder demonstrated very good oxidation resistance compared to other carbide-based composites.

Table 20. Calculated oxidation rates of carbide-based composites wt% at air brazing temperature 900 °C (Paper V).

Material	85WC-Co	70TiC-NiMo	70TiC-FeCr	50Cr ₃ C ₂ -FeCr
Oxidation rate, mg/mm ²	0.9	0.03	0.04	< 0.01

An simple immersion test was carried out to evaluate corrosion resistance in a chloride containing solution (see Fig. 33). The samples were tested during 72 h in 3 wt% HCl solution. TiC-based cermets demonstrated relatively low corrosion resistance because the chromium content of the binder phase is very low – below 5 wt% (see Tables 6 and 10). Cr₃C₂-based cermets are featured by good corrosion resistance, especially those of Cr₃C₂-FeTi. The high resistance to corrosion is related to the high chromium content of the metallic binder phase (see Tables 14 and 18).

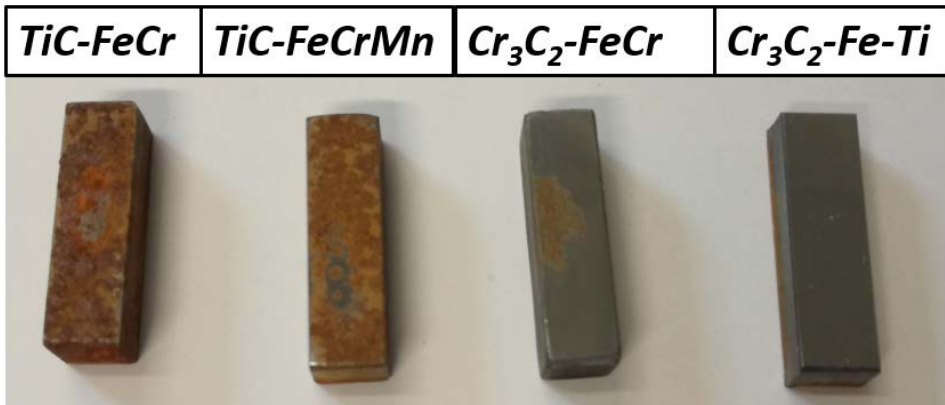


Figure 33. Immersion test results of different cermets.

4.3 Summary

Our research results of the influence of the composition and technological conditions on the structure formation and performance of chromium carbide-based (Fe-Cr and Fe-Ti alloys) bonded cermets can be summarized as follows:

- Cermets Cr₃C₂-FeCr and Cr₃C₂-FeTi are featured by excellent resistance to corrosion and oxidation but the mechanical characteristics are moderate because of coarse-grain structure.
- Cermets Cr₃C₂-FeTi outperform those of Cr₃C₂-FeCr in mechanical characteristics, in particular, in fracture toughness.
- During vacuum sintering of both Cr₃C₂-FeTi and Cr₃C₂-FeCr cermets, recrystallization of Cr₃C₂ into chromium-ferrous complex carbides (Cr,Fe)_xC_y takes place. The structure of Cr₃C₂-FeTi cermets consists essentially of three phases ((Cr,Fe)₂₃C₆, TiC and solid solution Fe(Cr)) while the structure of Cr₃C₂-FeCr primarily of two phases – (Cr,Fe)₇C₃ carbide and solid solution Fe (Cr).

- $\text{Cr}_3\text{C}_2\text{-FeTi}$ cermets are characterized by the formation of evenly distributed ultrafine TiC grains and two step recrystallization of chromium carbides ($\text{Cr}_3\text{C}_2 \rightarrow (\text{Cr, Fe})_7\text{C}_3 \rightarrow (\text{Cr, Fe})_{23}\text{C}_6$) during vacuum sintering. However, this structural peculiarity does not enable reduction of the size of chromium carbides in the microstructure.
- Marked decrease in grain size of chromium carbide-based cermets is feasible utilizing spark plasma sintering that enables rapid hot consolidation at reduced temperature and time.

5 CONCLUSIONS

Main conclusions from the microstructure evolution and phase transformations during sintering of TiC- and Cr₃C₂-based cermets bonded with Ni-free FeCr alloys and from the optimization of sintering parameters and chemical compositions are as follows:

Titanium carbide-based cermets

- Sintered Ni-free TiC based iron alloy bonded cermets TiC-FeCr and TiC-FeCrMn consist prevalently of two carbide phases (TiC with coaxial structure and secondary metal carbide M₇C₃ (M=Cr, Fe, Mn)) and iron based solid solution Fe(Cr).
- The decrease of Cr content in the alloy and in the metallic binder is caused by the evaporation, solution in TiC and formation of secondary complex carbides M₇C₃ during sintering. The latter is essentially the reason of heterogeneous distribution of Cr in composites and reduction of Cr content in the metallic binder.
- Alloying of TiC-FeCr cermets by strong carbide formers enables improvement of structural homogeneity – both of the metallic phase and Fe and Cr distribution.
- Alloying of TiC-FeCrMn cermets by silicon enables improvement of sinterability, resulting in improved structural homogeneity of cermets.
- Retaining both Cr and Mn in cermets is possible by sintering under low partial pressure of argon and using manganese “microatmosphere”. In terms of structure (porosity, structural homogeneity), sintering under such conditions is most effective.

Chromium carbide-based cermets

- Ni-free iron alloys bonded chromium carbide-based cermets are featured by excellent resistance to corrosion and oxidation but moderate mechanical characteristics because of coarse-grain structure. Cermets Cr₃C₂-FeTi outperform those of Cr₃C₂-FeCr in mechanical characteristics, in particular, in fracture toughness.
- During vacuum sintering of chromium carbide-based cermets, recrystallization of the starting Cr₃C₂ into the complex carbides (Cr,Fe)_xC_y takes place. The structure of Cr₃C₂-FeCr consists prevalently of (Cr,Fe)₇C₃ carbide and solid solution Fe(Cr) while the structure of Cr₃C₂-FeTi cermets consists essentially of two carbide phases ((Cr,Fe)₂₃C₆ and TiC) and solid solution Fe(Cr).
- Feature of Cr₃C₂-FeTi cermets is two step recrystallization of chromium carbides Cr₃C₂→(Cr, Fe)₇C₃→(Cr,Fe)₂₃C₆ as well as formation of evenly distributed submicron TiC grains during vacuum sintering.
- Carbide grain size refinement is most feasible by spark plasma sintering that enables rapid hot consolidation at decreased temperature and time.

Novelty and Further research

The novelty of present research can be attributed to:

TiC-based cermets:

- Assessment of microstructure evolution and phase transformation features of high-chromium TiC-FeCr and high-chromium and manganese TiC-FeCrMn cermets;
- Revealing technological and chemical (alloying) opportunities for improving structural homogeneity and mechanical performance of high-chromium TiC-based cermets characterized by high resistance to wear.

Cr₃C₂-based cermets:

- Elucidation of microstructure evolution and phase transformation features of Cr₃C₂-based cermets bonded with iron alloys (FeCr, FeTi);
- Revealing technological and chemical (alloying) opportunities that enable improvement of the structure and mechanical performance of Cr₃C₂-based cermets characterized by excellent resistance to corrosion.

For complementary increase of performance of TiC- and Cr₃C₂-based cermets bonded with Ni-free high-chromium Fe alloys, the following recommendations for further research are proposed:

- Revealing the possibilities to reach corrosion resistance of TiC-FeCrMn cermets that is comparable to that of nickel containing TiC-FeCrNi composites with austenitic structure of metallic binder;
- Study of Cr₃C₂-FeCrMn cermets with austenitic structure of metallic binder and opportunities to decrease grain size of such composites;
- Study of the corrosion and oxidation resistance of developed composites;
- Assessing the wear performance and degradation mechanism of developed composites in different wear conditions.

REFERENCES

- Aigner, K., Lengauer, W., & Ettmayer, P. (1997). Interactions in iron-based cermet systems. *Journal of Alloys and Compounds*, 262–263, 486–491.
- Akhtar, F., & Guo, S. J. (2008). Microstructure, mechanical and fretting wear properties of TiC-stainless steel composites. *Materials Characterization*, 59(1), 84–90.
- Akhtar, F., Guo, S., Askari, J., & Tian, J. (2007). Sintering behavior, microstructure and properties of TiC-FeCr hard alloy. *Journal of University of Science and Technology Beijing, Mineral, Metallurgy, Material*, 14(1), 89–93.
- Al-Mangour, B. (2015). Powder metallurgy of stainless steel: State-of-the art, challenges, and development. *Stainless steels, Nova Science Publishers*, 37–80.
- Alvaredo, P., Tsiapas, S. A., & Gordo, E. (2013). Influence of carbon content on the sinterability of an FeCr matrix cermet reinforced with TiCN. *International Journal of Refractory Metals and Hard Materials*, 36, 283–288.
- Brookes, K. (2011). There's more to hard materials than tungsten carbide alone. *Metal Powder Report*, 66(2), 36–45.
- Brookes, K. J. A. (1997). World directory and handbook of hardmetals: and hard materials (6 edition). *Metal Powder Industry*, East Barnet, Hertfordshire.
- Dai, H. Y., Li, J. F., Zhai, F. X., Cheng, X. R., & Wang, Y. B. (2012). Effect of molybdenum on the microstructure and mechanical properties of TiC-Fe cermets. *Advanced Materials Research*, 557–559, 205–208.
- Davis, J. R. (1994). *Stainless steels. ASM International.*
- Davis, J. R. (2001). *Alloying: understanding the basics. ASM International.*
- Deevi, S. C., & Sikka, V. K. (1996). Nickel and iron aluminides: an overview on properties, processing, and applications. *Intermetallics*, 4(5), 357–375.
- Desai, P. D. (1987). Thermodynamic properties of manganese and molybdenum. *Journal of Physical and Chemical Reference Data*, 16(1), 91–108.
- Durlu, N. (1999). Titanium carbide based composites for high temperature applications. *Journal of the European Ceramic Society*, 19(13), 2415–2419.
- ECHA Homepage. <https://echa.europa.eu/information-on-chemicals>, (accessed January 15, 2018).
- Eisen, W. B. (1998). *ASM Handbook Vol. 7: Powder metal technologies and applications: 2Rev Ed edition. ASM International*, Materials Park, Ohio.
- Ettmayer, P. (1989). Hardmetals and cermets. *Annual Review of Materials Science*, 19(1), 145–164.
- EuMaT homepage. <http://eumat.eu/>, (accessed February 25, 2018).
- European Commission homepage. http://ec.europa.eu/growth/sectors/raw-materials/specific-interest/critical_et, (accessed February 20, 2017).

- Evans, A. G., & Charles, E. A. (1976). Fracture toughness determinations by indentation. *Journal of the American Ceramic Society*, 59(7–8), 371–372.
- Exner, H. E. (1979). Physical and chemical nature of cemented carbides. *International Metals Reviews*, 24(1), 149–173.
- Fahlman, B. (2011). *Materials chemistry* (2. tr). Springer, Netherlands.
- Fischbein, A., Luo, J. C., Solomon, S. J., Horowitz, S., Hailoo, W., & Miller, A. (1992). Clinical findings among hard metal workers. *British Journal of Industrial Medicine*, 49(1), 17–24.
- Frage, N., Froumin, N., Dariel, M. P. (2002). Wetting of TiC by non-reactive liquid metals. *Acta Materialia*, 50, 237–245.
- German, R. M. (1998). *Powder metallurgy of iron and steel*. Wiley-Interscience Publication.
- Guo, Z., Xiong, J., Yang, M., Wang, J., Sun, L., Wu, Y., Chen, J., Xiong, S. (2009). Microstructure and properties of Ti(C,N)–Mo₂C–Fe cermets. *International Journal of Refractory Metals and Hard Materials*, 27(4), 781–783.
- Guyot, P., Rat, V., Coudert, J. F., Jay, F., Maître, A., & Pradeilles, N. (2012). Does the Branly effect occur in spark plasma sintering? *Journal of Physics D: Applied Physics*, 45(9), 092001.
- Hryha, E., & Dudrova, E. (2011). The Sintering Behaviour of Fe-Mn-C Powder System, Correlation between thermodynamics and sintering process, manganese distribution and microstructure composition, effect of alloying mode. *Application of Thermodynamics to Biological and Materials Science*.
- Humenik, M., & Parikh, N. M. (1956). Cermets: I, fundamental concepts related to micro-structure and physical properties of cermet systems. *Journal of the American Ceramic Society*, 39(2), 60–63.
- Jin, C., & Plucknett, K. P. (2016). Microstructure instability in TiC-316L stainless steel cermets. *International Journal of Refractory Metals and Hard Materials*, 58, 74–83.
- Jonsson, S. (1998). Assessment of the Fe-Ti-C system, calculation of the Fe-TiN system, and prediction of the solubility limit of Ti(C,N) in liquid Fe. *Metallurgical and Materials Transactions B*, 29(2), 371–384.
- Klar, E., & Samal, P. K. (2007). *Powder metallurgy stainless steels: processing, microstructures, and properties*. ASM International.
- Kocich, R., Szurman, I., & Kurska, M. (2013). The Methods of preparation of Ti-Ni-X alloys and their forming. *Shape Memory Alloys Francisco Manuel Braz Fernandes*, IntechOpen
- Krasnowski, M., & Kulik, T. (2007). Nanocrystalline FeAl matrix composites reinforced with TiC obtained by hot-pressing consolidation of mechanically alloyed powders. *Intermetallics*, 15(10), 1377–1383.
- Kuroda, D., Hiromoto, S., Hanawa, T., & Katada, Y. (2002). Corrosion behavior of nickel-free high nitrogen austenitic stainless steel in simulated biological environments. *Materials Transactions*, 43(12), 3100–3104.

- Kübarsepp, J., Valdma, L., & Kallast, V. (1980). Corrosion resistance of sintered TiC-steel alloys. *Soviet Powder Metallurgy and Metal Ceramics*, 19(4), 293–294.
- Kübarsepp, J., & Kallast, V. (1994). Stainless hardmetals and their electrochemical corrosion resistance. *Materials and Corrosion*, 45(8), 452–458.
- Kübarsepp, J., Pirso, J., Juhani, K., & Viljus, M. (2014). Developments in cermet design, technology and performance. *International Journal of Materials and Product Technology*, 49(2–3), 160–179.
- Kübarsepp, J., Reshetnyak, H., & Annuka, H. (1993). Characterization of the serviceability of steel-bonded hardmetals. *International Journal of Refractory Metals and Hard Materials*, 12(6), 341–348.
- Kübarsepp, J. (1986). Production of high chromium alloys TiC-Fe-Cr alloyed with silicon. *Soviet Powder Metallurgy and Metal Ceramics*, 25(5), 410–414.
- Kübarsepp, J. (1988). Oxidation of components of the TiC-Fe-Cr system in presintering a powder carbide steel. *Soviet Powder Metallurgy and Metal Ceramics*, 27(3), 215–218.
- Lenel, F. V. (1980). Powder metallurgy: principles and applications. *Metal Powder Industries Federation*.
- Li, J., Liu, Q., Shi, R., Wen, Y., & Yin, Y. (2008). Preparation and mechanical properties of Fe₃Al(Ti)/TiC composites. *Journal of Materials Processing Technology*, 208(1), 105–110.
- Mari, D., Miguel, L., & Nebel, C. (2014). Comprehensive hard materials. *Newnes*.
- Maslyuk, V. A. (2014). Tungsten-free hardmetals and carbide steels with chromium carbides. *Powder Metallurgy and Metal Ceramics*, 53(3–4), 162–169.
- Maslyuk, V. A., Yakovenko, R. V., Potazhevskaya, O. A., & Bondar, A. A. (2013). Hard powder alloys and carburized chromium steels in the Cr–Fe–C system. *Powder Metallurgy and Metal Ceramics*, 52(1–2), 47–57.
- Mohrbacher, H. (2008). The effect of niobium microalloying in second generation advanced high strength steels. *International Steel Technologies Symposium*.
- Nayar. (2000). The steel handbook. *Tata McGraw-Hill Education*.
- Norgren, S., García, J., Blomqvist, A., & Yin, L. (2015). Trends in the P/M hard metal industry. *International Journal of Refractory Metals and Hard Materials*, 48, 31–45.
- OCSPP. (TSCA homepage). <https://www.epa.gov/tsca-inventory>, (accessed February 20, 2018).
- Panasyuk, A. D., Maslyuk, V. A., Klimenko, V. N., & Kayuk, V. G. (1985). Contact reactions of chromium carbide base materials with copper alloys. *Soviet Powder Metallurgy and Metal Ceramics*, 24(9), 703–707.
- Reshetnyak, H., & Kübarsepp, J. (1994). Mechanical properties of hard metals and their erosive wear resistance. *Wear*, 177(2), 185–193.
- Roberts, G. A., Kennedy, R., & Krauss, G. (1998). Tool steels, 5th Edition. *ASM International*.

- Schatt, W., Association, E. P. M., & Wieters, K.-P. (1997). Powder metallurgy: processing and materials. *European Powder Metallurgy Association*.
- Schubert, W. D., Fugger, M., Wittmann, B., & Useldinger, R. (2015). Aspects of sintering of cemented carbides with Fe-based binders. *International Journal of Refractory Metals and Hard Materials*, 49, 110–123.
- Subramanian, R., Schneibel, J. H., & Alexander, K. B. (1996). Iron aluminide-titanium carbide composites: Microstructure and mechanical properties. *University of North Texas Libraries, Digital Library*, Tennessee.
- Tarraste, M., Kübarsepp, J., Juhani, K., Mere, A., Kolnes, M., Viljus, M., & Maaten, B. (2018). Ferritic chromium steel as binder metal for WC cemented carbides. *International Journal of Refractory Metals and Hard Materials*, 73, 183–191.
- Tolochin, A. I., Laptev, A. V., Yakovenko, R. V., & Maslyuk, V. A. (2017). Shock-wave sintering of the 70 vol.% Kh13M2–30 vol.% Cr₃C₂ carbonized steel in a wide temperature range. *Powder Metallurgy and Metal Ceramics*, 55(9–10), 518–529.
- V. Yakovenko, R., A. Maslyuk, V., N. Gripachevskii, A., & B. Deimontovich, V. (2011). Dissolution of chromium carbide Cr₃C₂ in Kh17N2 steel during sintering. *Powder Metallurgy and Metal Ceramics*, 50, 182–188.
- Vlasyuk, R. Z., Gripachevskii, A. N., & Radomysel'skii, I. D. (1984). Changes in the chemical and phase compositions of A Cr₃C₂ particle in contact with an iron matrix during sintering. *Soviet Powder Metallurgy and Metal Ceramics*, 23(8), 597–602.
- Wang J., & Wang Y. (2007). In-situ production of Fe–TiC composite. *Materials Letters*, 61(22), 4393–4395.
- Yang, K., & Ren, Y. (2010). Nickel-free austenitic stainless steels for medical applications. *Science and Technology of Advanced Materials*, 11(1).

ACKNOWLEDGEMENTS

First, I would like to thank my supervisor prof. Jakob Kübarsepp, co-supervisor assoc. prof. Fjodor Sergejev for providing excellent working conditions and continuous support throughout my studies.

I would like to thank co-authors of the papers related to the thesis and colleagues in the Department of Mechanical and Industrial Engineering for their support, especially Marek Tarraste, Jüri Pirso and Lauri Kollo for numerous scientific discussions. Also, I would like to thank Arvo Mere, Mart Viljus and Rainer Traksmäa for materials characterization.

Finally, my sincere thanks are due to my family for support and encouragement.

The study was supported by the following projects:

- IUT 19-29 – Multi-scale structured ceramic-based composites for extreme applications (Institutional research funding of the Estonian Ministry of Education and Research);
- IUT 19-4 – Thin films and nanomaterials by wet-chemical methods for next-generation photovoltaics (Institutional research funding of the Estonian Ministry of Education and Research);
- TK141 – Advanced materials and high-technology devices for energy recuperation systems (European Regional Development Fund project);
- VA 580, VA 683, VA 16002 – Different Research and Development agreement between The Swatch Group Research and Development Ltd and Tallinn University of Technology, 2012 – 2016.

This work has been partially supported by ASTRA “TUT Institutional Development Programme for 2016-2022” Graduate School of Functional Materials and Technologies (2014-2020.4.01.16-0032).

KOKKUVÕTE

Koobalti- ja nikli-vabad titaankarbiid- ja kroomkarbiidkermised

Kulutused, mis on tingitud tööriistade ja konstruktsioonielementide püsivuse vähenemisest seoses nende kulumisega on märkimisväärsed. Sellest tingituna on alatine vajadus arendada uusi töökindlaid ja hinna poolest konkurentsivõimelisi kulumiskindlaid materjale ja nende valmistustehnoloogiad. Keraamilis-metalsed komposiidid (kermised) on materjalid, kus keraamilise komponendina kasutatakse valdavalt karbiide ja karbonitriide (WC, TiC, Ti(C,N), Cr₃C₂). Pehmema ja sitkema metalse sideainena kasutatakse aga tavapäraselt raua grupi metalle (Co, Ni, Fe). Selliseid komposiitmaterjale kasutatakse, sest neil on kõrge kulumiskindlus ning sitkus. Keraamika-baasil komposiitmaterjalidest kasutatakse WC-Co kõvasulameid kõige enam, sest neid iseloomustab suurepärase kombinatsioon kõvadusest ja sitkusest. Tingituna W ja Co piiratud kättesaadavusest on tehtud suuri pingutusi asendamaks neid metalle ning välja töötada W- ja Co-vabu kermiseid. Kõige rohkem on tähelepanu olnud suunatud TiC- ja Ti(C,N)-NiMo kermistele. Alternatiivina neile kasutatakse korrosiivsetes keskkondades ka kroomkarbiidseid Cr₃C₂-Ni keraamilis-metalseid komposiite. Samas, nikkel ja koobalt on liigitatud mürgisteks metallideks. Seepärast on raua-baasil sideaine, mis ei sisalda mürgiseid, allergiat tekitavaid komponente parim lahendus asendamaks nii niklit kui koobaltit.

Käesoleva uurimistöö ajendiks oli asendada laia kasutusalauga WC-Co kõvasulamid samuti ja TiC-NiMo ja Cr₃C₂-Ni kermised W-, Ni- ja Co-vabade komposiitidega. Peamiseks eesmärgiks oli välja töötada, valmistada ja karakteriseerida TiC- ja Cr₃C₂-baasil alternatiivsete Ni- ja Co-vabade raua-baasil sideainetega kermised. Uurimistöö fookuses oli nende komposiitide mikrostruktuuri moodustumise ja faasilise koostise muutuste parem mõistmine ning nende teadmiste alusel uute tehnoloogiliste lahenduste välja töötamine.

Kermised valmistati kasutades üldlevinud pulbermetallurgilist meetodit – mehaanilisele jahvatamisele järgnes üheteljeline pressimine ja paagutamine. Kasutati kahte paagutustehnoloogiat – vaakumpaagutus ja plasma-aktiveeritud paagutus. Uurimaks mikrostruktuuri moodustumist ja välja toomaks faasimuutused paagutuse käigus kasutati optilist ja elektronmikroskoopi (OM ja SEM), röntgen-spektroskoopi (EDS) ja röntgenstruktuuranalüüsi (XRD). Keemiliste reaktsioonide ja füüsiliste muunduste mõõtmiseks kasutati skaneerivat diferentsiaal kalorimeetriat (DSC) ning mehaanilistest omadustest määrati Vickersi kõvadust ja purunemissitkust.

Käesoleva töö esimeses osas uuritakse TiC-baasil kermiseid, milliste sideaineks on suure kroomisisaldusega FeCr ja FeCrMn sulamid. Fookuses oli parem arusaam tehnoloogilistest iseärasustest, mikrostruktuuri ja faasilise koostise muutustest paagutamisel. Selgus, et TiC-FeCr kermiste struktuuris on esindatud peamiselt kahte tüüpi karbiidseid faase – TiC (koaksiaal struktuuriga) ja metallkarbiid M₇C₃ (M=Cr,Fe,Mn) - ning raua-baasil tardlahus. Märkimisväärne kroomisisalduse

väheneb sulamis ja metallses sideaines on tingitud sekundaarse metallkarbiidi M_7C_3 tekkest, krooni lahustumisest titaankarbiidis ja lendumisest. Kirjeldatud protsessid põhjustavad krooni heterogeense jagunemise sulamis ning märgatava kroonisisalduse vähenemise sideaines. Tõestust leidis, et sobivalt legerides TiC-FeCr kermist on võimalik parandada struktuurset homogeensust – nii krooni kui ka metalse faasi jaotumist komposiidis. TiC-FeCrMn kermiste korral on suureks väljakutseks Mn ja Cr säilumine sulamis vaakumpaagutusel. Peamiseks lahenduseks struktuurseid muutuseid ja mehaanilisi omadusi arvestades on paagutamine madala argooni alarõhu tingimustes ja mangaani „mikroatmosfääri“ kasutades. Lisaks on võimalik TiC-FeCrMn kermiste struktuuri homogeensust ja mehaanilisi omadusi parandada legerides neid tugeva taandaja ja paagutatavust parandava räniga.

Käesoleva töö teises osas käsitletakse kroomkarbiidi-baasil kermiseid, milliste sideaineks on FeCr ja FeTi sulamid. Peamiseks eesmärgiks oli välja töötada, valmistada ja karakteriseerida Cr_3C_2 -baasil alternatiivsete Ni- ja Co-vabade raua-baasil sideainetega korrosioonikindlad kermised. Selgitati, et raua-baasil sideainetega kermised on suurepärase korrosiooni- ja oksüdatsioonikindlusega, kuid suhteliselt tagasihoidlike mehaaniliste omadustega. See on peamiselt tingitud Cr_3C_2 -baasil kermiste jämedateralisest struktuurist. Cr_3C_2 -FeCr kermise struktuur koosneb peamiselt $(Cr,Fe)_7C_3$ karbiidist ja raua tardlahusest. Kuid Cr_3C_2 -FeTi kermise struktuuris sisaldub peamiselt karbiid $(Cr,Fe)_{23}C_6$ (kahe-astmelise rekristallisatsiooni $Cr_3C_2 \rightarrow (Cr, Fe)_7C_3 \rightarrow (Cr,Fe)_{23}C_6$ tulemus) ja TiC. Alamikroonse TiC moodustumine paagutamisel siiski ei pidurda märkimisväärselt kroomkarbiidi terade kasvu. Sellele vaatamata Cr_3C_2 -FeTi kermised ületavad Cr_3C_2 -FeCr kermiseid mehaaniliste omaduste (eelkõige purunemissitkus) poolest.

Kroomkarbiidsete kermiste terakasvu pidurdamiseks annab parima tulemuse plasma-aktiveeritud paagutuse tehnoloogia, mis võimaldab rakendada kiiret konsolideerimist tavapärase vaakumpaagutusega võrreldes madalamal temperatuuril ja lühema aja jooksul.

ABSTRACT

Cobalt- and Nickel-free titanium and chromium carbide-based cermets

Losses resulting from wear in the life cycle costs of equipment in the processing of materials, mining, building materials production etc. are pronounced. Therefore the challenge is to develop new reliable and cost-effective wear resistant materials and related production technologies. Carbides and carbonitrides cemented with metals of the iron group (Co, Ni, Fe) are composites where hard phase (prevalently WC, TiC, Ti(C,N), Cr₃C₂) is cemented in more soft and tough metal matrix. Such composite materials are known due to their higher wear resistance and higher toughness in comparison with ceramics. Because of the good combination of hardness and toughness, tungsten carbide-based cemented carbides WC-Co are the most widely used. First of all, because of the strategic nature of tungsten supply and shortage of cobalt, efforts have been made to replace these metals and elaborate W- and Co-free ceramic-metal composites (cermets). Most of the efforts have been centred on TiC- and Ti(C,N)-based cermets bonded with Ni-Mo alloys. An alternative to these cermets is composites based on chromium carbide (Cr₃C₂) bonded with Ni and Ni-alloys. However, Ni and Co are classified as metals toxic for human health. Non-toxic Fe-based binders are therefore the top-of-the-line solution for replacing Ni and Co and also WC.

The motivation of the present study is the need for tungsten-, nickel- and cobalt-free cermets replacing regular WC-Co cemented carbides and TiC-NiMo or Ti(C,N)-NiMo cermets. The general objective is to develop, produce and characterize TiC- and Cr₃C₂-based cermets bonded with an alternative Ni- and Co-free Fe-based alloys (steels). The aim was to acquire better understanding of the microstructure evolution of high-chromium FeCr alloys bonded cermets, phase transformation and to find possibilities of performance improvement utilizing and/or technological opportunities.

Cermets were produced by the conventional powder metallurgy method - mechanical milling (in ball mill or attritor), followed by uniaxial pressing and sintering. Two sintering techniques were used - vacuum sintering and spark plasma sintering. An optical and scanning electron microscopy (OM and SEM), X-ray spectroscopy (EDS), X-ray diffraction (XRD) and differential scanning calorimetry (DSC) were used to study microstructure evolution and to reveal changes in the phase composition during sintering. Mechanical characteristics (hardness and fracture toughness) were used as the main performance characteristics of cermets.

The first part of the research addresses TiC-based cermets with two different high-chromium binders – FeCr and FeCrMn. The aim was to acquire better understanding of technological peculiarities, microstructure evolution and phase transformations of these composites during sintering. It was revealed that the structure of both Ni- and Co-free cermets TiC-FeCr and TiC-FeCrMn consists prevalently of two carbide phases – TiC (with coaxial structure) and complex metal carbides M₇C₃ (M= Cr, Fe, Mn) and iron-based solid solution. Formation of secondary complex carbides M₇C₃, solution in TiC

and vacuum evaporation leads to a marked decrease of Cr content in the alloy and in the metallic binder. The former is essentially the reason behind the heterogeneous distribution of Cr in composites and marked reduction of this element in the metallic binder. It was revealed that alloying of TiC-FeCr cermets enables improvement of the structure homogeneity - both of the metallic phase of the composite and Cr distribution. A challenge in TiC-FeCrMn cermets is how to retain both Cr and Mn during sintering. It was revealed that in terms of structure (porosity, structural homogeneity) and mechanical properties, sintering under low partial pressure of Ar and using Mn "microatmosphere" is an effective technological procedure for such composites. Also, alloying of TiC-FeCrMn cermets by silicon enables enhancement of sinterability, resulting in improved structural homogeneity and mechanical performance.

The second part of the research is focused on Cr_3C_2 -based cermets. Two different binders – FeCr and FeTi were studied. The aim was to acquire better understanding of microstructure evolution, phase transformations and technological peculiarities of these Ni- and Co-free cermets. It was revealed that Fe alloy-bonded cermets are featured by excellent resistance to corrosion and oxidation but moderate mechanical characteristics - first of all, because of coarse-grain microstructure. During sintering of chromium carbide-based cermets, recrystallization of starting Cr_3C_2 into complex carbides $(\text{Cr,Fe})_x\text{C}_y$ takes place. The structure of Cr_3C_2 -FeCr cermets consists prevalently of $(\text{Cr,Fe})_7\text{C}_3$ carbide and solid solution Fe(Cr). The structure of Cr_3C_2 -FeTi cermets due to the two-stage recrystallization of chromium carbides ($\text{Cr}_3\text{C}_2 \rightarrow (\text{Cr, Fe})_7\text{C}_3 \rightarrow (\text{Cr,Fe})_{23}\text{C}_6$) consists essentially of two carbide phases ($(\text{Cr,Fe})_{23}\text{C}_6$ and TiC) and solid solution Fe(Cr). Surprisingly, submicron TiC particles in the structure do not provide reduction of the size of chromium carbides. However, cermets Cr_3C_2 -FeTi outperform Cr_3C_2 -FeCr in mechanical characteristics, in particular, in fracture toughness.

It was revealed that the grain size refinement of chromium carbide-based cermets is most feasible by spark plasma sintering that enables rapid hot consolidation at decreased temperature and time.

APPENDIX

Paper I

Kolnes, M., Mere, A., Kübarsepp, J., Viljus, M., Maaten, B., Tarraste, M. Microstructure evolution of TiC cermets with ferritic AISI 430L steel binder. *Powder Metallurgy*, 2018, published online: 15 Mar 2018.



Microstructure evolution of TiC cermets with ferritic AISI 430L steel binder

Märt Kolnes^a, Arvo Mere^b, Jakob Kübarsepp^a, Mart Viljus^a, Birgit Maaten^c and Marek Tarraste^a

^aDepartment of Mechanical and Industrial Engineering, Tallinn University of Technology, Tallinn, Estonia; ^bDepartment of Materials and Environmental Technology, Tallinn University of Technology, Tallinn, Estonia; ^cDepartment of Energy Technology, Tallinn University of Technology, Tallinn, Estonia

ABSTRACT

From the outlook of healthcare, economic importance and supply risk, utilisation of raw materials like tungsten, cobalt and nickel should be reduced or replaced with other metals. Nontoxic titanium carbide and iron are the top-of-the-line solution for displacing these materials. Our focus was on conventionally fabricated titanium carbide-based cermets with a chromium ferritic steel binder. To study microstructural evolution, specimens were sintered at different temperatures (600–1500°C). We used a scanning electron microscopy, X-ray diffraction and differential scanning calorimetry to analyse the microstructure and phase formation of the cermets. Our results showed that during the solid and liquid phase sintering of the TiC–FeCr cermet, chromium ferrous complex carbides M_7C_3 are formed and as a result, chromium content in the binder phase is decreased. Alloying TiC–FeCr cermets with strong carbide formers improves the structural homogeneity of the cermets. Also, mechanical characteristics (hardness, fracture toughness) were evaluated.

ARTICLE HISTORY

Received 20 July 2017
Accepted 18 February 2018

KEYWORDS

Titanium carbide-based cermets; alternative steel binders; microstructure evaluation; phase formation

1. Introduction

Cemented carbides are composite materials known for their excellent wear resistance, coupled with a good combination of mechanical properties. Hard and brittle carbide phase is ‘cemented’ in a more ductile metal matrix. Tungsten and titanium carbide-based cemented carbides are most well-known systems. Usually, Fe-group metals (Fe, Co, Ni) are employed as the binder phase. Among the tungsten-free ceramic-metallic composites, TiC–NiMo cermets are most widespread.

A leading direction in the studies of cemented carbide is to use cheaper and more environment friendly materials. Throughout the 1930s, partly because of the strategic nature of tungsten deposit and partly driven by the sheer excitement of technological achievement, great efforts were made to displace or supplement tungsten carbide as hard phase and cobalt as binder [1].

The European Commission has created a list of critical raw materials which combine a high economic importance to the European Union with a high risk associated with their supply. In addition to many materials, tungsten is included in that list [2]. Additionally, recent worldwide demand has driven the price of nickel and molybdenum skyward. Alloys containing significant amounts of these elements, such as the austenitic and duplex grades, have experienced significant price increases and spot shortages have resulted in some regions. With low nickel and reasonable molybdenum content, super-ferritic

stainless steels have proved to be the most cost-effective [3]. Gries and Prakash explained the toxicity of WC–Co and to exploit the Fe to reduce toxicity [4]. In addition, Ni has been declared as a carcinogen [5]. Therefore, it is of interest to find a satisfactory alternative binder phase to replace critical materials totally or partially, thereby reducing the dependence on these strategic materials in the future. Low-cost and abundant Fe, which is not harmful to human body, is the most popular alternative as a binder for Ni- and Co-free cemented carbides [6]. Ti(C,N)-based cermets have demonstrated high performance in wear parts and semi-finishing or finishing cutting tools. Also, iron-based alloys have demonstrated quite satisfactory mechanical, corrosive and wear performance as a binder system of cermets.

Since the 1970s, the focus has been on titanium carbide with iron-based binder systems. However, findings show that such cermets have insufficient wettability between iron and titanium carbide [7]. Still, sinterability and mechanical properties of these cermets can be considerably improved by alloying them with elements that act as surfactants and have high affinity to oxygen [8]. Titanium carbide cermet bonded with intermetallic FeAl alloy has demonstrated the combination of excellent high-temperature stability, high hardness, low density and low raw material cost [9,10]. In previous decades, different kinds of steel grades (austenitic and

ferritic) have been used as a binder of TiC-based cermets [11–14]. Alvaredo et al. investigated the sinterability, microstructural development and mechanical properties of a FeCr matrix cermet reinforced with TiCN [15]. They confirmed the presence of M_7C_3 carbides using thermodynamic calculations and data from thermal analysis.

Austenitic stainless steel as a binder phase of TiC-based cermets is relatively popular today among researchers [14,16,17]. Chenxin Jin et al. fabricated TiC-316L stainless steel cermets using a simple melt-infiltration process. They show that a complex core-rim structure was developed and no intermediate or reaction phases were observed [18]. The most commonly used steel is AISI 316L because of its excellent corrosion resistance and good mechanical characteristics. However, there is little information about the use of ferritic stainless steel as a metal matrix for cermets. The reason probably is that chromium containing ferrite has high requirements for thermal processing to maintain the homogeneity of chromium for proper corrosion-resistance performance [19]. The limit of solubility of carbon is much lower in ferritic stainless steels, and the diffusion rates of interstitials are much higher owing to their body-centered cubic structure. In contrast to the face-centered cubic austenitic stainless steels, the diffusion rate of chromium atoms in the body-centered cubic ferritic matrix is approximately 100 times faster [20]. In addition, chromium is known as a very active carbide former and carbon solubility in ferrite is fractional. Chromium carbide formation in cermets decreases the chromium content in stainless steel [19]. It affects the mechanical properties and corrosion resistance of TiC-based chromium containing cermets.

Our aim was to develop and produce TiC-based cermets using ferritic stainless steel as a bonding. Our focus was on the phase transformations, microstructural evolution and sintering peculiarities of TiC-based ferritic corrosion-resistant steel-bonded cermets. Further, based on our studies of microstructural

evolution, we concentrated on the improvement of the microstructure and performance of TiC–FeCr-based cermets.

2. Experimental

Chemical composition and characteristics of initial powders are presented in Table 1. Stoichiometric TiC and ferritic stainless steel (AISI 430L) powder produced by Pacific Particulate Materials Ltd and Sandvik Osprey Ltd., respectively, were used to fabricate TiC–FeCr cermets with the carbide content of 70 wt-%. Additionally, Realizer's austenitic stainless steel (AISI 316L) powder was used to produce reference cermets TiC-316L (see Table 2).

TiC-based cermets were produced using the conventional powder metallurgy method. Titanium carbide and ferritic stainless steel powders were mechanically milled in isopropyl alcohol using a ball mill (WC-Co balls and lining) with a rotating speed of 60 rev min⁻¹ and the charge ratio (ball to powder mass ratio) was 10:1. Powder mixture milling in the ball mill during 72 h using WC-Co balls and lining results in some contamination of alloy with tungsten (see Table 2). After milling, the powder was dried and plasticised with paraffin wax (approximately 1 wt-%). Uniaxially consolidated samples were liquid phase sintered in a vacuum (vacuum level was approximately 0.04 mbar) using a furnace with graphite heaters. Specimens were sintered in vacuum during 30 min at different sintering temperatures (600–1500°C) and the heating rate was 10°C·min⁻¹.

The stability of different phases can be predicted using thermodynamic modelling by the calculation of the phase diagram (CALPHAD) approach. In this approach, free energy from binary systems is extrapolated to obtain free energies of ternary systems by fitting an excess free energy term. Similar extrapolations can be extended to quaternary and quinary systems. A detailed analysis and application of this approach can be found elsewhere [15,21,22].

Table 1. Chemical composition and particle size of initial powders.

Powder	C	Ti	Cr	Ni	Mo	Mn	Si	Fe	Other	Average particle size
	wt-%									μm
TiC	19.1	81.9	–	–	–	–	–	–	0.32	2.6
AISI 430L	–	–	16.8	–	–	0.7	0.6	Bal.	0.04	10 ... 45
AISI 316L	–	–	17.1	10.9	2.3	1.2	0.7	Bal.	0.13	10 ... 45

Table 2. Average calculated chemical composition of TiC-based cermets after milling.

Material	C	Ti	Cr	Ni	Mo	W ^a	Mn	Si	Me ^b	Fe
	wt-%									
TiC-430L	12.7	54.6	4.8	–	–	4.5	0.2	0.2	–	23.0
TiC-430LMe	12.7	54.6	4.6	–	–	4.5	0.2	0.2	1.2	22.0
TiC-316L	12.7	54.6	4.8	3.6	0.8	4.5	0.4	0.3	–	18.3

^aContamination with tungsten as a result of ball milling with WC-Co balls.

^bStrong carbide-forming element.

For thermal analysis, the samples were analysed using a NETZSCH STA 449 F3 Jupiter® TG-DSC apparatus. The samples were heated in a pure argon (5.0) atmosphere from 40°C to 1240°C using constant heating rates set to 5°C/min and 20°C/min. A protective gas flow of 50 mL/min was used. The samples were analysed in Pt/Rh alloy crucibles with removable thin-walled liners of Al₂O₃. In order to eliminate buoyancy effects during the furnace heat-up cycle, background mass data were recorded during empty crucible experiments and subtracted from each of the measurement data sets. The temperature of the apparatus was calibrated using In, Sn, Zn, Al and Au standards.

Microstructural analysis was carried out using a scanning electron microscope (SEM) JOEL JSM 840A. Distribution of chemical elements in the cermets was analysed using X-ray spectroscopy (EDS). Phase identification of cermets was carried out using X-ray diffraction (XRD) with a Rigaku (D.Max.C) X-ray diffractometer (having CuK α ($\lambda = 1.5405\text{\AA}$) radiation and Ni filter operated at 30 kV and 20 mA). The porosity of the cermets was determined using an optical microscope Axiovert25 and software Buehler Omnimet. The density was measured according to the Archimedes' method. The porosity was evaluated by measuring the surface area of pores on the optical image of the microstructure at magnification 200 times.

Indentation fracture toughness and hardness were determined using ground and polished specimens of 5 × 5 × 17 mm. Hardness (Vickers hardness) was measured in accordance with the standard EN-ISO-6507. The fracture toughness (K_{IC} , MPa·m^{1/2}) was determined using the method of fracture by indentation with the most commonly used empirical equations for fragile materials proposed by Evans [23]: $K_{IC} = 0.16 \cdot (c/a)^{-1.5} \cdot (H \cdot a^{1/2})$, where c is the average length of the cracks obtained in the tips of the

Vickers indentations (μm); a is the half average length of the diagonal of Vickers indentations (μm); H is Vickers hardness (MPa).

3. Results and discussion

3.1. Densification

Density (measured and relative densities as against calculated density) and mass loss of TiC-430L cermets depending on sintering temperatures are presented in Figure 1. Density values clearly shows that densification of samples starts at temperatures over 1100°C. It shows the formation of the liquid phase at even low sintering temperatures below 1300°C. The mass loss during sintering does not include the loss due to the evaporation of paraffin wax. In the calculated density of cermet composition, the formation of new phases and dissolution or evaporation of chemical elements were not taken into account. The microstructure of the cermets clearly showed the increased apparent density with increasing sintering temperature, as shown in Figure 1. Fully dense cermets were obtained at the sintering temperature of 1500°C.

Results of Aigner et al.'s experiments [24] with Fe-TiC cermets demonstrate that oxygen is almost completely removed within solid-state reactions at temperatures lower than 1150°C. It is also known that Cr₂O₃ starts to decompose because of the low stability of this oxide at temperatures above 900°C [20]. In our research, also minor mass loss took place at temperatures below 1300°C. Significant changes in the mass loss of the cermets (see Figure 1) occurred during sintering at temperatures exceeding 1300°C when the liquid phase of eutectic nature was formed (see Figure 2(a)). Eutectic transformation of α -Fe-TiC takes place at temperatures around 1300°C [25]. One of the reasons for mass loss is the high vapour pressure of chromium – the vacuum level during

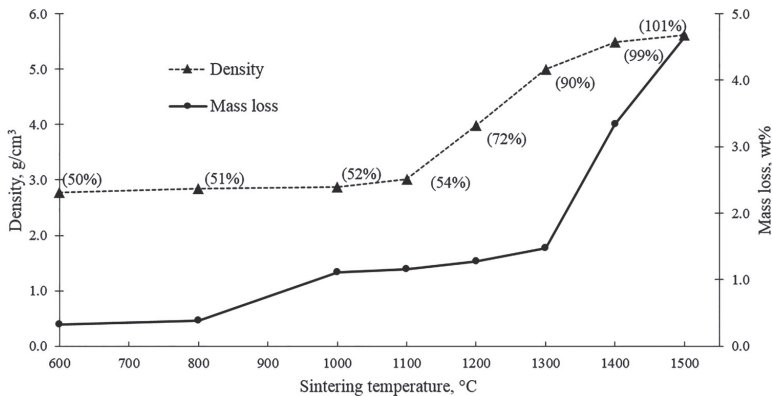


Figure 1. Relative (in brackets) and measured density and mass loss of TiC-430L cermets depending on the sintering temperature.

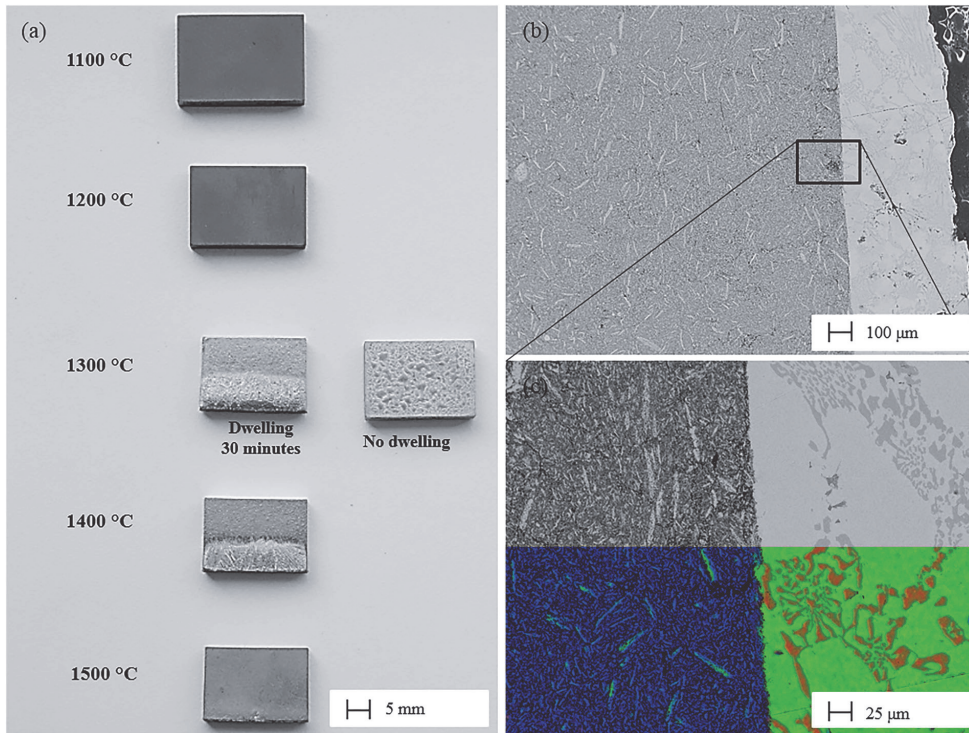


Figure 2. TiC-430L cermet specimens after sintering at different temperatures, dwelling time 30 min (a); SEM image of the cross-section (b) and results of EDS mapping (c): blue – titanium, red – chromium and green – iron.

sintering was approximately 0.04 mbar and the vapour pressure of chromium at 1400°C was approximately 0.01 mbar. Vacuum sintering with the presence of the liquid phase also intensifies the evaporation of iron (compare the calculated chemical composition of TiC-430L cermet in Tables 2 and 4). The higher the sintering temperature, the higher is Fe and Cr loss (see Figure 1).

Figure 2 demonstrates the appearance of specimens after sintering at different temperatures and SEM images of the cross-sections of the liquid phase on the surface of samples. Samples were sintered on the longer edge of specimens with dwelling during 30 min. Therefore, the liquid phase is perched down along the side surfaces but in the case of samples sintered without dwelling at final temperature, the liquid phase is spread out along the surface. Although the liquid phase is formed during sintering at the temperature of 1300°C, the liquid binder is not fully soaked up by the porous core. This is a sign of insufficient sinterability. Wetting ability of the liquid phase improves significantly with the increase of the sintering temperature.

The cross-section clearly demonstrates that the metallic phase on the surface of samples has a two-phased structure (see Figure 2(c)). According to

EDS analysis, those phases are ferrite (light grey) and metal carbide (dark grey, see Table 3). It shows that during the liquid phase sintering, carbon from TiC interacts with chromium and iron and forms complex carbides. In ferrite, the chromium content is lower than in the initial powder – 9.6 and 16.8 wt-%, respectively. In the second phase, the high content of carbon clearly indicates the presence of metal carbide with Cr:Fe ratio about 1:1. Our continuing research with WC-FeCr systems also demonstrated the formation of metal carbides with similar chemical composition.

3.2. Phase transformations

In general, metal carbides do not exist as an isolated pure species. When several carbide-forming elements that share the same crystal structure are present, the

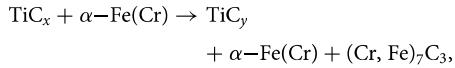
Table 3. EDS analysis of the metallic phase on the surface of TiC-430L cermets (sintering temperature 1300°C, see Figure 2).

	Chemical composition, wt-%						
	C	Ti	Cr	W	Mn	Si	Fe
Total	5.2	0.5	16.7	–	3.3	0.6	73.7
Ferrite	–	–	9.6	–	3.5	1.0	85.9
Metal Carbide	9.7	0.6	46.0	–	3.3	–	40.4

formed carbide will be present as a combination of those elements. As an example, an iron-based alloy containing Cr will consist of complex carbide $(\text{Cr, Fe})_x\text{C}_y$, rather than simple Cr_xC_y carbide [26]. Because of the differences in solubility of carbon in $\gamma\text{-Fe}$ and $\alpha\text{-Fe}$, there evolve free carbon during cooling from sintering temperature and different types of metal carbides can be formed.

XRD patterns of TiC–FeCr cermet after sintering at 800–1500°C are presented in Figure 3. As it follows from the figure, as-milled powder mixture consists of three phases: titanium carbide, ferrite and tungsten carbide. The latter is the result of contamination from the milling equipment. After sintering at 800°C for 30 min, the transformation of phases took place – additional M_7C_3 phase appeared during solid-state sintering. After sintering at 1200°C for 30 min, WC lines disappeared as WC dissolves mainly in the inner rim of titanium carbide [6]. During the sintering in the temperature range 1200–1500°C for 30 min, no remarkable changes in phase composition occurred (see Figure 3). The composite consists of three main phases: chromium ferrous complex carbide $(\text{Cr, Fe})_7\text{C}_3$, solid solution $\text{Fe}(\text{Cr})$ and titanium carbide TiC. The phase transformation during the liquid

phase (1300–1500°C) sintering of the TiC–FeCr alloy can be described as follows:



where $x > y$.

Although during sintering at temperatures over 1200°C, XRD patterns (see Figure 3) demonstrate three main phases (TiC, M_7C_3 , $\alpha\text{-Fe}$), additional traces of the following phases have been detected: M_{23}C_6 , M_3C , M_6C and $\gamma\text{-Fe}$ (see Figure 4). The residual $\gamma\text{-Fe}$ is the result of the unfinished allotropic change $\text{Fe}_\gamma\text{-Fe}_\alpha$ during cooling. Traces of different types of carbides M_xC_y , are results of the decomposition $\gamma\text{-Fe}$ during cooling with sintering furnace and formation of a metastable structure. The similar phase transformations show also reference TiC-316L cermet (see Figure 4).

Phase transformation calculations indicate that it is highly probable to have both TiC and M_7C_3 -type carbide particles in sintered samples. The following thermodynamic equations provide information about the reactions in the system Ti–C–Fe–Cr [26,27]:

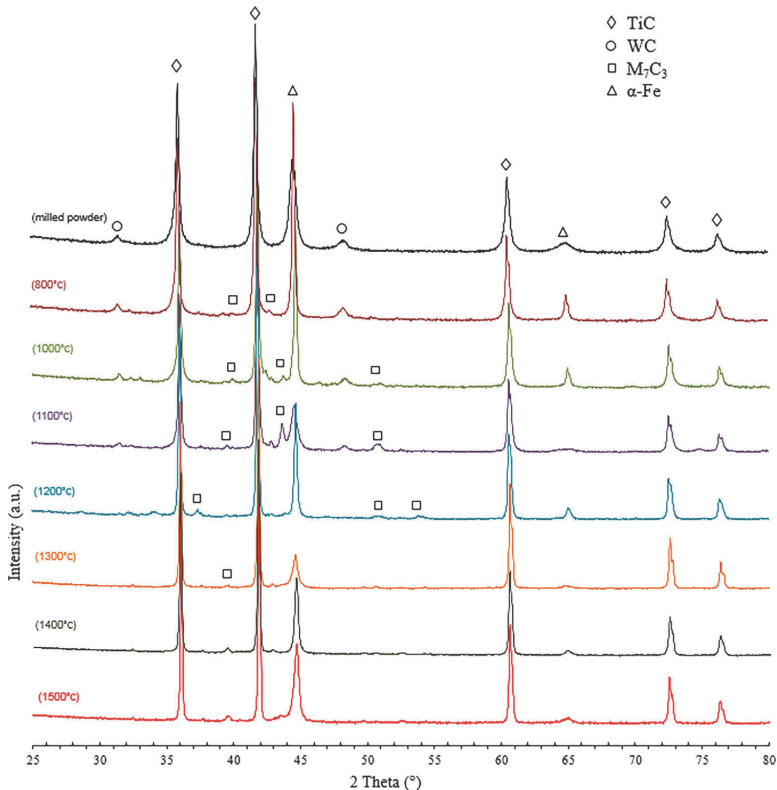
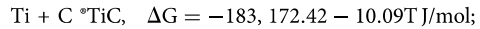


Figure 3. XRD pattern of TiC-430L cermet sintered at different temperatures.

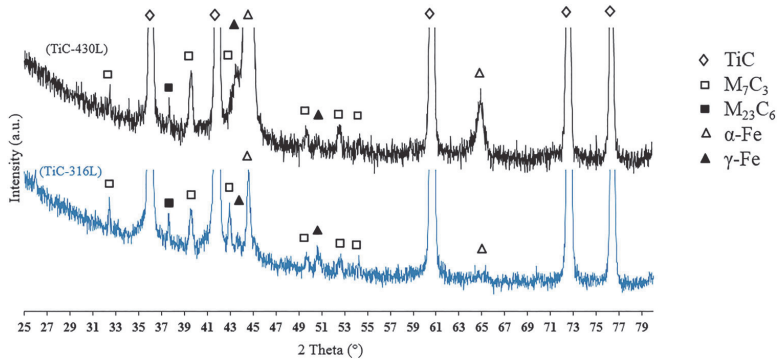


Figure 4. XRD pattern of TiC-based cermets: TiC-316L (bottom) and TiC-430L (top).

$$\begin{aligned} \frac{23}{6}\text{Cr} + \text{C} &\rightarrow \frac{1}{6}\text{Cr}_{23}\text{C}_6, \Delta G \\ &= -53,729.18 - 12.77T \text{ J/mol}; \end{aligned}$$

$$\begin{aligned} \frac{7}{27}\text{Cr}_{23}\text{C}_6 + \text{C} &\rightarrow \frac{23}{27}\text{Cr}_7\text{C}_3, \Delta G \\ &= -125,541.14 - 31.02T \text{ J/mol}; \end{aligned}$$

$$\begin{aligned} \frac{3}{5}\text{Cr}_7\text{C}_3 + \text{C} &\rightarrow \frac{7}{5}\text{Cr}_3\text{C}_2, \Delta G \\ &= -41,198.09 - 11.05T \text{ J/mol}; \end{aligned}$$

$$3\text{Fe} + \text{C} \rightarrow \text{Fe}_3\text{C}, \Delta G = -53,416.00 + 55.68T \text{ J/mol}.$$

The equations prove that the Gibbs free energy of TiC and Cr_7C_3 formation are thermodynamically more probable than those of other metal carbides. Although the equations are useful in equilibrium conditions, they enable us to predict phase transformation. According to the equilibrium phase diagram composed using Thermocalc software obtained by Alvaredo et al., in the case of the higher content of carbon (4–5 wt-%) at room temperatures, TiCN-FeCr cermets have a three-phased structure: TiCN, α -Fe and M_7C_3 carbide [15].

The differential scanning calorimetry analysis (DSC) was carried out to determine the temperatures of phase transformations. Heat-up followed by cooling was used to imitate real sintering cycle up to 1240°C (see Figure 5) when most of the carbides formed. The two pronounced changes in the DSC curve at the temperature of 600°C (heating and cooling) are due to the change in the heating and cooling rates. Also, at the end of heating at 1240°C, the DSC curve showed a marked change. The DSC curve indicates that endothermic effects dominate during the sintering process over the measured temperature range. On the DSC graph, three endothermic peaks were observed. The first one peak at temperatures up to 600°C arises from the reduction of oxides [20,21]. The second peak with a maximum at approximately 1200°C is thought to arise from the formation and the decomposition of different metal carbides. The result is in line with the XRD analysis (see Figure 3), where remarkable changes occurred in the XRD diagrams at sintering at temperatures up to 1200°C. The third endothermic reaction with a maximum at 1150°C is attributed to the M_7C_3 formation from the decomposed γ -Fe during cooling.

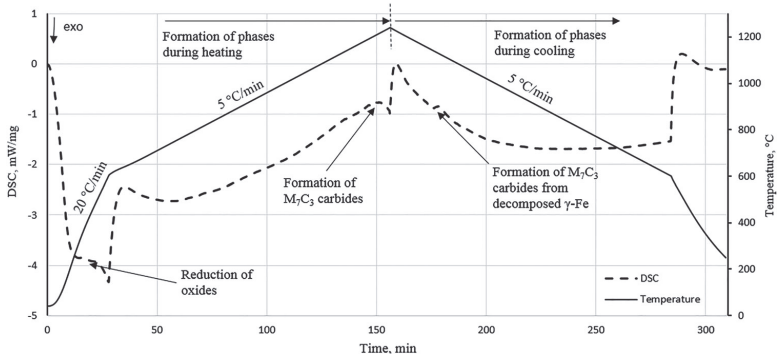


Figure 5. Differential scanning calorimetry thermogram for the TiC-430L system (heating and cooling).

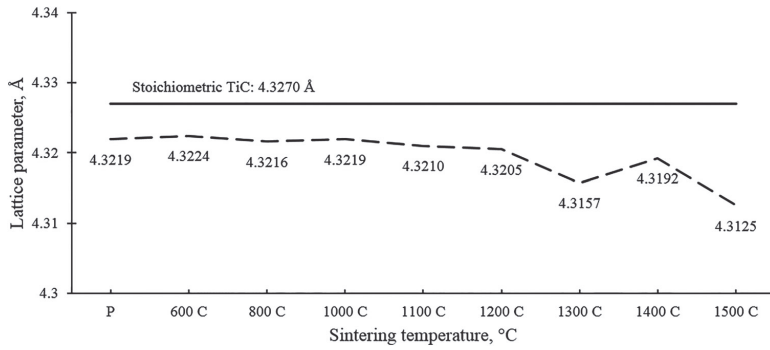


Figure 6. Lattice parameter of TiC particles from samples sintered at different temperatures and lattice parameter of stoichiometric TiC.

Carbon content in TiC after sintering at 1500°C is much lower than in the initial carbide powder. Figure 6 demonstrates the lattice parameter of TiC dependent on the sintering temperature. For comparison, the lattice parameter of stoichiometric TiC is also plotted [27]. The displacement of the diffraction angle of the peaks respective to the TiC phase confirms the decrease of the lattice parameter. This clearly indicates that TiC is nonstoichiometric in TiC-FeCr cermets and other carbides can be formed.

3.3. Evolution of microstructure

Figure 7 shows the microstructures of cermets sintered at different temperatures. Distribution of the binder is significantly improving with the increase of the sintering temperature. The reason is that the wetting angle between the binder and the carbide grains decreases with the increase of the sintering temperature. Also, the liquid phase is soaked up by the porous core at higher sintering temperatures. Despite that, cermets

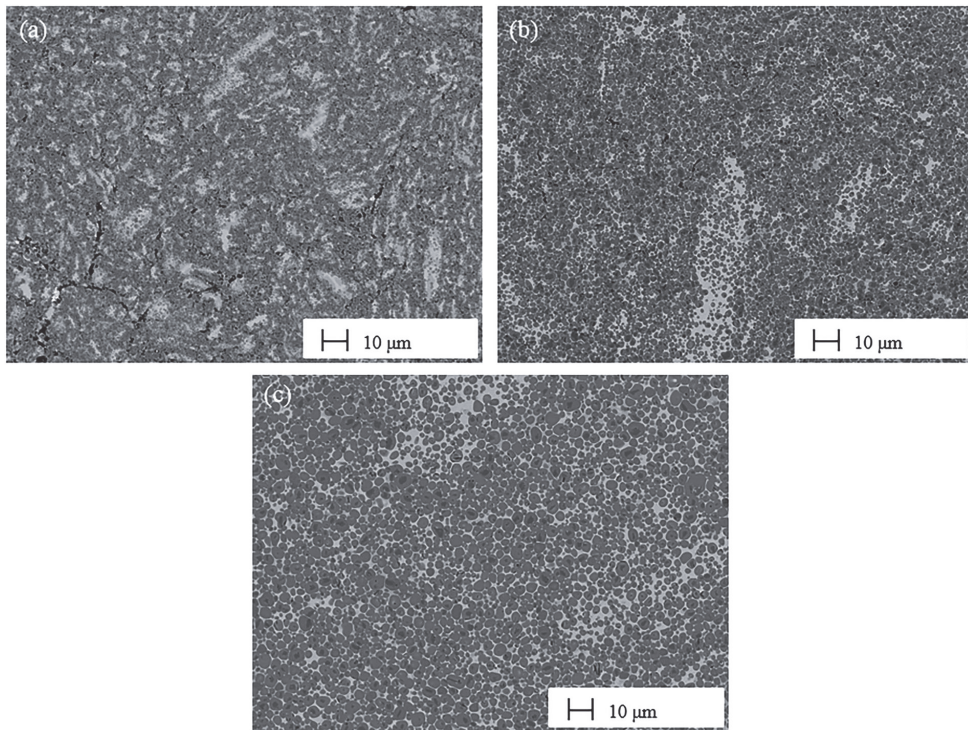


Figure 7. Microstructure of cermets sintered at different temperatures: 1300°C (a), 1400°C (b), 1500°C (c).

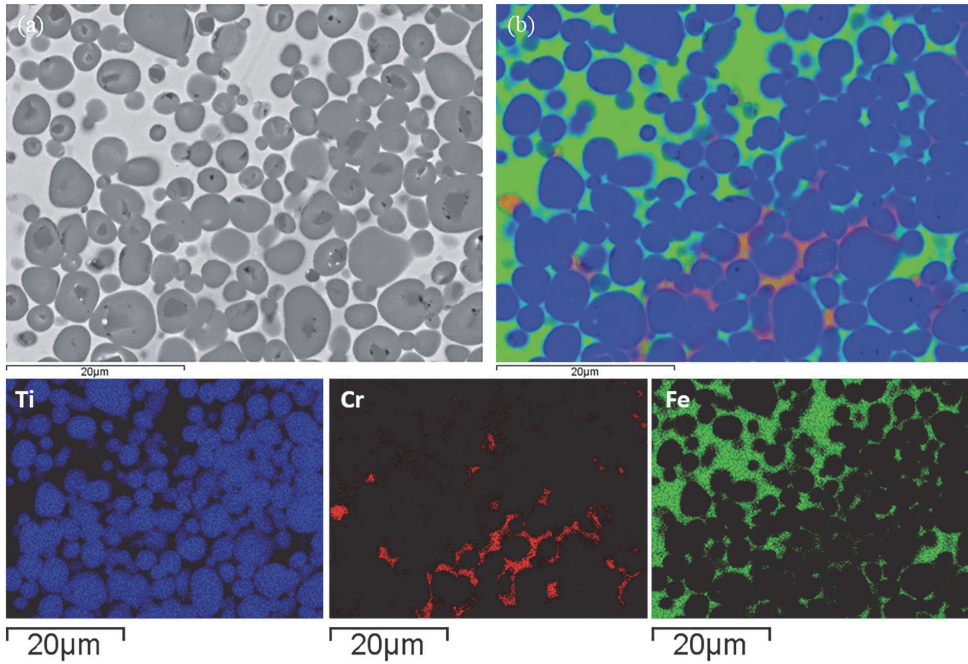


Figure 8. SEM image (a) and EDS mapping of TiC-430L cermet sintered at 1500°C during 30 min (b): blue – titanium, red – chromium and green – iron.

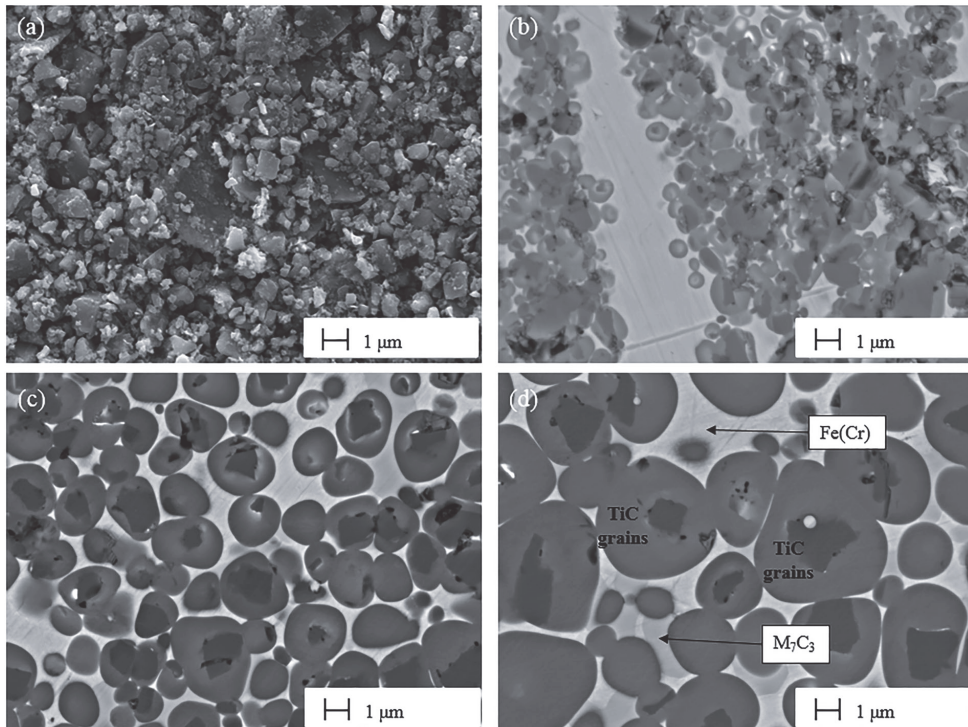


Figure 9. Microstructures of milled powder (a) and TiC-430L cermet sintered at different temperatures: 1300°C (b), 1400°C (c), 1500°C (d).

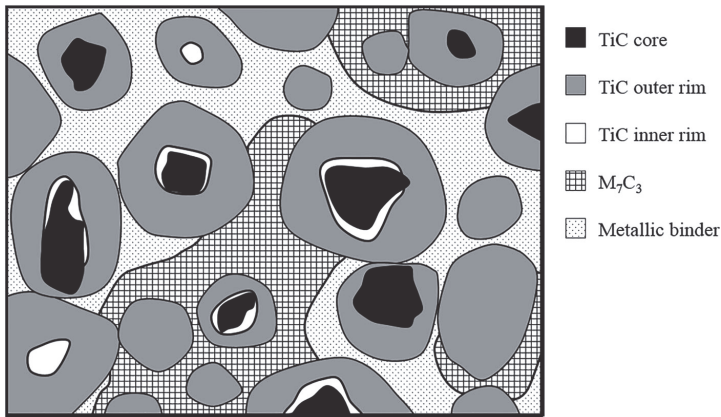


Figure 10. A SEM schematic of TiC-430L cermet.

Table 4. EDS analysis of TiC-430L cermet after sintering at 1500°C.

1500°C	Chemical composition, wt-%						
	C	Ti	Cr	W ^a	Mn	Si	Fe
Total	14.2	58.4	4.5	4.8	0.5	–	17.6
Binder	–	6.6	4.6	–	1.8	1.0	86.0
Metal Carbide	10.2	10.1	37.3	0.8	2.1	–	39.5
TiC outer rim	15.1	77.4	0.9	6.0	–	–	0.6
TiC inner rim	16.5	68.2	1.2	12.0	–	–	2.1
TiC core	15.9	81.4	0.3	2.0	–	–	0.4

^aContamination with tungsten as a result of ball milling using WC-Co balls.

Table 5. EDS analysis of TiC-430LMe (Me – strong carbide former) cermet after sintering at 1400°C.

	Chemical composition, wt-%							
	C	Ti	Cr	W ^a	Mn	Si	Me	Fe
Total	14.8	53.4	5.2	4.5	–	–	1.1	21.0
Binder	–	4.7	6.7	0.3	0.5	0.9	–	86.9
Metal Carbide, M ₇ C ₃	12.8	21.6	35.8	2.0	–	–	0.5	27.3
TiC outer rim	16.4	72.3	1.0	5.6	–	–	1.5	3.2
TiC inner rim	16.5	63.0	1.3	12.1	–	–	3.2	3.9
TiC core	17.5	76.6	1.2	2.3	–	–	0.7	1.7

^aContamination with tungsten as a result of ball milling using WC-Co balls.

sintered at 1500°C do not exhibit fully homogeneous microstructure (Figure 7(c)).

Figure 8 demonstrates elemental signals of three metals (Ti, Fe and Cr). As can be seen, both chromium and iron are unevenly distributed in the microstructure of the cermets. It is the result of the formation of the M₇C₃ carbides during sintering, and consequently, chromium content in the metallic binder is significantly decreased.

Microstructure of TiC-based cermets consolidated during vacuum sintering is characterised by carbides with TiC core, exhibiting a ‘core-rim’ structure and M₇C₃ carbides, bonded with a metallic phase (Figures 9). The inner and outer rim of TiC could be differentiated; the inner rim is very thin and unevenly distributed around the cores. Figure 9 (see the dark grey region of binder) shows the formation of M₇C₃. The light grey region is the solid solution of chromium in the iron matrix. Figure 10 shows schematically of the microstructure of sintered TiC-FeCr cermet.

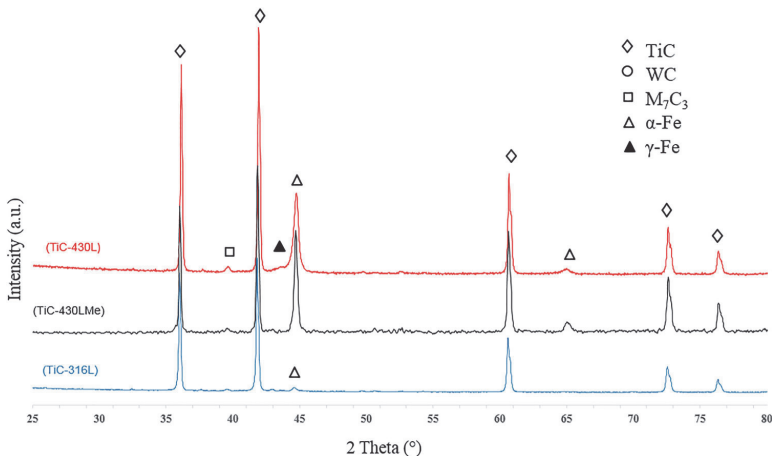


Figure 11. XRD patterns of TiC-based cermets: TiC-430L (top), TiC-430LMe (middle) and TiC-316L (bottom).

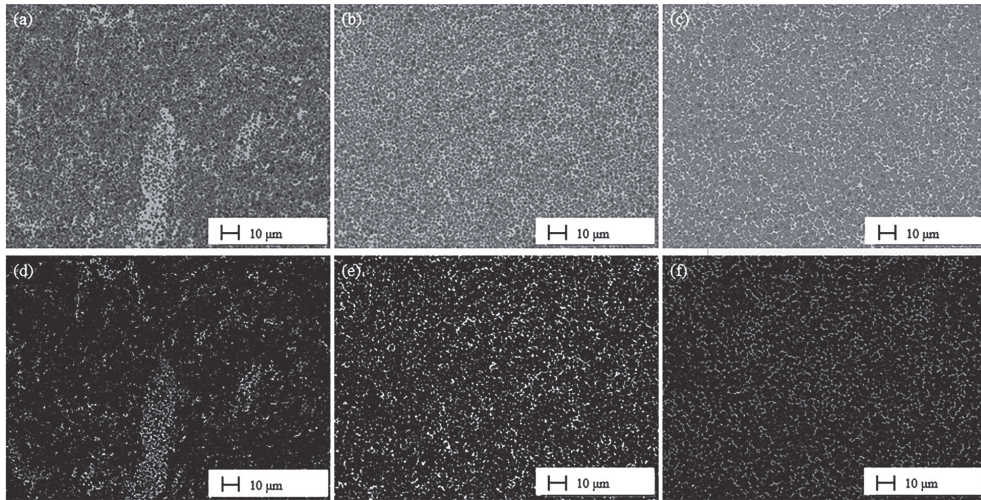


Figure 12. Microstructures (SEM) and binder distribution of TiC-430L, 1500°C (a and d, respectively), TiC-430LMe, 1400°C (b and e) and TiC-316L, 1500°C (c and f).

The EDS results summarised in Table 4 indicate that the total content of chromium and iron has decreased due to the evaporation during vacuum sintering. Here, the metallic binder phase contains approximately 5 wt-% of chromium, which is markedly less than in the initial ferritic steel powder (16.8 wt-%). Therefore, in addition to volatilisation in vacuum, some part of chromium dissolves in TiC and takes part in the formation

of M_7C_3 carbides. According to the EDS results, the TiC rim phase contains a large amount of tungsten. The inner rim had a significantly higher tungsten content than the outer one.

The hypothesis is that it should be possible to improve microstructural homogeneity and increase chromium content in the metallic binder by alloying with elements exhibiting higher affinity to carbon

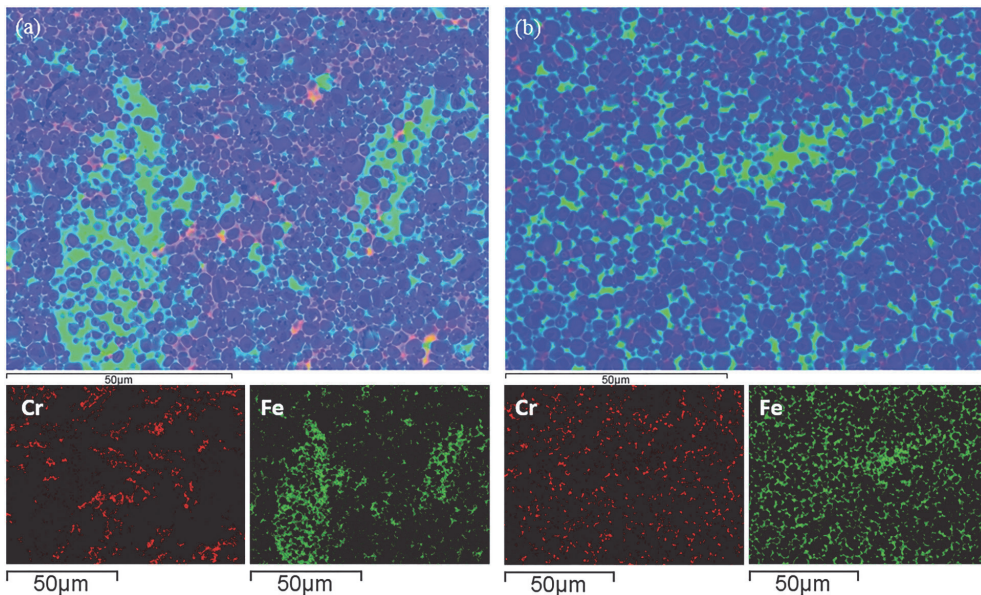


Figure 13. EDS mapping results of TiC-430L (a) and TiC-430LMe (b) cermets sintered at 1500 and 1400°C, respectively during 30 min, : red – chromium and green – iron.

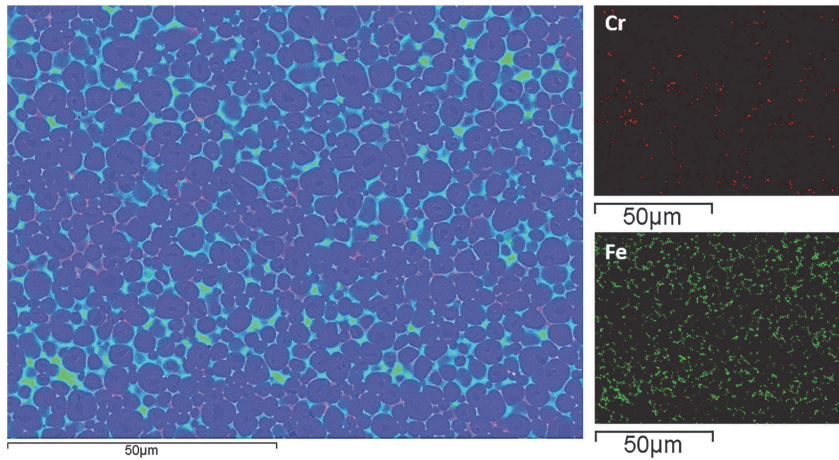


Figure 14. EDS mapping results of TiC-316L (left) and elemental distribution (right): red – chromium and green – iron.

Table 6. Mechanical properties of TiC-430L and TiC-430LMe cermet.

	Sintering temperature, °C	Hardness, HV30	Indentation fracture toughness, MPa·m ^{1/2}	Porosity, %	Density, g/cm ³
TiC-430L	1300	1081 (±47)	n/a	10.81	5.00
	1400	1388 (±16)	10.1 (±0.2)	0.45	5.49
	1500	1459 (±36)	10.0 (±0.3)	0.34	5.62
TiC-430LMe	1400	1104 (±10)	10.4 (±0.2)	0.31	5.66
TiC-316L	1500	1158 (±20)	11.0 (±0.3)	0.56	5.55

than chromium. It is known that elements with high affinity to carbon (Ti, Nb, Ta) are used for alloying of corrosion-resistant steels. These elements improve the grain refining and retard recrystallisation and precipitation hardening. These effects, in turn, increase the toughness, strength, formability and weldability [28]. These elements have low solubility in ferrite and they are strong carbide formers. In cermet TiC-430LMe, the majority of strong carbide former dissolve in the rim of TiC (more in the inner rim, like tungsten) but it also dissolves in the M_7C_3 carbide (see Table 5). The most significant differences between EDS patterns of TiC-430L and TiC-430LMe (compare Tables 4 and 5) are the marked increase of Ti content in M_7C_3 carbide and the increase of chromium fraction in the metallic binder. Nevertheless, according to the XRD analysis, no remarkable differences were found in the phase composition of TiC-430L and TiC-430LMe cermets because the majority of Me dissolves in TiC (see Table 5). Both cermets and reference one exhibit mainly three-phased structure: TiC, α -Fe and M_7C_3 carbide (see Figure 11).

Strong carbide former improves the distribution of the binder phase and the structural homogeneity (see Figure 12) of the cermets even at lower sintering temperatures (1400°C), which has a positive effect on the distribution of the chromium and iron in the structure of the cermets. Figure 13 clearly demonstrates the more

even distribution of Cr (red) and Fe (green). Increase in the binder chromium content of TiC-430LMe cermets is proved by the EDS analysis (Table 5).

Prevalently austenitic stainless steel is used as a binder phase [14,16,17]. The most commonly used steel is AISI 316L. In our research, cermet with austenitic AISI 316L steel was used as the reference material. Our result demonstrated that both TiC-316L and TiC-430LMe cermets exhibit microstructural homogeneity (compare Figure 12(b,e and c,f)) and also homogeneity of Cr and Fe distribution (compare Figure 13(b) and Figure 14). In all cermets, the formation of M_7C_3 -type carbides was revealed (see XRD patterns on Figure 11). This result is different from C. Jin et al.'s where no intermediate or reaction phases formed during sintering of TiC-316L cermets [18].

3.4. Mechanical characteristics

Mechanical properties and porosity of TiC-AISI 430L and TiC-AISI 430LMe cermets as well as reference on TiC-316L are presented in Table 6.

4. Conclusion

Our focus was on the phase transformations, microstructural evolution and sintering peculiarities of TiC-based corrosion-resistant ferritic AISI 430L

steel-bonded cermets. Cermet with austenitic AISI 316L steel was used as the reference material. Microstructure analysis (SEM), X-ray spectroscopy (EDS), XRD and DSC resulted in the following conclusions:

- Sintered TiC–ferritic FeCr (AISI 430L) as well as TiC austenitic FeCrNi (AISI 316L) steel composites consist of three main phases – titanium carbide TiC with coaxial structure, metal carbide M_7C_3 , iron-based solid solution Fe(Cr). Formation of the M_7C_3 phase takes place at temperatures below 1200°C.
- Evaporation during vacuum sintering, formation of metal carbides M_7C_3 and solution in TiC result in a decrease of Cr content in the metallic binder. Formation of metal carbides M_7C_3 causes the heterogeneous distribution of Cr in a composite.
- Formation of M_7C_3 -type carbides is accompanied by the formation of nonstoichiometric TiC during sintering.
- Alloying by strong carbide formers enables us to improve both the metallic phase and the elemental Fe and Cr distribution of TiC-AISI 430L steel cermets.

Disclosure statement

No potential conflict of interest was reported by the authors.

Funding

This work was supported by institutional research fundings IUT (19–29) and IUT (19–4) of the Ministry of Education and Research and by the European Regional Development Fund project TK141 ‘Advanced materials and high-technology devices for energy recuperation systems’.

Notes on contributors

Märt Kolnes is an early Stage Researcher at Department of Mechanical and Industrial Engineering.

Jakob Kübarsepp is a Professor at Department of Mechanical and Industrial Engineering.

Arvo Mere is an Associate Professor at Department of Cybernetics and Senior Research Scientist at Department of Materials and Environmental Technology.

Mart Viljus is a Senior Research Scientist at Department of Mechanical and Industrial Engineering.

Birgit Maaten is an Early Stage Researcher at Department of Energy Technology.

Marek Tarraste is an Early Stage Researcher at Department of Mechanical and Industrial Engineering.

ORCID

Arvo Mere  <http://orcid.org/0000-0001-9070-3970>

Birgit Maaten  <http://orcid.org/0000-0002-4641-1484>

Marek Tarraste  <http://orcid.org/0000-0003-3269-9648>

References

- [1] Kenneth JA. Brooks, world directory and handbook of hardmetals and hard materials. 6th ed. London: International Carbide Data; 1996.
- [2] European Commission homepage. [cited 2017 Feb 28]. Available from: <https://ec.europa.eu/growth/sectors/raw-materials/specific-interest/critical/>.
- [3] Janikowski DS. Super-ferritic stainless steels rediscovered. Proc. Stainless Steel World 2005, Holland; 2005.
- [4] Gries B, Prakash L. Acute inhalation toxicity by contact corrosion – the case of WC–Co. Proceedings of Euro PM 2007; Toulouse. 2007.
- [5] European Chemicals Agency homepage. 2017 [cited 2017 Mar 8]. Available from: <http://echa.europa.eu/substance-information/-/substanceinfo/100.028.283/>.
- [6] Mari D, Llanes L. Hardmetals. In: VK Sarin, editor. Comprehensive hard materials. Oxford: Elsevier; 2014. p. 3–538.
- [7] Humenik Jr M, Parikh NM. Cermets: I, fundamental concepts related to micro-structure and physical properties of cermet systems. J Amer Ceram Soc. 1956;39:60–63.
- [8] Kübarsepp J. Production of high chromium alloys TiC-FeCr alloyed with silicon. Powder Metall Met Ceram. 1986;25:410–414.
- [9] Subramanian R, Schneibel JH, Alexander KB. Iron aluminide-titanium carbide composites – microstructure and mechanical properties. Scr Mater. 1996;35:583–588.
- [10] Li J, Liu Q, Shi R, et al. Preparation and mechanical properties of Fe3Al(Ti)/TiC composites. J Mater Process Tech. 2008;208:105–110.
- [11] Kübarsepp J, Reshetnyak H, Annuka H. Characterization of the serviceability of steel-bonded hardmetals. Int J Refr Met Hard Mater. 1993;12:341–348.
- [12] Akhtar F, Guo SJ. Microstructure, mechanical and fretting wear properties of TiC-stainless steel composites. Mater Charact. 2008;59:84–90.
- [13] Kolnes M, Kübarsepp J, Viljus M, et al. Effect of sintering conditions on microstructure and performance of TiC-FeCrMn cermets. Proc. World PM 2016; Hamburg. 2016.
- [14] Onuoha CC, Kipouros GJ, Farhat ZN, et al. The effects of metal binder content and carbide grain size on the aqueous corrosion behaviour of TiC-316L stainless steel cermets. Int J Refr Met Hard Mater. 2014;44:129–141.
- [15] Alvaredo P, Tsipas SA, Gordo E. Influence of carbon content on the sinterability of an FeCr matrix cermet reinforced with TiCN. Int J Refr Met Hard Mater. 2013;36:283–288.
- [16] Onuoha CC, Jin C, Farhat ZN, et al. The effect of TiC grain size and steel binder content on the reciprocating wear behaviour of TiC-316L stainless steel cermets. Wear. 2016;350–351:116–129.
- [17] Jin C, Onuoha CC, Farhat ZN, et al. Reciprocating wear behaviour of TiC-stainless steel cermets. Tribol Int. 2017;105:250–263.
- [18] Jin C, Plucknet KP. Microstructure instability in TiC-316L stainless steel cermets. Int J Refract Met Hard Mater. 2016;58:74–83.
- [19] McGuire MF. Metallurgy. In: Stainless steels for design engineers. ASM Int., Ohio; 2008. p. 1–11.
- [20] Klar E, Samal PK. Sintering and corrosion resistance. In: Powder Metallurgy Stainless Steels: Processing,

- Microstructures, and Properties. ASM Int., Ohio; 2007. p. 59–100.
- [21] Shatynski SR. The thermochemistry of transition metal carbides. *Oxid Met.* 1979;13:105–118.
- [22] Emamian A, Corbin SF, Khajepour A. In-situ deposition of metal matrix composite in Fe-Ti-C system using laser cladding process. In: Cuppoletti J editor. *Metal, Ceramic and Polymeric Composites for Various Uses*, InTech; 2011.
- [23] Evans AG, Charles EA. Fracture toughness determinations by indentation. *J Amer Ceram Soc.* 1976;59:371–372.
- [24] Aigner K, Lengauer W, Ettmayer P. Interactions in iron-based cermet systems. *J Alloy Comp.* 1997;262–263:486–491.
- [25] Jonsson S. Assessment of the Fe-Ti-C system, calculation of the Fe-Ti-N system, and prediction of the solubility limit of Ti(C,N) in liquid Fe. *Metall Mater Trans B.* 1998;29:371–384.
- [26] Fahlman BD. *Materials chemistry*. Heidelberg: Springer; 2011.
- [27] Potanin AY, Levashov EA, Pogozhev YS, et al. The features of combustion and structure formation of ceramic materials in the TiC-Ti₃PO_x-CaO system. *Ceram Int.* 2015;41:8177–8185.
- [28] Mohrbacher H. The effects of niobium microalloying in second generation advanced high strength steels. *International Steel Technologies Symposium 2008*; Taiwan. 2008.

Paper II

Kolnes, M., Kübarsepp, J., Kollo, L., Viljus, M. Characterization of TiC-FeCrMn cermets produced by powder metallurgy method. *Materials Science (Medžiagotyra)*, 2015, 21 (3), 353–357.

Characterization of TiC-FeCrMn cermets produced by powder metallurgy method

Märt KOLNES^{1*}, Jakob KÜBARSEPP¹, Lauri KOLLO¹, Mart VILJUS²,

¹ Department of Materials Engineering, Tallinn University of Technology, Ehitajate tee 5, 19086 Tallinn, Estonia

² Centre for Materials Research, Tallinn University of Technology, Ehitajate tee 5, 19086 Tallinn, Estonia

crossref <http://dx.doi.org/10.5755/j01.ms.21.3.7364>

TiC-NiMo cermets combine relatively low density with high hardness. Because nickel is known as a toxin and allergen and allergy to nickel is a phenomenon which has assumed growing importance in recent years there has been a flurry of activity to find alternatives to the nickel binder in cermets. It is also the global research and technical development trend in the powder metallurgy cermets industry. In present research TiC-based cermets with FeCrMn binder system were fabricated. Three different sintering conditions were used (vacuum sintering, sinter/HIP and sintering under low Ar pressure). Because of high vapor pressure of manganese different sintering conditions and technologies were investigated to depress the Mn-loss during sintering. Chemical composition of TiC-FeCrMn cermets after different sintering conditions were analyzed by energy-dispersive X-ray spectroscopy (EDS) and mechanical properties – hardness and fracture toughness were evaluated on samples. Results of research showed that Ni-free TiC-based CrMn-steels bonded cermets compare unfavourably with cermets bonded with CrNi austenitic steels in terms of fracture toughness and corrosion resistance. Noticeable Mn-loss during vacuum sintering can be avoided when sintering under low Ar gas pressure.

Keywords: Ni-free cermets, austenitic stainless steel, titanium carbide-base cermets, pressurized sintering, manganese loss.

1. INTRODUCTION

Stainless steels containing more than 12% Cr have been proved to be the most used corrosion resistant materials due to their good mechanical properties and fabricability. The most frequently used corrosion resistant materials are conventional stainless austenitic steels. Such steels contain in addition to chromium (16 ... 23 wt%) a large amount (10 ... 28 wt%) of nickel because nickel is the primary austenite stabilizing element. However, the greatest drawback with conventional stainless steel is susceptibility to localized corrosion in chloride-containing aqueous solutions. The alloying elements that increase the resistance of corrosion resistant steels to pitting and crevice corrosion are chromium, molybdenum and nitrogen [1]. Content of molybdenum in austenitic steels used in chloride containing aqueous solutions is usually 2 ... 8 wt%.

REACH (The Regulation on Registration, Evaluation, Authorization and Restriction of Chemicals) is classifying Ni and Co as very toxic for human health [2]. The reports of metallic allergy and toxicity caused by these metals is increasing. Therefore removal of Ni from stainless steel for a number of applications is largely demanded.

Ni-free austenitic stainless steels having a large amount (wt %) of manganese and nitrogen such as Fe- (15-23)Cr- (10-24) Mn- (0.5-6) Mo- (0.85-1.1)N have been developed. In such steels manganese and nitrogen are employed instead of nickel to obtain austenitic phase [3, 4].

Hardmetals (WC-based ceramic metal composites) are extensively used in applications demanding wear resistance, e.g. metal cutting or forming tools. The excellent wear resistance exhibited by the hardmetals is due to their combination of high hardness, wear resistance and moderate fracture toughness [5]. The most common are hardmetals WC-Co. Cobalt is widely used as the binder metal because of its good wetting behaviour and good mechanical properties. However, cobalt has been in short supply and there are toxicity concerns. Additionally, in accordance to United States National Toxicology Program (NTP) the tungsten carbide-cobalt hardmetal dust has been shown to be more toxic in combination than either pure cobalt or tungsten carbide alone [6]. Therefore, there have been activities to find alternatives to the cobalt binder in hardmetals. The alternative to cobalt as a binder is either iron based or nickel based. From the health and safety aspect, nickel as a binder metal in hardmetals does not offer any advantage. On the other hand, the complete substitution of nickel for cobalt has proven to be the most effective means of extending the life of hardmetal in highly corrosive environments. Literature on the advantages and disadvantages of using iron as an alternative base component of binder shows that replacing cobalt (as well as nickel) by application tailored iron base grades is possible, but more research work is necessary [7, 8].

Previous research carried out in Tallinn University of Technology has proved possibility to produce and employ cobalt and tungsten free cermets on basis of titanium carbide produced using powder metallurgy press-and-sinter process. Vacuum sintering has been and is usually used for titanium carbide based cermets [9, 10, 11].

¹ Corresponding author. Tel.: +372-620-3357; fax: +372-620-3196.
E-mail address: mart.kolnes1@ttu.com (M. Kolnes)

Mechanical properties (hardness, transverse rupture strength, plasticity, strain energy and fracture toughness) of iron-alloy (steel) bonded TiC-based cermets have been investigated to characterize their serviceability as material for tools and wear resistant parts of equipment. Both hardenable martensitic and austenitic steels, in particular corrosion resistant grades were used as metallic binder of carbide-metal composites [9]. Corrosion and corrosion-abrasive resistance of such corrosion resistant TiC-based cermets under neutral, acid and alkaline conditions have also been investigated [10]. Both high mechanical characteristics and corrosion resistance are characteristic of TiC-based cermets bonded with austenitic Fe-Cr-Ni stainless steels. Transverse rupture strength and fracture toughness of such composites are comparable to those of WC-Co hardmetals. At the same time TiC-based cermets bonded with Cr-Ni austenitic steels compare favourably with corrosion resistance of hardmetals. From the health aspect it is better to replace Ni in austenitic steels by alternative austenite stabilizing elements.

Performance and reliability of ceramic-metal composites depends to a great extent on their production technology in particular sintering technology (mode). Investigation of the influence of a sintering mode (vacuum sintering, sinter/HIP and sinter + HIP in different cycles) on the performance and reliability of TiC- and Cr₃C₂-based cermets revealed that sinter/HIP-ed TiC-based cermets are featured by a microstructure of high homogeneity and are characterized by decreased porosity when compared to vacuum sintered cermets. In general the positive effect of sinter/HIP on performance increases with an increase in the carbide fraction in the composite. HIP conducted in two different cycles (sinter + HIP) is at a disadvantage as compared to the one-cycle sinter/HIP technology [11].

In present work the aim was to develop and produce TiC-based cermets bonded with Ni-free austenitic steels. The cermets should demonstrate the following minimum characteristics: Vickers hardness (HV) upper than of silica sand (HV 1100...1200), fracture toughness (K_{IC}) upper than ceramics (K_{IC} ≥ 6.0 MPa·m^{1/2}) and corrosion resistance in chloride containing solutions.

2. EXPERIMENTAL DETAILS

Characteristics of starting powders used in production of composite are listed in Table 1.

Cermets were produced using conventional PM route: mechanical milling (grinding and mixing in ball mill) in liquid media (ethanol) using ball mill (WC-Co lining and

balls) with rotating speed of 60 rpm, ball-to-powder ratio of 1:10. Milling time was set at 72 hours.

The uniaxially pressed specimens were sintered under vacuum (vacuum level was approximately 5×10⁻² mbar), by sinter/HIP (30 bar) and by sintering under low Ar gas pressure (see Fig. 1).

Table 1. Characterization - chemical composition (wt%), average particle size (μm) of powders used for production of TiC-FeCrMn cermets

Powder	Basic components, %	Impurities	Average particle size, μm
TiC	Ti, C _{comb} ^{19,12} , C _{free} ^{0,15}	O – 0.30; N – 0.02	2.6
Fe	99.72	Si – 0.01; P – 0.07; Mn – 0.02	< 100
Mn	Mn – 99.84	O - rest	7.95
Cr	Cr – 99.5	O ≤ 0.38; Fe – 0.01	6.65
Mo	>99.80	Fe – 0.0025; O – 0.110	2.48
Fe-Si	Si - 48.2, Fe - 50.1	Al – 1.1; Cr – 0.2; Mn – 0.4	< 100

Fracture toughness and hardness were determined using ground test pieces of 5 x 5 x 17 mm. Hardness measurements (Vickers hardness) were carried out in accordance with the standard EN-ISO-6507.

Indentation fracture toughness (K_{IC}) was measured using one of the most used empirical equation proposed by Evans [12].

$$K_{IC} = 0.16 \cdot \left(\frac{c}{a}\right)^{-1.5} \cdot \left(H \cdot a^2\right)^{\frac{1}{2}}, \quad (1)$$

where *c* is the average length of the cracks obtained in the tips of the Vickers indentations, (μm); *a* is the half average length of the diagonal of Vickers indentations, (μm); *H* is Vickers hardness, (MPa).

Corrosion resistance was assessed using immersion test in NaCl containing (3%) water solutions during 72 hours. The corrosion resistance was evaluated using observation method (quality).

Microstructural analysis was carried out using scanning electron microscope (SEM) JOEL JSM 840A. Chemical composition of cermets after sintering was analysed using X-ray spectroscopy (EDS). The porosity of cermets was determined using optical microscope Axiover25 microscope and software Buehler Omnimet.

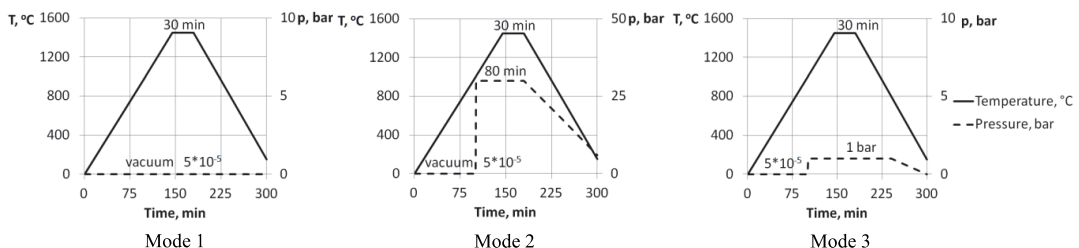


Fig. 1. Sintering modes of cermets TiC-FeCr26Mn20 (Mode 1 – vacuum sintering, 5·10⁻² mbar; Mode 2 – sinter/HIP, 30 bar; Mode 3 – sintering in Ar, 1 bar)

Table 2. Calculated chemical composition and mechanical characteristics of TiC-based (70 wt% TiC) vacuum sintered (sintering mode 1) and sinterhipped (sintering mode 2) cermets

Grade	Sint. Mode	Chemical composition (calculated), wt%					Porosity, %	Hardness, HV ₃₀	K _{IC} , MPa·m ^{1/2}
		TiC	Cr	Mn	Mo	Ni			
T70/FeCr21Mn14	1	70	6.3	4.2	-	-	0.60	1400	7.0
T70/FeCr26Mn20	1	70	7.8	6.0	-	-	0.56	1520	6.9
T70/FeCr26Mn20	2	70	7.8	6.0	-	-	2.34	1350	9.8
T70/FeCr26Mn20Mo5	1	70	7.8	6.0	1.5	-	0.24	1310	5.7
T70/FeCr22Ni16	1	70	6.6	-	-	4.8	0.30	1230	13.8

3. RESULTS AND DISCUSSION

The study covers the TiC-based cermets cemented with Ni-free corrosion resistant CrMn and CrMnMo steels. Manganese was used as austenitizing element replacing nickel while molybdenum was used as alloying element which in combination with chromium is effective in terms of stabilizing the passive film in presence of chlorides. Cermet bonded with regular austenitic nickel containing corrosion resistant steel was used as reference material. Calculated chemical composition and mechanical characteristics of TiC-based cermets are presented in Table 2.

Results of screening experiments demonstrate that Ni-containing austenitic steel-bonded cermet (reference material) is characterized by higher performance characteristics – fracture toughness (Table 2) and corrosion resistance in presence of chlorides in water in comparison with TiC-FeCrMn-type cermets. Marked decrease in austenitizing Mn content during vacuum sintering should probably account for such a result first of all because binder of TiC-FeCrMn cermets, unlike TiC-FeCrNi ones is not austenitic (nonmagnetic).

Depression of manganese loss during sintering can be achieved using gas compression during sintering. Manganese loss in different sintering modes (regular

vacuum liquid-phase sintering, sinter/HIP under isostatic gas (Ar) pressure of 30 bar and sintering in argon gas pressure of 1 bar) was determined. Chemical composition of cermet grades after sintering using different sintering modes is presented in Table 3.

Results in Table 3. prove drastical reduction of manganese content during vacuum sintering. Both sintering under gas pressure 1 bar and 30 bar enable to retain the majority of Mn in alloy (calculated Mn content in cermet 6 wt%). There are no remarkable differences in chemical compositions using two pressurized sintering modes (Ar gas pressure of 30 bar or 1 bar, respectively sintering mode 2 and 3).

Sinterability evaluated by residual porosity of alloys is in general the better the lower gas compression during sintering. Therefore mechanical characteristics of cermets of different chromium content in binder (20 and 26 wt%) were determined after sintering using sintering mode 3 – sintering at 1450°C under gas pressure of 1 bar, sintering time 0.5 h (see Table 4).

Most cermets have acceptable mechanical characteristics. However, cermets alloyed by silicon (used in high chromium cermets for better sinterability [9, 10]) demonstrate more homogenous microstructure (compare microstructures Fig. 2 and 3) and reduced porosity.

Table 3. Sintering technology vs chemical composition of TiC-based cermet grade T70/FeCr26Mn20 (EDS analysis)

Sintering mode	Sintering Technology	Chemical composition, wt%						
		C	Ti	Cr	Mn	Fe	W	Total
1	T=1450°C, vacuum p=5·10 ⁻⁵ bar	14.49	60.26	5.25	0.45	12.38	7.19	100.00
2	T=1450°C, p=30bar (Ar)	15.43	59.15	3.47	3.69	11.16	7.09	100.00
3	T=1450°C, p=1bar (Ar)	14.21	54.13	7.20	4.05	13.62	6.01	100.00

Table 4. Calculated chemical composition and mechanical characteristics of 70TiC-FeCrMn cermets (sintering mode 3 in Fig. 1.)

Grade	Binder composition (calculated), wt%				Porosity, %	Hardness, HV ₃₀	K _{IC} , MPa·m ^{1/2}
	TiC	Cr	Mn	Si			
T70/FeCr20Mn20	70	6.0	6.0	-	0.83	1450	5.6
T70/FeCr20Mn30Si2	70	6.0	9.0	0.06	0.23	1305	7.6
T70/FeCr26Mn20	70	7.8	6.0	-	2.33	1220	6.6
T70/FeCr26Mn20Si2	70	7.8	6.0	0.06	0.67	1590	8.7
T70/FeCr30Mn20	70	9.0	6.0	-	1.54	1300	8.9
T70/FeCr30Mn20Si2	70	9.0	6.0	0.06	0.81	1380	6.4

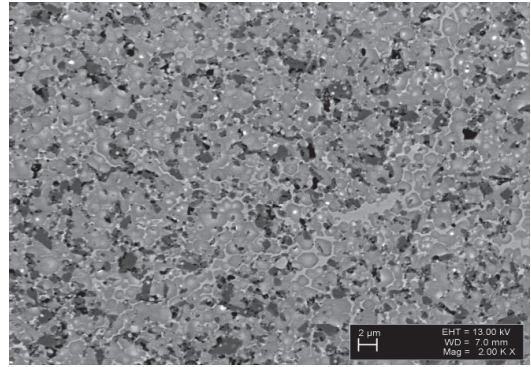
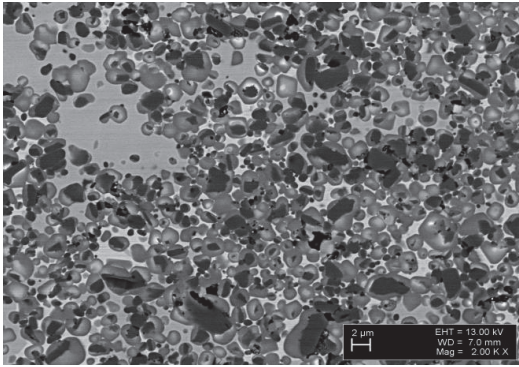


Fig. 2. Microstructure of cermets 70TiC-FeCr26Mn20 (left) and 70TiC-FeCr26Mn20Si2 (right) after sintering in argon (sintering mode 3 in Fig. 1)

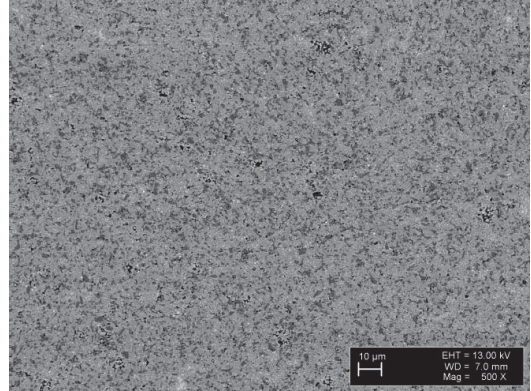
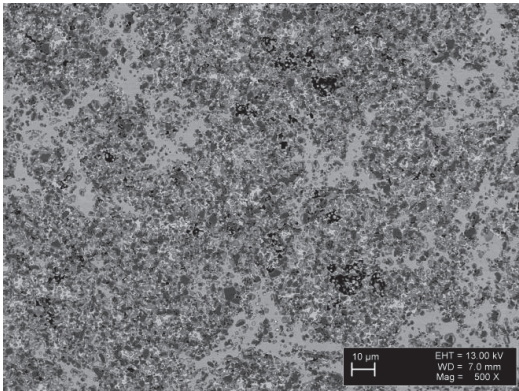


Fig. 3. Microstructure of cermets 70TiC-FeCr26Mn20 (left) and 70TiC-FeCr26Mn20Si2 (right) after sintering in argon (sintering mode 3 in Fig. 1)

Higher homogeneity in microstructure and acceptable mechanical characteristics do not ensure sufficient corrosion resistance of such cermets in chloride containing water solutions. TiC-FeCrNi cermets with austenitic steel binder compare favourably with Ni-free TiC-FeCrMn cermets in terms of corrosion resistance (Fig. 4) and fracture toughness (Fig. 5). Further research must be done to optimize both composition and technological peculiarities of Ni-free cermets.



Fig. 4. Corrosion resistance immersion tests in chloride containing solution: TiC-FeCr20Mn30Si2 (left) and 70TiC-FeCr22Ni16 (right)

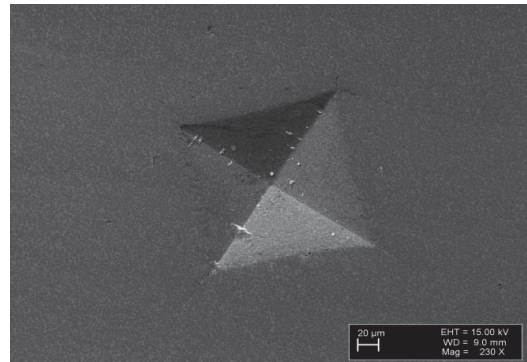
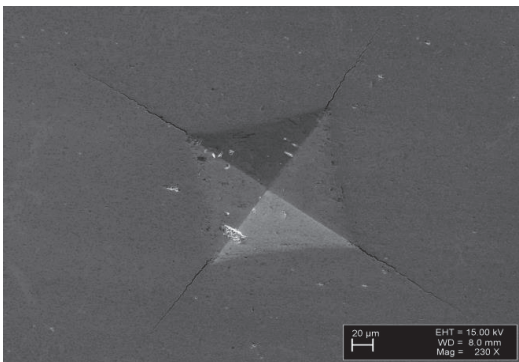


Fig. 5. SEM images of Vickers indentation (HV_{30}) of cermet 70TiC-FeCr22Ni16 (left) and TiC-FeCr20Mn30Si2 (right)

4. CONCLUSIONS

- Goals of research were achieved in terms of mechanical characteristics – hardness and fracture toughness. Corrosion resistance in chloride containing solutions of TiC-FeCrMn composites is not acceptable.
- Ni-free TiC-based CrMn-steels bonded cermets compare unfavourably with cermets bonded with CrNi austenitic steels in terms of fracture toughness and corrosion resistance.
- Marked decrease in austenitizing manganese content during vacuum sintering takes place.

- Depression of Mn loss can be achieved using gas compression during sintering leading, however to decrease in sinterability (increase in porosity).
- Further research must be done to optimize both composition and technological peculiarities of Ni-free cermets.

Acknowledgment

The research was supported by Estonian Ministry of Education and Research (projects No 140062s08 and No IUT1929).

REFERENCES

1. Metals Handbook. Volume 1. Properties and selection: steels and high performance alloys. ASM International, 2002 p. 843 - 847
2. European Commission homepage: <http://ec.europa.eu/>, 13.05.2014.
3. **Kuroda, D. Hiromoto, S. Hanawa, T. Katada, Y.** Corrosion behavior of Nickel-free High Nitrogen Austenitic Stainless Steel in Simulated Biological Environments *Materials Transactions* 43 (12) 2002: pp. 3100 – 3104.
4. **Ren, Y. Yang, K. Bingchun, Z. Yaqing, W. Yong, L.** Nickel-free Stainless Steel for Medical Applications *Journal of Materials Science and Technology* 20 (5) 2004: pp. 571 – 573.
5. **Brookes, K. J.** World Dictionary and Handbook of Hardmetals and Hard Materials. London, 1996.
6. National Toxicology Program homepage: <http://ntp.niehs.nih.gov/>, 11.06.2014.
7. **Hanyaloglu, C. Aksakal, B. Bolton, J. D.** Production and Indentation Analysis of WC/Fe-Mn as an Alternative to Cobalt-bonded Hardmetals *Materials Characterization* 47 (3 - 4) 2001: pp. 315 – 322.
8. **Prakash, L. J.** Plansee Seminar 2013: The Global Refractory Metals and Hard Materials Industry Meets in Austria *Powder Metallurgy Review* 2 (3) 2013: pp. 41 – 48.
9. **Kübarsepp, J. Reshetnyak, H. Annuka, H.** Characterization of the Serviceability of Steel-bonded Hardmetals International *Journal of Refractory Metals and Hard Materials* 12 (6) 1993, pp. 341 – 348.
10. **Kübarsepp, J. Kallast, V.** Stainless Hardmetals and Their Electrochemical *Corrosion Resistance Werkstoffe und Korrosion* 45 (8) 1994, pp. 452 – 458.
11. **Kübarsepp, J. Pirso, J. Juhani, K. Viljus, M.** Developments in Cermet Design, Technology and Performance International *Journal of Materials and Product Technology* 49 (2 - 3) 2014, pp. 160 – 179.
12. **Evans, A. G. and Charles, E. A.** Fracture toughness determinations by indentation. *J. Am. Ceram. Soc.* 59 1976, pp. 371–372.

Paper III

Kolnes, M., Kübarsepp, J., Viljus, M., Traksmäa, R., Illopmägi, S. Effect of sintering conditions on microstructure and performance of TiC-FeCrMn cermets. *World PM2016 proceedings*, 2016.

Manuscript refereed by Dr Ralph Useldinger (Cerazit, Luxembourg)

Effect of Sintering Conditions on Microstructure and Performance of TiC-FeCrMn Cermets

Märt Kolnes (Tallinn University of Technology, Ehitajate tee 5, 19086 Tallinn, Estonia) mart.kolnes1@ttu.ee; Jakob Kübarsepp (Tallinn University of Technology, Ehitajate tee 5, 19086 Tallinn, Estonia) jakob.kubarsepp@ttu.ee; Mart Viljus (Tallinn University of Technology, Ehitajate tee 5, 19086 Tallinn, Estonia) mart.viljus@ttu.ee; Rainer Traksmäa (Tallinn University of Technology, Ehitajate tee 5, 19086 Tallinn, Estonia) rainer.traksmaa@ttu.ee; Siim Illopmägi (Tallinn University of Technology, Ehitajate tee 5, 19086 Tallinn, Estonia) siim.illopmagi@hotmail.com

Abstract

High chromium and manganese TiC-FeCrMnSi cermets were investigated. In our experiments, three different sintering conditions were used: vacuum, low-partial pressure and spark plasma sintering (SPS). Because of high vapor pressure of manganese, different sintering conditions and technologies were investigated to depress the Mn- and Cr-loss during sintering. Chemical composition of TiC-FeCrMn cermets was analyzed by energy-dispersive X-ray spectroscopy (EDS) and structure formation was studied using X-ray diffraction (XRD). Also, mechanical properties – hardness and fracture toughness - were evaluated on the samples. It was found that noticeable Mn- and Cr-loss during vacuum sintering can be avoided when sintering under partial Ar gas pressure or using SPS. In terms of structure (residual porosity) and mechanical characteristics, it is most effective to utilize sintering under moderate partial argon pressure combined with manganese microatmosphere.

Introduction

Hardmetals are liquid-phase sintered WC-based ceramic metal composites used as the working elements of tools and machine parts because of their combination of high wear resistance, hardness and fracture toughness. Most widely used WC-based hardmetals are bonded with cobalt because of its excellent wetting behavior and good mechanical performance. However, for the shortage of cobalt, its high cost and insufficient corrosion resistance, alternatives to cobalt as the binder phase have been searched [1]. In addition, hardmetal (tungsten carbide-cobalt composite) dust is the reason for a kind of malady known as “hard metal disease”[2]. Therefore, tungsten and cobalt free ceramic-metal composites – cermets, have been elaborated. The most widespread among them are TiC- and TiCN-based cermets bonded with Ni-Mo alloys [3]. But nickel, also classified as an allergen, is very toxic for human health [4]. The best method to set a limit to nickel allergy is to use completely Ni-free alloys in applications where these alloys may have direct contact with human skin. Therefore, efforts have been made to replace the toxic elements in the binder phase and to offer a nontoxic alternative to cobalt and nickel containing hard materials [5 - 9]. Iron-based binder systems are most widely used to replace toxic metals because iron is known as a nontoxic and very cost-effective metal. Also, iron-based Ni- and Co-free alloys as binders have acceptable mechanical characteristics and sufficient corrosion resistance in corrosive media [7, 10].

Stainless steel is a steel alloy with a minimum of 10.5-% chromium content by mass. Austenitic stainless steels are the most commonly used types of stainless steel [11]. To transform the structure of stainless steel to austenite, it is necessary to add a substantial amount of austenite stabilizing elements (Ni, Mn, N). Manganese is added to steels to increase toughness, strength and to improve hot working properties. Manganese, like nickel, is also an austenite forming element but its austenite stabilizing ability is half of that of nickel in stainless steels. Despite this, fully nickel-free stainless steels have been developed recently [12]. The aim of these studies was to replace nickel by cheap and nontoxic manganese.

Manganese is the most widely used alloying element in the production of classic steels. However, as compared to classic steels, production of manganese steel is affected by many more mutually interacting factors. Manganese, chromium and partly silicon, especially manganese, have not been widely used to produce sintered alloy steels [13]. The main reason from a thermodynamic point of view has been and still is in their high affinity to oxygen and stringent requirements on the sintering atmospheres. In addition to high affinity to oxygen, manganese has a high vapor pressure, which is its physical property that cannot be controlled [13]. Although vacuum sintering of stainless steels offers superior oxide reduction, vacuum sintering is unacceptable for stainless steel because it causes the depletion of chromium from the surfaces of sintered parts. Therefore, vacuum sintering of stainless steels is combined with partial pressure (1...4 mbar) of argon or nitrogen to minimize chromium losses

due to its relatively high vapor pressure [14].

WC- and TiC-based ceramic metal composites bonded with iron-based binder alloyed with manganese have been developed [7, 9]. As the vapor pressure of manganese is even three orders of magnitude higher than that of chromium, higher partial pressures during sintering have been used [7]. Furthermore, the sintering temperature should be decreased as low as possible and in the presence of 10 mbar of argon pressure, evaporation losses of manganese can be limited to about 20% [9]. Manganese losses can be further minimized by creating a manganese vapor “microatmosphere” in the sintering device by surrounding the samples with manganese metal.

Our focus in this study is on the processing and technological peculiarities of TiC-FeCrMn cermets. The goal is to develop and produce a Ni-free corrosion resistant austenitic stainless steel bonded TiC-based cermet. The main objective was to investigate Mn and Cr losses using different liquid-phase sintering modes and spark plasma sintering (SPS). SPS technology is known as a relatively rapid process and therefore manganese loss during sintering could be minimized.

Experimental Details

Nickel-free TiC-FeCrMnSi cermets with TiC content of 30 wt% were investigated (see Table 1). Well-known super ferritic stainless steel (AISI 446) powder and elemental powders of manganese and silicon were used. Chemical composition and characteristics of powders used in the production of specimens are listed in Table 2. Ni-containing TiC-FeCrNi stainless steel cermet with an austenitic binder was used as reference material.

Table 1. Calculated chemical composition of TiC-based cermets

Grade	Chemical composition, wt%					
	TiC	Fe	Cr	Mn	Ni	Si
70TiC-FeCr18Mn20Si4	70	16.86	5.52	6.27	-	1.35
70TiC-FeCr22Ni16	70	18.6	6.6	-	4.8	-

Table 2. Chemical composition and average particle size of used powders

Powder	Basic components, wt%	Impurities, wt%	Average particle size, μm
TiC	Ti, C_{comb} – 19.12; C_{free} – 0.15	O – 0.30; N – 0.02	2.6
AISI 446	Fe – 73.45; Cr – 24.2; Mn – 1.2; Si – 0.85	N – 0.25; C – 0.03; P – 0.011; S – 0.008	10...45
Mn	Mn – 99.84	O – rest	8
Si	Si – 99.50	Al – 0.15; Ti – 0.002; P – 0.004; Fe – 0.2; Ca – 0.05; B – 0.0005	44

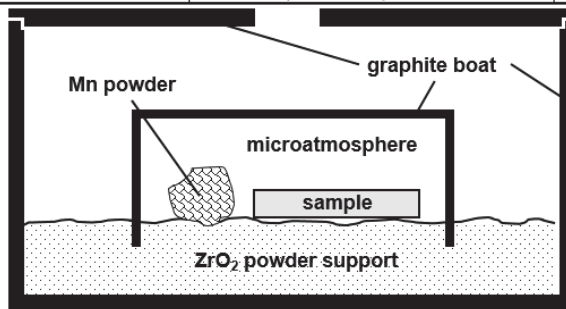


Figure 1. Schematic built up of a graphite crucible (sintering mode 4)

Cermets were produced using a common powder metallurgy route: wet (ethanol) mechanical milling in a ball mill using WC-Co balls with a rotating speed of 60 rpm. The milling time was 72 h and the ball-to-powder ratio 1:10 was used. Pressed specimens were liquid-phase sintered using six sintering modes on a ZrO₂ powder support. Different partial pressure levels and different sintering temperatures were applied: vacuum 0.04 mbar; argon partial pressure 4 and 400 mbar; temperatures of 1375, 1425 and 1475 °C (see Figure 2 and Table 3). Sintering mode 3 includes a manganese vapor “microatmosphere” within the graphite crucible in the presence of 4 mbar of argon partial pressure at 1475 °C (Figure 1). The compacted samples were sintered during 30 min at the sintering temperature

and the heating rate was 10 °C·min⁻¹. During SPS, the powder was consolidated in a partial pressure of 4·10⁻² mbar under a load of 60 MPa. The sample was heated up to the sintering temperature of 1300 °C with the heating rate of 100 °C·min⁻¹ and was dwelled at this temperature for 2 min. Natural cooling was followed.

Fracture toughness and hardness were determined using ground test pieces of 5 x 5 x 17 mm. Hardness measurements (Vickers hardness) were carried out in accordance with the standard EN-ISO-6507. The fracture toughness (K_{IC}, MPa·m^{1/2}) was determined by the method of fracture by indentation with the most commonly used empirical equations for fragile materials proposed by Evans [15].

$$K_{IC} = 0.16 \cdot \left(\frac{c}{a}\right)^{-1.5} \cdot \left(H \cdot a^{\frac{1}{2}}\right),$$

where c is the average length of the cracks obtained in the tips of the Vickers indentations, (μm); a is the half average length of the diagonal of Vickers indentations, (μm); H is Vickers hardness, (MPa). The weight loss during sintering does not include the mass loss due to the evaporation of paraffin wax.

Microstructural analysis was carried out using a scanning electron microscope (SEM) JOEL JSM 840A. Chemical composition of the cermets after sintering was analyzed using X-ray spectroscopy (EDS). Phase identification of cermets was carried out using XRD method (Bruker AXS D5005). The porosity of the cermets was determined using an optical microscope Axiovert25 and software Buehler Omnimet. The porosity was evaluated by measuring the surface area of pores on the optical image of microstructure.

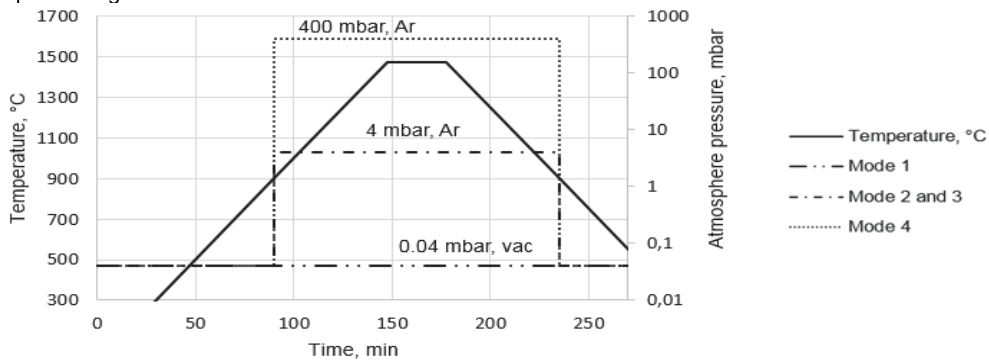


Figure 2. Sintering regimes (modes 1, 2, 3 and 4) of TiC-FeCrMnSi cermets

Results and Discussion

The study covers the Ni-free TiC-based cermet bonded with manganese containing steels. Well-known super ferritic stainless steel powder was used because of its high chromium content and to achieve homogeneous chromium distribution in the binder phase. In addition, this steel has quite high content of nitrogen (0.25 wt%) – an element with 30 times higher austenitizing effect than Ni. Manganese was used as a replacing element of nickel to stabilize austenite. One percent nickel can be replaced by about two percent of manganese as long as nitrogen is present [11]. Silicon addition was used to improve the sinterability and reduce porosity of cermets [10].

Results of W. D. Schubert's experiments [9] with WC-FeMn hardmetals and previous work by authors [7] with TiC-FeCrMn cermets demonstrate that vacuum liquid-phase sintering is inappropriate for manganese containing cemented carbides. This is because manganese has relatively high vapor pressure and the sublimation and evaporation occurs during solid- and liquid-phase sintering. Therefore, manganese vapor "microatmosphere" within the graphite crucible and partial pressure of argon were used to produce TiC-FeCrMnSi cermets. Manganese loss during different sintering modes (conventional vacuum sintering, sintering in two different partial pressures of argon and sintering in manganese vapor) was determined using X-ray spectroscopy. Chemical composition after milling (calculated) and after different sintering modes is presented in Table 3. As a result of ball milling using WC-Co balls, tungsten (up to 4...6 wt%) was revealed in all cermets.

Results in Table 3 and Figure 3 demonstrate a substantial reduction of manganese and a fractional loss of chromium and silicon during vacuum (0.04 mbar, mode 1) liquid-phase sintering. Also, mass loss confirms a considerable depression of different metals (Table 3). Sintering under 4 mbar of argon (mode 2) also reduces the manganese content drastically but it does not affect the content of chromium. Furthermore, the mass loss is slightly smaller as compared to vacuum sintering. Additionally, cermet sintered under 400 mbar of argon (mode 4) has minor manganese loss.

Spectacular difference in the manganese content was revealed during partial pressure sintering (4 mbar) and in manganese vapor “microatmosphere” within the graphite crucible. The mass loss and manganese depletion were noticeably smaller using sintering in the manganese vapor atmosphere (mode 3).

Table 3. Sintering conditions vs chemical composition and mass loss of TiC-FeCrMnSi cemet (EDS)

Sintering mode	Sintering Technology	Chemical composition, wt%							Mass loss
		Ti	C	Fe	Cr	Mn	Si	W	
	After milling, calculated	53.9	12.9	16.0	5.3	6.0	1.3	4.8	–
1	T=1475 °C, p=0.04 mbar (vac)	62.0	15.1	12.5	4.0	0.3	0.6	5.4	7.81
2	T=1475 °C, p=4 mbar (Ar)	58.9	14.3	14.8	5.3	0.8	0.7	5.2	6.81
3*	T=1475 °C, p=4 mbar(Ar), G boat	56.7	13.9	14.8	5.2	3.6	0.7	5.0	3.80
4	T=1475 °C, p=400 mbar (Ar)	53.9	13.7	16.5	5.8	4.6	0.8	4.6	2.27
5	T=1425 °C, p=400 mbar (Ar)	52.2	13.7	17.0	5.7	6.0	0.9	4.5	1.04
6	T=1375 °C, p=400 mbar (Ar)	50.5	13.4	18.2	6.5	6.3	1.0	4.0	1.11
7	SPS, T=1300 °C, p=4 mbar (Ar)	51.8	14.1	17.2	5.9	5.5	1.2	4.2	n/a

*Cermets sintered in manganese vapor within the graphite boat

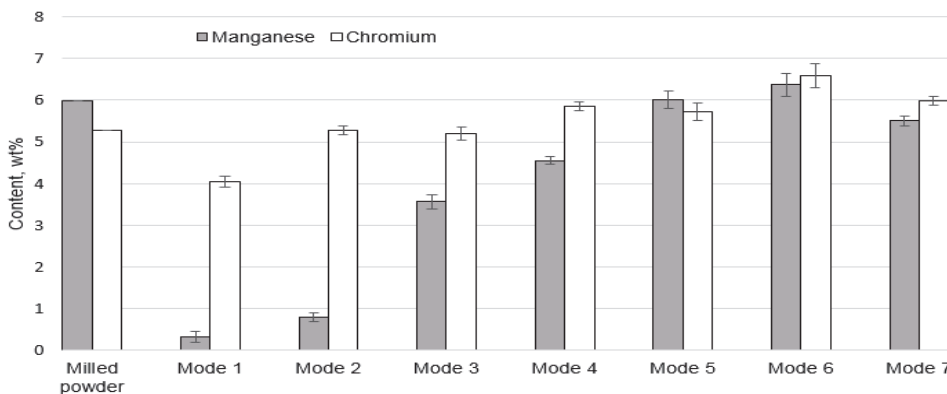


Figure 3. Manganese and chromium content in the alloy using different sintering regimes of TiC-FeCrMnSi cermets (see Table 3)

In sintering modes 5 and 6, lower temperatures (1425 °C and 1375 °C) were used to minimize manganese evaporation during liquid-phase sintering. Lower temperatures have a positive effect on retaining manganese in the cermets and the mass loss is as minimal as possible. Most of manganese remained in the content of cermets (see Table 3). SPS employs very high heating rates and external pressure for powder consolidation in a short time and decreased temperature. Therefore, it is not surprising that SPS enables to retain Mn and Cr in alloy.

Most cermets have acceptable mechanical characteristics (see Table 4). However, vacuum sintered and specimens sintered using lower temperatures have quite high residual porosity (see also Figure 4). Furthermore, cermets sintered using modes 5 and 6 (lower temperatures) also demonstrate considerably lower Vickers hardness. Cermets sintered using sintering mode 3, which includes a manganese vapor “microatmosphere” within the graphite crucible in the presence of 4 mbar of argon partial pressure at 1475 °C, demonstrate an auspicious combination of hardness and fracture toughness and also have an acceptable value of porosity.

TiC-FeCrMnSi cermets produced using liquid phase sintering show a medium size grain microstructure, which is a typical core-rim structure when formed during liquid-phase sintering (see Figure 4; a, b). Most of the carbide grains consist of black TiC cores and gray (Ti, W,...)C rims (inner and outer rim). Sintering under partial argon gas pressure enables to retain prevalent part of Mn in alloy and XRD pattern of cemet proves possibility to produce cemet with mostly austenitic structure of binder (see Figure 5). XRD analysis also show that M_7C_3 (M=Fe, Cr) carbide has formed during sintering.

World PM2016 – HM - Cermets

The fast nature of SPS technology helps drastically reduce average grain size of cermet (see Figure 4; c) and decrease residual porosity. Structural peculiarity (particularly decreased grain size) results in low fracture toughness of spark plasma sintered cermets.

Table 4. Sintering conditions vs mechanical characteristics of TiC-FeCrMnSi cermet

Sintering mode	Sintering Technology	Hardness	Fracture toughness, K_{IC}	Porosity	Density
		HV ₃₀	MPa·m ^{1/2}	%	g/cm ³
1	T=1475 °C, p=0.04 mbar (vac)	1321	n/a	2.0	5.56
2	T=1475 °C, p=4 mbar (Ar)	1315	7.1	0.6	5.59
3*	T=1475 °C, p=4 mbar (Ar), G boat	1232	11.4	0.4	5.65
4	T=1475 °C, p=400 mbar (Ar)	1244	9.6	0.6	5.59
5	T=1425 °C, p=400 mbar (Ar)	1156	n/a	2.3	5.57
6	T=1375 °C, p=400 mbar (Ar)	1081	n/a	3.0	5.52
7	SPS, T=1300 °C, p=4 mbar (Ar)	1341	4.1	0.2	5.42
Reference material: 70TiC-FeCr22Ni16					
1	T=1475 °C, p=0.04 mbar (vac)	1230	13.8	0.3	5.50

*Cermets sintered in manganese vapor within the graphite boat

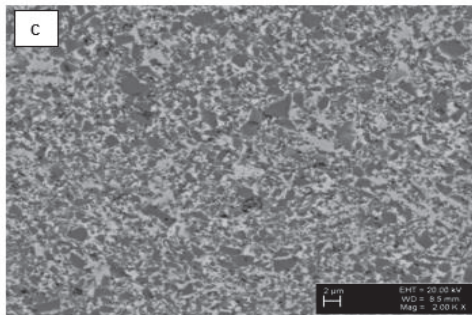
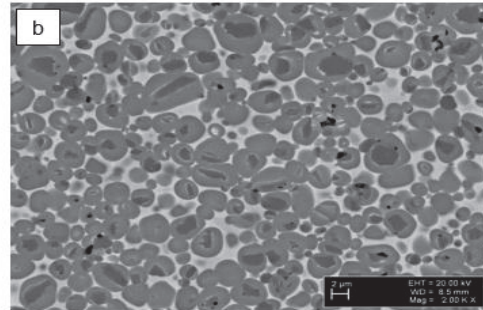
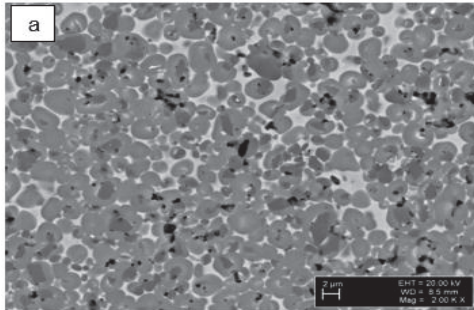


Figure 4. Microstructure of TiC-FeCrMnSi cermets using sintering modes: 1 (a), 3 (b) and 7 (c)

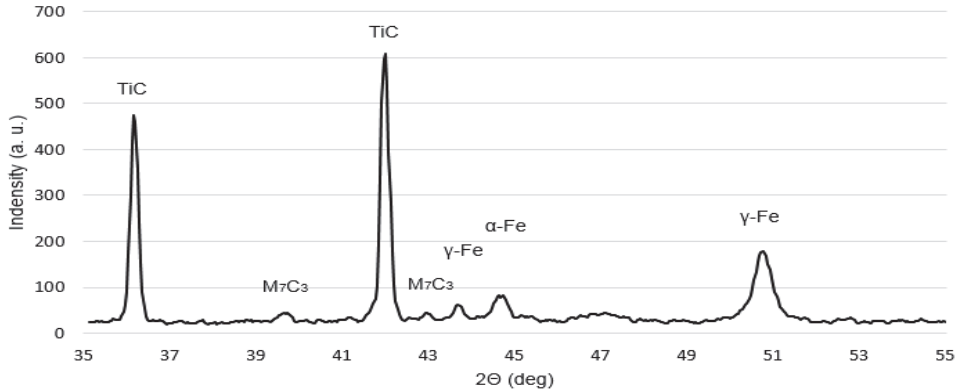


Figure 5. X-ray diffraction pattern of TiC-FeCrMnSi cemet (sintering mode 4)

Conclusions

Results from the investigation of the influence of manganese and chromium losses using different sintering modes provide for the following conclusions:

- Vacuum ($p=0.04$ mbar) and partial argon pressure ($p=4$ mbar) sintering of TiC-FeCr18Mn20Si4 cermets results in a remarkable decrease in Mn and Cr content.
- The higher the partial pressure of argon and the lower the temperature of sintering, the higher is the effectiveness of reduction of Mn and Cr losses during sintering. In terms of structure (residual porosity) and mechanical characteristics (fracture toughness), use of sintering under moderate partial argon pressure ($p=4$ bar) combined with manganese microatmosphere is most effective.
- Spark plasma sintering at decreased temperature enables retaining the Mn and Cr in the alloy and producing low porosity cermets. Structural peculiarities (decreased carbide grain size) result in low fracture toughness of spark plasma sintered ceramic and metal composites.
- Sintering modes enabling retaining of manganese during sintering allow to produce TiC-FeCrMn type cermets with prevalently austenitic structure of metallic binder.

Acknowledgement

This work was supported by institutional research funding IUT 19-29 of the Estonian Ministry of Education and Research.

References

- [1] M. Tarraste, K. Juhani, J. Kübarsepp, J. Pirso, V. Mikli, The Effect of Cr and C on the Characteristics of WC-FeCr Hardmetals, Proceedings of Euro PM2015.
- [2] A. Fischbein, J. C. Luo, S. J. Solomon, S. Horowitz, W. Hailoo, A. Miller, Clinical Findings Among Hard Metal Workers, British Journal of Industrial Medicine. 1992 (49), pp. 17-24.
- [3] Comprehensive Hard Materials, Volume 1, Elsevier 2014, p. 4.
- [4] European Chemicals Agency homepage: <http://echa.europa.eu/substance-information/-/substanceinfo/100.028.283>, 18.04.16
- [5] L. J. Prakash, Plansee Seminar 2013: The Global Refractory Metals and Hard Materials Industry Meets in Austria Powder Metallurgy Review 2013 (2), pp. 41-48.
- [6] C. Hanyaloglu, B. Aksakal, J. D. Bolton, Production and Indentation Analysis of WC/Fe-Mn as an Alternative to Cobalt-bonded Hardmetals, Materials Characterization, 2001 (47), pp. 315-322.
- [7] M. Kolnes, J. Kübarsepp, L. Kollo, M. Viljus, Characterization of TiC-FeCrMn Cermets Produced by Powder Metallurgy Method, Materials Science (Medžiagotyra), 2015 (21), pp. 353-357
- [8] M. Kolnes, J. Pirso, J. Kübarsepp, M. Viljus, R. Traksmäa, Structure Formation and Characteristics of Chromium Carbide-iron-titanium Cermets, Proceedings of the Estonian Academy of Sciences, 2016 (65), pp. 138-143.
- [9] W. D. Schubert, M. Fugger, B. Wittmann, R. Useldinger, Aspects of Sintering of Cemented Carbides with Fe-based Binders, Int. Journal of Refractory Metals and Hard Materials, 2015 (49), pp. 110-123.

World PM2016 – HM - Cermets

- [10] J. Kübarsepp, V. Kallast, Stainless Hardmetals and Their electrochemical Corrosion Resistance, *Werkstoffe und Korrosion*, 1994 (45), pp 452-458.
- [11] M. F. McGuire, *Stainless Steels for Design Engineers*, ASM International, 2008.
- [12] J. Menzel, W. Kirschner, G. Stein, High Nitrogen Containing Ni-free Austenitic Steels for Medical Applications, *ISIJ International*, 1996 (36), pp. 893-900.
- [13] A. Šalák, M. Selecká, *Manganese in Powder Metallurgy Steels*, ASM International, 2012.
- [14] E. Klar, P. K. Samal, *Powder Metallurgy Stainless Steels: Processing, Microstructures, and Properties*, 2007, p. 61.
- [15] A. G. Evans, E. A. Charles, Fracture toughness determinations by indentation, *Journal of American Ceramic Society*, 1976 (59), pp. 371-372.

Paper IV

Kolnes, M., Pirso, J., Kübarsepp, J., Viljus, M., Traksmäa, R. Structure formation and characteristics of chromium carbide-iron-titanium cermets. *Proceedings of the Estonian Academy of Sciences*, 2016, 65 (2), 138–143.



Structure formation and characteristics of chromium carbide–iron–titanium cermets

Märt Kolnes^{a*}, Jüri Pirso^a, Jakob Kübarsepp^a, Mart Viljus^b, and Rainer Traksmaa^b

^a Department of Materials Engineering, Tallinn University of Technology, Ehitajate tee 5, 19086 Tallinn, Estonia

^b Centre for Materials Research, Tallinn University of Technology, Ehitajate tee 5, 19086 Tallinn, Estonia

Received 30 June 2015, revised 14 January 2016, accepted 21 January 2016, available online

Abstract. Structure formation and properties of chromium carbide-based cermets with iron–titanium binder were investigated. Chromium carbide (50–70 wt%), Fe, and Ti (Fe:Ti ratio 4:1 as the binder phase) powders were milled in an attritor and a ball mill, compacted, and sintered at different temperatures and for different periods in vacuum. The microstructure, phase formation and the composition of cermets were studied using XRD and EDS analysis and SEM. The results show that during the sintering of the Cr_3C_2 –Fe–Ti composite at temperatures above 1000 °C, diffusion of chromium and carbon into the ferritic matrix and Cr_3C_2 recrystallization into the chromium ferrous dicarbide $(\text{Cr,Fe})_{23}\text{C}_6$ and the formation of chromium solid solution in the iron matrix (Fe(Cr) take place. Titanium participates actively in the interaction process, which leads to the formation of TiC carbides even at 1200 °C. The mechanical properties (hardness, fracture toughness) and corrosion resistance in salt water were studied. Cermets sintered at lower temperature during a longer period demonstrated the best complex of mechanical properties.

Key words: chromium carbide-based cermets, structure formation, iron alloys bonded cermets, mechanical characteristics, corrosion resistance.

1. INTRODUCTION

Chromium carbide-based cermets are materials of interest in different application areas due to their unique properties. The hardness of Cr_3C_2 –Ni cermets is high and they exhibit excellent corrosion, oxidation, abrasion, and erosion resistance [1–8]. The main disadvantages of these cermets are relatively low mechanical properties (transverse rupture strength (TRS), fracture toughness) because of their coarse-grained structure [9].

Chromium carbide cermets with iron as the binder can replace the expensive and toxic nickel, thus extending the application of chromium carbide materials [10–16]. However, Cr_3C_2 –Fe cermets have not been used because of their high brittleness and low TRS (190 MPa), a successful solution can be achieved only at an iron content above 40 wt% [10]. When the iron content is lower, almost all of it forms a complex carbide $(\text{Cr}_{0.43}\text{Fe}_{0.37})_7\text{C}_3$ [13].

Sintering temperature and sintering time are the most important technological factors determining the structure and properties of Cr_3C_2 -based cermets. A pronounced growth of carbide grains during sintering is one of the main disadvantages of Cr_3C_2 -based cermets [9].

One of the objectives of this investigation was to prevent carbide grain growth in Cr_3C_2 –Fe cermets by alloying them with titanium (20 wt% in Fe). The focus was on the influence of technological factors (milling method, sintering temperature, and sintering time) on the structure formation and mechanical properties of Cr_3C_2 –Fe–Ti cermets.

2. MATERIALS AND EXPERIMENTAL METHODS

The chromium carbide-based composites were produced in the Laboratory of Powder Metallurgy of Tallinn University of Technology using conventional powder metallurgy technology. Chromium carbide (Cr_3C_2) and

* Corresponding author, mart.kolnes1@ttu.ee

pure iron (Fe) and titanium (Ti) powders were used as starting materials milled in an attritor or a ball mill. The attritor and the ball mill lining were reinforced with a WC–Co alloy. To minimize contamination WC–Co balls (diameter 6 mm) were used as the milling balls. The charge ratio (ball to powder mass ratio) in the attritor was 5 : 1. The rotation speed of the impellers was 560 rpm. Kerosene was used as the milling environment, which allows adding the plasticizer (paraffin) solution during the initial stage of milling. The plasticizer forms a thin film on the powder particles, thus preventing additional access of air to the ultra-fine active powder particles. Powder mixtures with similar composition were also milled in the ball mill during 72 h. The charge ratio was 10 : 1.

The compacts (22 mm × 6 mm × 6 mm) were sintered in a furnace with graphite heaters. The compacted samples were sintered in vacuum during 30 and 60 min at 800–1470 °C, heating rate 10 °C min⁻¹. Different Cr₃C₂ contents (50, 60, and 70 wt%) and Fe:Ti ratio of 4 : 1 in the metallic binder were tested. The main focus was on cermet with 70 wt% of chromium carbide, which

ensures acceptable hardness (~1200 HV) and resistance to wear (Table 1).

Phase identification of the milled powders was carried out using X-ray diffraction (XRD) methods with Cu K α radiation (Bruker AXS D5005). The microstructure and grain size of the sintered samples were characterized using a scanning electron microscope (SEM) JEOL-840A.

Vickers hardness was determined in accordance with the standard EN ISO 6507-1 (HV₃₀). Fracture toughness was determined by the Palmqvist method. Each test point indicates the average value of five measured results [17]. The porosity of cermets was determined using an optical microscope Axiovert 25 and Buehler Omnimet software.

3. RESULTS AND DISCUSSION

3.1. Structure formation during sintering

XRD patterns of mechanically activated Cr₃C₂, Fe, and Ti powder mixtures after sintering at 800, 1000, 1200, and 1420 °C are presented in Fig. 1. As it follows from the figure, the as-milled powder mixture consists of

Table 1. Chemical composition, technological parameters, and mechanical properties of Cr₃C₂–Fe–Ti cermets

Grade	Composition, wt%			Milling device	Sint. temp, °C	Sint. time, min	Porosity, %	HV ₃₀ , GPa	K _{1C} , MPa·m ^{1/2}
	Cr ₃ C ₂	Fe	Ti						
E1-1	50	40	10	Attritor	1390	30	0.29	979 ± 95	7.8 ± 0.8
E2-1	60	32	8	Attritor	1450	30	0.55	995 ± 11	4.8 ± 0.5
E3-1	60	32	8	Ball mill	1450	30	2.01	1008 ± 21	5.5 ± 0.4
E4-1	70	24	6	Attritor	1420	30	0.37	1180 ± 19	5.6 ± 0.9
E4-2	70	24	6	Attritor	1470	30	0.84	1349 ± 17	3.9 ± 0.2
E4-3	70	24	6	Attritor	1420	60	0.47	1067 ± 20	7.7 ± 0.7
E5-1	70	24	6	Ball mill	1420	30	1.38	1274 ± 33	5.4 ± 0.1
E5-2	70	24	6	Ball mill	1470	30	0.15	1133 ± 31	5.4 ± 0.1
E5-3	70	24	6	Ball mill	1420	60	0.92	1163 ± 6	6.0 ± 0.4

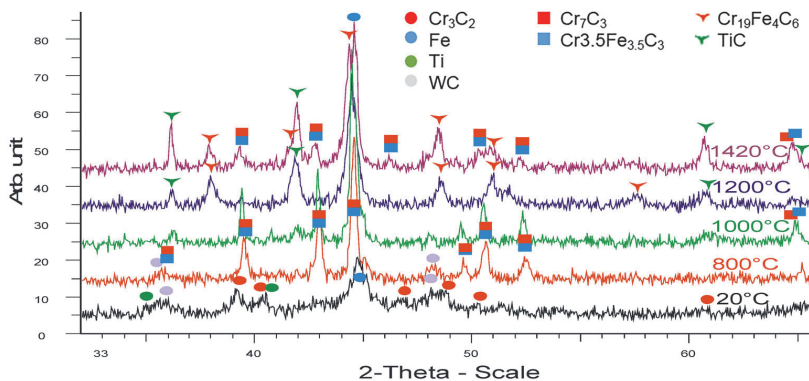
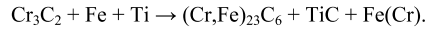


Fig. 1. X-ray diffraction pattern of the 70 wt% Cr₃C₂–Fe–Ti composite at different sintering temperatures.

three phases: Cr₃C₂, Fe, and Ti. After sintering at 800 °C for 30 min, the transformation of phases took place: additional Cr₇C₃ and (Cr_{3.5},Fe_{3.5})C₃ phases appeared and Cr₃C₂ disappeared. The presence of the Cr₇C₃ phase may be indicative of a low stability of Cr₃C₂ at high temperatures. In the Fe matrix Cr₃C₂ dissolves and forms a complex carbide (Cr_{3.5},Fe_{3.5})C₃ and a solid solution of Cr in iron Fe(Cr). After sintering at 1000 °C, additional TiC lines appeared. This means that Ti reacts with carbon and forms TiC already at a temperature below 1000 °C.

Significant changes in the XRD pattern (see Fig. 1) took place after sintering at 1200 °C during 30 min. The reason probably was the formation of liquid eutectic at

this temperature. A liquid phase was formed and a new phase (Cr,Fe)₂₃C₆ appeared (Fig. 1). The exact content of the phase was (Cr_{18.93},Fe_{4.07})C₆. During the sintering at 1420 °C for 30 min, no remarkable changes in the XRD diagram were noticed. The composite consists of three main phases: chromium ferrous complex carbide (Cr,Fe)₂₃C₆, solid solution Fe(Cr), and titanium carbide TiC. The reaction during the sintering of the alloy can be described as follows:



Also the EDS analysis confirmed this. The dark grey region in Fig. 2a is dicarbide (Cr,Fe)₂₃C₆. The light grey

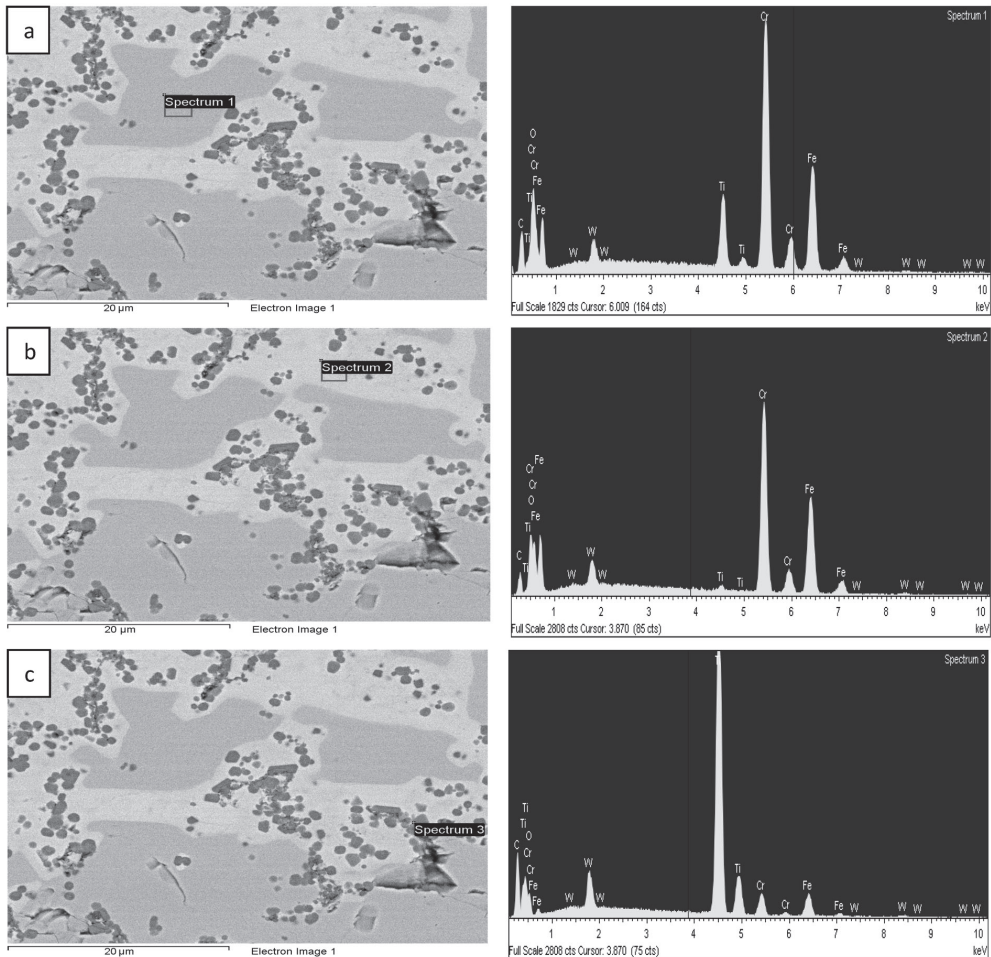


Fig. 2. Results of the EDS analysis at three points (spectra 1, 2, and 3; 1420 °C): (a) (Cr₁₉,Fe₄)C₆; (b) Fe(Cr); (c) TiC.

region (Fig. 2b) is the solid solution of chromium in the iron matrix. The content of Cr is approximately 33 wt% in Fe. Ultrafine (below 1 μm) black near-spherical particles are TiC grains (Fig. 2c). We can see that dispersed TiC grains precipitate in the metallic Fe(Cr) phase.

3.2. Microstructure

The formation of microstructure during the sintering of $\text{Cr}_3\text{C}_2\text{-Fe-Ti}$ cermets was examined using SEM. The results are given in Fig. 3. The carbide grain size in the cermets is determined by sintering parameters and by the particle size of the powder. The rapid grain growth during solid and liquid phase sintering is one of the main disadvantages of chromium carbide-based cermets [9]. As seen in Fig. 3b, the cermets sintered at 1000 $^\circ\text{C}$ during 30 min have fine particles: the average carbide grain size is below 1 μm . In these cermets no carbide grain growth can be observed as compared to the initial particle size (Fig. 3a). A remarkable carbide grain growth occurs in

alloys sintered at 1200 $^\circ\text{C}$ (Fig. 3c). The average carbide grain size is 2–3 μm . The structure contains many pores. The high porosity of these cermets is caused by the low liquid phase content at this sintering temperature.

The microstructure of the cermets sintered at 1420 $^\circ\text{C}$ has coarse $(\text{Cr,Fe})_2\text{C}_6$ carbide grains, making the cermets weak and brittle (Fig. 3d). The in situ synthesized titanium carbide grains are fine-grained and are situated mainly in the Fe(Cr) solid solution and between the carbide grains.

An alternative approach to reduce the grain size of chromium carbide-based cermets is using additions of TiC as a grain size inhibitor (compare Fig. 4b and c). The grain size of $\text{Cr}_3\text{C}_2\text{-Fe-Ti}$ and $\text{Cr}_3\text{C}_2\text{-TiC-Fe}$ cermets is similar.

3.3. Mechanical properties

The mechanical properties of $\text{Cr}_3\text{C}_2\text{-Fe-Ti}$ cermets are summarized in Table 1. The properties of sintered cermets depend on their composition and microstructure. A coarse

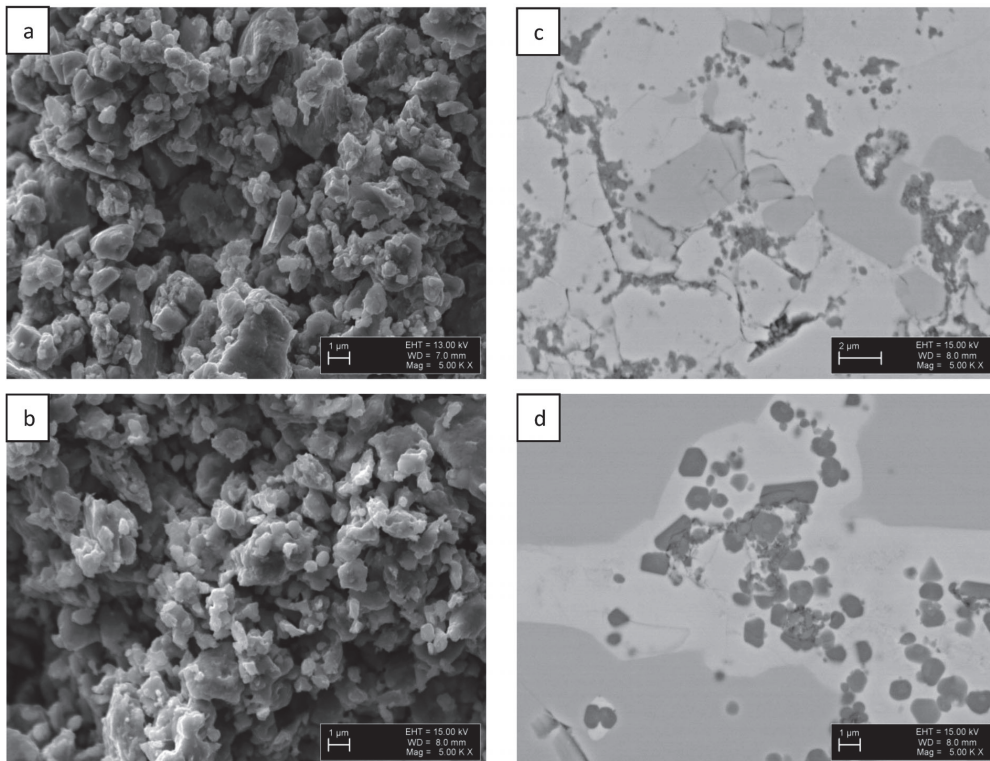


Fig. 3. SEM images of $\text{Cr}_3\text{C}_2\text{-Fe-Ti}$ composite structure formation sintered at different temperatures: (a) as-milled powder mixture; (b), (c), (d) sintered at temperatures 1000, 1200, and 1420 $^\circ\text{C}$, respectively.

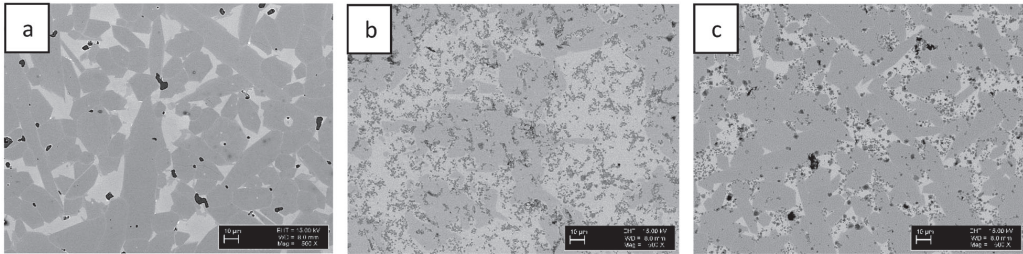


Fig. 4. SEM images of $\text{Cr}_3\text{C}_2\text{-Fe}$ (a), $\text{Cr}_3\text{C}_2\text{-Fe-Ti}$ (b), and $\text{Cr}_3\text{C}_2\text{-TiC-Fe}$ (c).

microstructure of chromium carbides is the reason of moderate mechanical properties (fracture toughness). Like most ceramics, chromium carbides are intrinsically brittle. On the atomic level, this brittleness of carbides is related to their strong hybrid ionic-covalent bonds, which prevent plastic deformation similar to that encountered in ductile metals [15].

The hardness of the cermets depends mainly on the Cr_3C_2 content in the initial powder mixture, being between 980 and 1350 HV. This demonstrates that the hardness increases with the increasing carbide content due to an increase in the fraction of the hard carbide phase. Hardness is practically independent of the milling device (attritor or ball mill) used. Fracture toughness of chromium carbide-based cermets is comparatively low ($4\text{--}8 \text{ MPa}\cdot\text{m}^{1/2}$). The lower the sintering temperature, the smaller is the carbide grain size and the higher is the fracture toughness.

Salt corrosion tests of $\text{Cr}_3\text{C}_2\text{-Fe-Ti}$ cermets showed that they were resistant to corrosion in 3.5% NaCl water solution at room temperature for 72 h. Corrosion resistance did not depend on the composition of cermets and technological parameters used.

4. CONCLUSIONS

Results obtained from the investigation of the influence of the composition of cermets and technological factors on the structure formation and mechanical characteristics of $\text{Cr}_3\text{C}_2\text{-Fe-Ti}$ cermets provide basis for the following conclusions:

- During the sintering of the $\text{Cr}_3\text{C}_2\text{-Fe-Ti}$ composite at a temperature above 1000°C , diffusion of chromium and carbon into the ferritic matrix, Cr_3C_2 recrystallization into chromium ferrous complex carbide $(\text{Cr,Fe})_{23}\text{C}_6$, and formation of chromium solid solution in the iron matrix $\text{Fe}(\text{Cr})$ take place. Titanium participates actively in the interaction process, which leads to the formation of TiC carbides even at 1200°C .

- There is no significant difference in the structure and mechanical properties of composites milled in an attritor or in a ball mill. At the same time, sintering temperature and time affect the structure and properties of the cermets.
- Cermets sintered at lower temperature during a longer time demonstrated the best complex of hardness-toughness properties.

ACKNOWLEDGEMENT

This work was supported by institutional research funding IUT 19-29 of the Estonian Ministry of Education and Research.

REFERENCES

1. Pirso, J. and Kallas, P. Abrasive erosion of non-tungsten cemented carbides. In *Proceedings of European Conference on Advances in Hard Materials Production*. Stockholm, 1996, 333–338.
2. Kayuk, V. G., Masljuk, V. A., and Yuga, A. I. Production, mechanical and tribological properties of layered composite materials based on a chromium carbide alloy. *Powder Metall. Met. Ceram.*, 2003, **42**, 31–37.
3. Pirso, J., Viljus, M., and Kübarsepp, J. Abrasive erosion of chromium carbide based cermets. In *Proceedings of the 9th International Conference on Tribology*. Porvoo, 2000, 959–967.
4. Hussainova, I., Kübarsepp, J., and Pirso, J. Mechanical properties and features of cermets. *Wear*, 2001, **250**, 818–825.
5. Kayuk, V. G., Masljuk, V. A., and Kostenko, A. D. Tribological properties of hard alloys based on chromium carbide. *Powder Metall. Met. Ceram.*, 2003, **42**, 257–261.
6. Letunovits, S., Viljus, M., and Pirso, J. Sliding wear of $\text{Cr}_3\text{C}_2\text{-Ni}$ base cermets. *Mater. Sci. (Medžiagotyra)*, 2002, **8**(4), 477–480.
7. Hussainova, I., Pirso, J., and Viljus, M. Processing and tribological properties of chromium carbide based

- cermets. In *Proceedings of World Congress on Powder Metallurgy and Particulate Materials*. USA, 2002, **6**, 166–173.
8. Pirso, J., Viljus, M., and Letunovits, S. Friction and wear behaviour of cemented carbides. *Wear*, 2004, **257**, 257–265.
 9. Pirso, J. and Viljus, M. Structure formation of Cr_3C_2 -based cermets during sintering. In *Proceedings of Powder Metallurgy World Congress*. Kyoto, 2000, **2**, 1265–1268.
 10. Radomyselskii, I. D. and Klimenko, V. N. Method of producing cermet alloys. USSR patent No. 140582, 1961, **16**.
 11. Vlasyuk, R. Z., Gripachevskii, A. N., and Radomyselskii, I. D. Changes in the chemical and phase compositions of a Cr_3C_2 particle in contact with an iron matrix during sintering. *Powder Metall. Met. Ceram.*, 1984, **23**, 597–602.
 12. Yakovenko, R. V., Maslyuk, V. A., Gripachevskii, A. N., and Deimontovich, V. B. Dissolution of chromium carbide Cr_3C_2 in Kh17N2 steel during sintering. *Powder Metall. Met. Ceram.*, 2011, **50**, 182–188.
 13. Maslyuk, V. A., Yakovenko, R. V., Potazhevskaya, O. A., and Bondar, A. A. Hard powder alloys and carburized chromium steels in the Cr–Fe–C system. *Powder Metall. Met. Ceram.*, 2013, **52**, 47–57.
 14. Maslyuk, V. A., Bondar, A. A., Kuras', V. B., Pidoprygora, M. I., and Varchenko, V. M. Structure and properties of iron–high-carbon ferrochrome powder composites. *Powder Metall. Met. Ceram.*, 2013, **52**, 291–297.
 15. Maslyuk, V. A. Tungsten-free hardmetals and carbide steels with chromium carbides. *Powder Metall. Met. Ceram.*, 2014, **53**, 162–169.
 16. Yakovenko, R. V., Maslyuk, V. A., Mamonova, A. A., Gripachevskii, A. N., and Denisenko, N. I. Interaction of chromium carbide with a Kh13M2 steel matrix. *Powder Metall. Met. Ceram.*, 2014, **52**, 644–650.
 17. Evans, A. G. and Charles, E. A. Fracture toughness determinations by indentation. *J. Am. Ceram. Soc.*, 1976, **59**, 371–372.

Kroomkarbiidkermiste struktuuri moodustumine ja karakteristikud

Märt Kolnes, Jüri Pirso, Jakob Kübarsepp, Mart Viljus ja Rainer Traksmaa

Käesolevas töös uuriti kroomkarbiidi baasil kermiste omadusi ja struktuuri moodustumise protsesse. Kroomkarbiid (50–70 massiprotsenti), raud (Fe) ja titaan (Ti) (Fe:Ti = 4:1) jahvatati atriitoris ning kuulveskis, pressiti ja seejärel paagutati, kasutades erinevaid režiime (temperatuur, kestus). Struktuuri moodustumise protsesside, faasilise ja keemilise koostise uurimiseks kasutati skaneerivat elektronmikroskoopiat ning röntgendifraktsioonanalüüsi. Uuringute tulemusena selgus, et vaakumpaagutamisel toimuvad alljärgnevad protsessid: kroom ja süsinik difundeeruvad ferriitsesse sideainesse ning Cr_3C_2 rekrustilliseerub, moodustades rauaga kaksikkarbiidi $(\text{Cr,Fe})_{23}\text{C}_6$. Moodustub raua-kroomi tardlahus Fe(Cr), temperatuuridel alates 1200 °C tekivad peeneteralised titaankarbiidi osakesed. Määrati kermiste mehaanilised omadused (kõvadus, purunemissitkus), samuti hinnati korrosioonikindlust NaCl vesilahuses (3,5% NaCl). Parimate mehaaniliste omadustega on kermised, mis on paagutatud võimalikult madalal temperatuuril pikema aja jooksul.

Paper V

Kolnes, M., Kübarsepp, J., Viljus, M., Traksmäa, R. Technological Peculiarities of Chromium Carbide-Based Iron Alloy Bonded Cermet. *Solid State Phenomena, Trans Tech Publications Ltd.*, 2017, 267, 82–86.

Technological Peculiarities of Chromium Carbide-Based Iron Alloy Bonded Cermet

Märt Kolnes^{a*}, Jakob Kübarsepp^b, Mart Viljus^c and Rainer Traksmaa^d

Department of Mechanical and Industrial Engineering, Tallinn University of Technology, Ehitajate tee 5, Tallinn, Estonia

^amart.kolnes1@ttu.ee, ^bjakob.kubarsepp@ttu.ee, ^cmart.viljus@ttu.ee, ^drainer.traksmaa@ttu.ee

Keywords: chromium carbide-based cermets; structure formation; spark plasma sintering; oxidation resistance.

Abstract. Cr₃C₂-Ni cermets exhibit high hardness and excellent corrosion, oxidation, abrasive and erosion resistance. However, because nickel is toxic and carcinogenic, great efforts have been made to displace or replace nickel in the composition of cermets. In this research, chromium carbide-based cermets with FeCr-type ferritic binder were fabricated and investigated. Composites were sintered at different conditions: vacuum and spark plasma sintering. Spark plasma sintered cermets demonstrated acceptable structure and mechanical characteristics. Chemical composition of chromium carbide-based iron alloy bonded cermets was analyzed by energy-dispersive X-ray spectroscopy and in the structural analysis, X-ray diffraction was used. Sintered cermet consists of two main phases: α -Fe and (Cr,Fe)₇C₃ complex dicarbide. Mechanical properties – hardness and fracture toughness were characterized. Also, oxidation rates were determined.

Introduction

The European Commission has created a list of critical raw materials which combine high economic importance to the European Union with a high risk associated with their supply. Therefore, efforts have been made to replace the toxic elements in the binder phase and the high-priced elements in the hard phase [1-4]. Iron-based binder systems are most widely used to replace toxic metals because iron is known as a nontoxic and very cost-effective metal.

Development of nickel-free chromium carbide-based cermets is an important area of focus in modern materials science because of the toxicity and high price of nickel. According to Maslyuk et al., iron-based alloys could replace expensive and carcinogenic nickel as a binder phase in chromium carbide materials [5]. Considering that chromium carbide Cr₃C₂ is completely wetted by iron and carbon steel (0.45 %), replacing nickel with low-cost and available iron-based alloys is reasonable. They also demonstrated that iron and steel powders, as well as high-carbon ferrochromium powder, can be used successfully as starting materials to produce chromium carbide cermets and carbide steels [6]. Also, it has been established that in case of steels with chromium carbide additions, as compared to free sintering, shock-wave sintering technique in vacuum improves mechanical properties [7].

Based on the vertical section of the Cr-Fe-C phase diagram along the Cr₃C₂-Fe line, it was concluded that development of chromium carbide cermets with an iron-based binder would be successful only at iron content not lower than 40 wt.%. Iron-based phase is not in equilibrium with Cr₃C₂, leading to the formation of a complex carbide (Cr, Fe)₇C₃ [5]. This confirms that the most promising chromium carbide-based iron alloy bonded cermets can be produced by liquid-phase sintering with 50 – 60 wt.% of Cr₃C₂.

Our focus in this study is on the phase and chemical composition of chromium carbide-based cermets prepared using different sintering techniques. Our goal is to develop and produce chromium carbide-based cermets with ferritic steel binder.

Experimental Details

Chromium carbide and ferritic stainless steel powders were used to fabricate chromium carbide-based cermets (see Table 1). Cr_3C_2 and AISI430L steel powder produced by Pacific Particulate Materials Ltd. and Sandvik Osprey Ltd., respectively, were mechanically ball milled (WC-Co balls and lining) in isopropyl alcohol with rotating speed of 60 rpm, charge ratio of 10:1 during 72 hours. Using WC-Co balls and lining results in some contamination of alloy with tungsten. The milled powder was plasticized with paraffin wax (approximately 1 wt.%). Uniaxially consolidated samples were sintered using two different technologies: liquid-phase sintering in vacuum and spark plasma sintering (SPS). During vacuum sintering (vacuum level was approximately 0.04 mbar), the samples densification was performed using a furnace with graphite heaters (samples were sintered during 30 min at 1300 °C with the heating rate of 10 °C·min⁻¹). During SPS, the powder was consolidated under a load of 35 MPa. The sample was heated up to the sintering temperature of 1100 °C with the heating rate of 100 °C min⁻¹ and was dwelled at this temperature for 2 min. Natural cooling was followed. Oxidation test was performed in air at 900 °C with holding of 60 min.

Table 1. Chemical composition and average particle size of the initial powders

Powder	C	Cr	Mn	Si	Fe	Impurities [wt.%]	Average powder particle size [μm]
	[wt.%]						
Cr_3C_2	13.2	86.7	–	–	–	0.10	1.9
AISI430L	–	16.8	0.7	0.6	81.9	0.04	10 – 45

Hardness measurements (Vickers hardness) were carried out in accordance with the standard EN-ISO-6507. The fracture toughness (K_{IC} , MPa·m^{1/2}) was determined by the method of fracture by indentation with the most commonly used empirical equations for fragile materials proposed by Evans [8]. The weight loss during sintering includes no mass loss due to the evaporation of paraffin wax.

Microstructural analysis was conducted using a scanning electron microscope (SEM) JOEL JSM 840A. In the phase identification of cermets, the XRD method (Bruker AXS D5005) was used. The porosity of the cermets was determined using an optical Axiovert25 microscope and software Buehler Omnimet. The porosity was evaluated by measuring the surface area of pores on the optical image of microstructure.

Results and Discussion

The study covers the chromium carbide-based cermets cemented with Ni-free corrosion resistant FeCr (AISI430L) steel fabricated using different sintering technologies: traditional vacuum sintering and spark plasma sintering. The particle size distribution of ball milled powder are presented in Fig. 1.

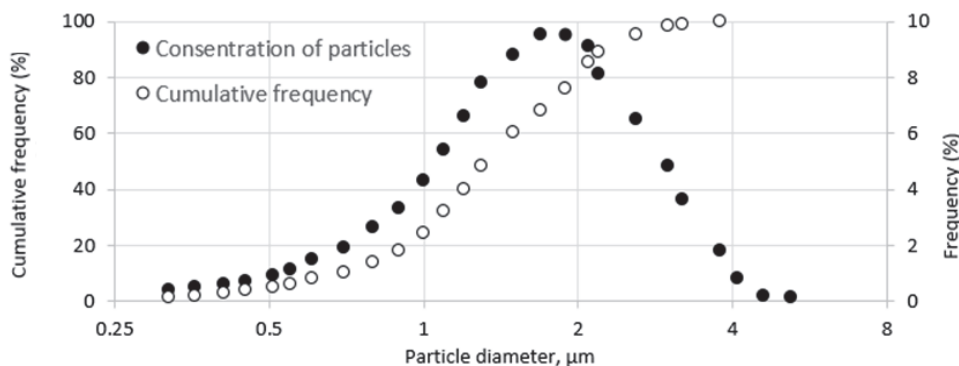


Fig. 1. Particle size distribution of milled chromium carbide based cermets, cumulative frequency and concentration of particles

The average particle size is below 2 μm . XRD pattern of Cr_3C_2 -430L cermet after sintering in vacuum is presented in Fig. 2. The pattern demonstrates that sintered cermet consists of two main phases: α -Fe and $(\text{Cr,Fe})_7\text{C}_3$ complex carbide.

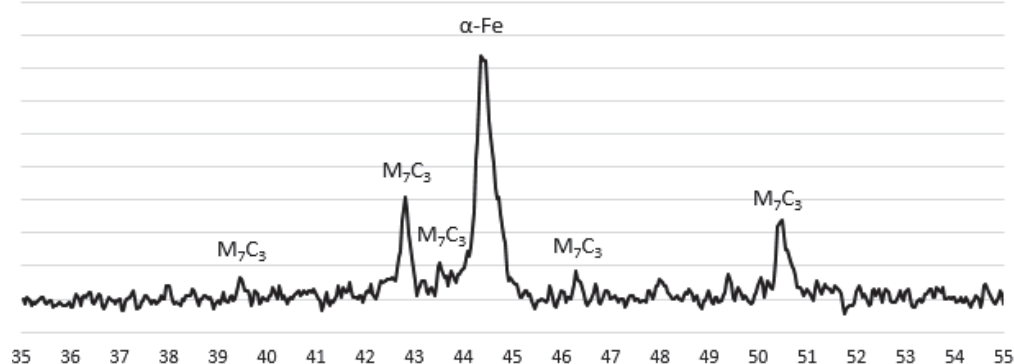


Fig. 2. X-ray diffraction pattern of chromium carbide-based FeCr steel bonded cermet

The change in the structure of chromium carbide observed during subsequent heating is also apparently linked with its composition, since in the carbide Cr_7C_3 , up to 60 % of chromium atoms can be replaced by iron atoms [9]. Therefore, the following sintering mechanism can be presented: depletion of carbon in Cr_3C_2 carbide and its recrystallization into lower carbon containing carbide, iron from metal matrix dissolves in the chromium carbide forming the complex $(\text{Cr,Fe})_x\text{C}_y$ carbide, chromium diffuse into the metallic matrix.

Microstructures of chromium carbide-based cermets are presented in Fig. 3. The dark grey region is complex $(\text{Cr,Fe})_7\text{C}_3$ carbide and light grey is a solid solution of chromium and iron. EDS analysis also confirms the recrystallization of the Cr_3C_2 into $(\text{Cr,Fe})_7\text{C}_3$ complex carbide (see Table 2).

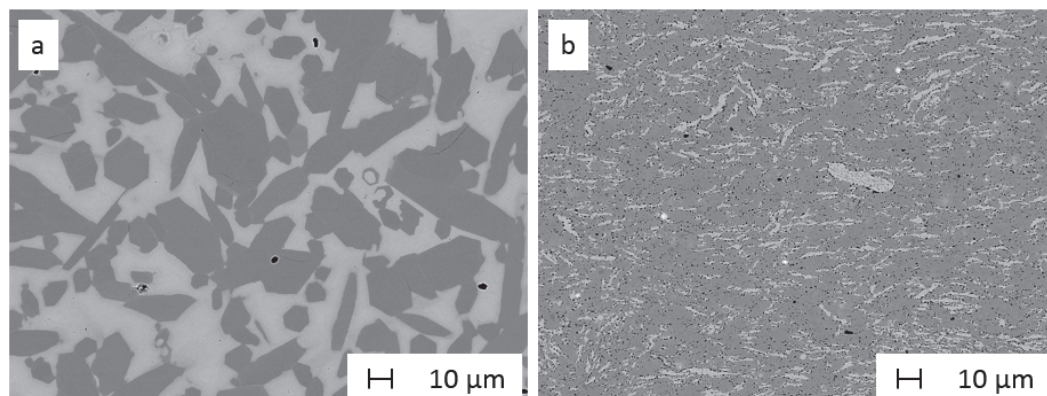


Fig. 3. Microstructure of cermets: a – after vacuum sintering; b – after spark plasma sintering

Table 2 indicates that carbon content in the complex carbide is 9 wt.% (~ 30 at.%). The phase and chemical composition of Cr_3C_2 -430L cermets after spark plasma sintering is similar to that of vacuum sintered samples. Pronounced growth of carbide grains during sintering is one of the main disadvantages of Cr_3C_2 -base cermets [10]. As seen from Figure 1, the milled powder has quite fine particles – the average carbide grain size is below 2 μm . Remarkable carbide grain growth takes place in the alloy during liquid phase sintering (see Figure 3). The average carbide grain size is above 20 μm . During spark plasma sintering, the grain size did not increase so rapidly. However, SPS sintered samples are characterized by very small (below 1 μm) pores.

Table 2. EDS analysis of chromium carbide - 430L steel cermets sintered in vacuum

Phase	C	Cr	W	Mn	Si	Fe
	[wt.%]					
Total	6.9	49.8	1.5	0.5	0.3	41.0
Binder	-	19.5	1.9	0.5	1.0	77.1
Carbide	9.1	69.3	1.0	0.4	-	20.2

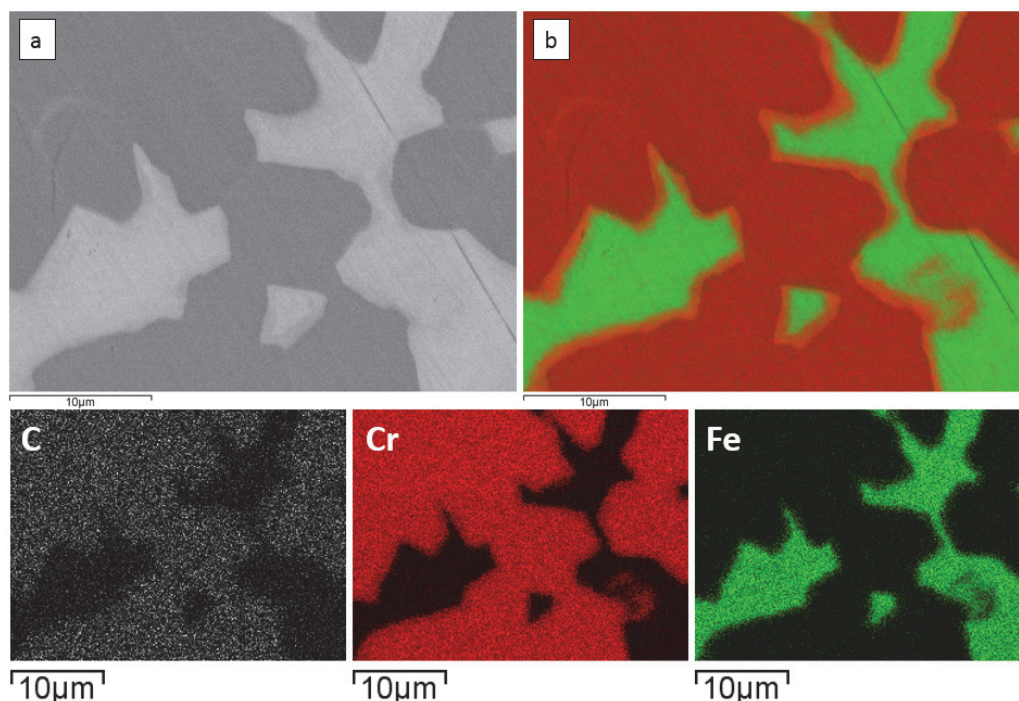


Fig. 4. SEM (a) and EDS mapping (b) images of chromium carbide – 430L steel cermets sintered in vacuum; red – chromium, green – iron

EDS mapping results demonstrate the two-phase structure of the vacuum sintered cermets (see Fig. 4) – complex $(Cr,Fe)_7C_3$ carbides and iron based binder. As can also be seen, at the boundaries of carbide grains, regions that consist less chromium and more iron are determined.

Mechanical characteristics of sintered cermets are demonstrated in Table 3. Cermets produced using SPS technology demonstrated acceptable mechanical characteristics (hardness and fracture toughness) compared with vacuum sintered cermets bonded with Fe-Ti alloys [3], although SPS-ed cermets have small evenly distributed porosity. Chromium carbide cermets bonded with Fe-Ti binder outperform alloys bonded with FeCr binder.

Table 3. Mechanical properties of chromium carbide – 430L steel cermets

Sintering technology	Hardness HV_{30} [kgf/mm ²]	Fracture toughness K_{IC} [MPa·m ^{1/2}]	Porosity [%]	Density [g/cm ³]
Vacuum	1132 ± 33	n/a	0.2 ± 0.1	7.2 ± 0.1
SPS	1167 ± 16	6.4 ± 0.3	0.6 ± 0.1	7.1 ± 0.1

Oxidation tests were performed to evaluate the oxidation rates of different cemented carbides at air brazing temperature – air brazing with Cu brazing filler (F-Bronze) with the melting temperature of 900 °C. Oxidation rates of different composites are presented in Table 4. Chromium carbide cermets with ferritic steel binder demonstrated very good oxidation resistance at higher temperatures compared to other carbide-based composites.

Table 4. Oxidation rates of different carbide-based composites at 900 °C

Material	WC-15wt%Co	TiC-25wt%NiMo	TiC-25wt%FeCr	Cr ₃ C ₂ -50wt%FeCr
Oxidation rate [mg/mm ²]	0.9	0.03	0.04	< 0.01

Summary

Our results from the investigation of the phase and chemical composition of chromium carbide-based cermets using different sintering modes provide for the following conclusions:

- The phase and chemical composition of chromium carbide-based cermets with FeCr binder is the same vacuum sintering or SPS technology.
- Spark plasma sintered Cr₃C₂-FeCr cermets demonstrate similar mechanical characteristics (hardness and fracture toughness) and smaller grain size than vacuum sintered Cr₃C₂-Fe-Ti cermets.
- Chromium carbide – FeCr cermets demonstrate very good oxidation resistance at higher temperatures (900 °C).

Acknowledgement

This work was supported by institutional research funding IUT 19-29 of the Estonian Ministry of Education and Research.

References

- [1] L.J. Prakash, Plansee Seminar 2013: The global refractory metals and hard materials industry meets in Austria, Powder Metallurgy Review. 2 (2013) 41-48.
- [2] C. Hanyaloglu, B. Aksakal, J.D. Bolton, Production and indentation analysis of WC/Fe-Mn as an alternative to cobalt-bonded hardmetals, Materials Characterization. 47 (2001) 315-322.
- [3] M. Kolnes, J. Pirso, J. Kübarsepp, M. Viljus, R. Traksmäa, Structure formation and characteristics of chromium carbide-iron-titanium cermets, Proc. Estonian Acad. Sci. 65 (2016) 138-143.
- [4] W.D. Schubert, M. Fugger, B. Wittmann, R. Useldinger, Aspects of sintering of cemented carbides with Fe-based binders, Int. J. Ref. Met. Hard Mater. 49 (2015) 110-123.
- [5] V.A. Maslyuk, R.V. Yakovenko, O.A. Potazhevskaya, A.A. Bodar, Hard powder alloys and carburized chromium steels in the Cr-Fe-C system, Powder Metall. Met. Ceram. 52 (2013) 47-57.
- [6] V.A. Maslyuk, Tungsten-free hardmetals and carbide steels with chromium carbides, Powder Metall. Met. Ceram. 53 (2014) 162-169.
- [7] A.I. Tolochin, A.V. Laptev, R.V. Yakovenko, V.A. Maslyuk, Shock-wave sintering of the 70 vol% Kh13M2-30 vol% Cr₃C₂ carbonized steel in a wide temperature range, Powder Metall. Met. Ceram. 55 (2017) 518-529.
- [8] A.G. Evans, E.A. Charles, Fracture toughness determinations by indentation, J. Am. Ceram. Soc. 59 (1976) 371-372.
- [9] R.Z. Vlasyuk, V.V. Deimontovich, A.A. Mamonova, Dissolution of the carbide Cr₃C₂ in an iron matrix, Powder Metall. Met. Ceram. 20 (1981) 689-693.
- [10] J. Pirso, M. Viljus, Structure formation of Cr₃C₂-based cermets during sintering, Proc. of Powder Metallurgy World Congress, 2 (2000) 1265-1268.

CURRICULUM VITAE

Personal data

Name: Märt Kolnes

Date of birth: 18/11/1987

Place of birth: Pärnu, Estonia

Citizenship: Estonian

Contact data

E-mail: mart.kolnes1@ttu.ee

Education

2013– 2018 Tallinn University of Technology—PhD

2011– 2013 Tallinn University of Technology—MSC,

2007– 2011 Tallinn University of Technology—BSC

1995– 2007 Pärnu Koidula Gymnasium—High school

Language competence

Estonian Mother Tongue

English Fluent

German Basic

Professional employment

2016– Early Stage Researcher, Tallinn University of Technology

2013– 2016 Engineer, Tallinn University of Technology

ELULOOKIRJELDUS

Isikuandmed

Nimi: Märt Kolnes
Sünniaeg: 18/11/2018
Sünnikoht: Pärnu, Eesti
Kodakondsus: Eesti

Kontaktandmed

E-post: mart.kolnes@ttu.ee

Hariduskäik

2013–2018 Tallinna Tehnikaülikool – PhD
2011–2013 Tallinna Tehnikaülikool – MSC
2007–2011 Tallinna Tehnikaülikool – BSC
1995–2007 Pärnu Koidula Gümnaasium – Keskkharidus

Keelteoskus

Eesti keel – emakeel
Inglise keel – kõrgtase
Saksa keel – algtase

Teenistuskäik

2016 – Nooremteadur, Tallinna Tehnikaülikool
2013 – 2016 Insener, Tallinna Tehnikaülikool